ΕΘΝΙΚΟ ΜΕΤΣΟΒΙΟ ΠΟΛΥΤΕΧΝΕΙΟ

ΣΧΟΛΗ ΗΛΕΚΤΡΟΛΟΓΩΝ ΜΗΧΑΝΙΚΩΝ & ΜΗΧΑΝΙΚΩΝ ΥΠΟΛΟΓΙΣΤΩΝ

ΤΟΜΕΑΣ ΗΛΕΚΤΡΟΜΑΓΝΗΤΙΚΩΝ ΕΦΑΡΜΟΓΩΝ, ΗΛΕΚΤΡΟΟΟΠΤΙΚΗΣ ΚΑΙ ΗΛΕΚΤΡΟΝΙΚΩΝ ΥΛΙΚΩΝ

Προβλήματα Δυναμικής Φορτισμένων Σωματιδίων σε Θερμοπυρηνικό Πλάσμα

ΔΙΔΑΚΤΟΡΙΚΗ ΔΙΑΤΡΙΒΗ

ΠΑΝΑΓΙΩΤΗ Α. ΖΕΣΤΑΝΑΚΗ

ΕΠΙΒΛΕΠΩΝ:
Κ. ΧΙΤΖΑΝΙΔΗΣ
Καθηγητής Ε.Μ.Π.

ΑΘΗΝΑ, Ιούλιος 2019

ΕΘΝΙΚΟ ΜΕΤΣΟΒΙΟ ΠΟΛΥΤΕΧΝΕΙΟ

ΣΧΟΛΗ ΗΛΕΚΤΡΟΛΟΓΩΝ ΜΗΧΑΝΙΚΩΝ & ΜΗΧΑΝΙΚΩΝ ΥΠΟΛΟΓΙΣΤΩΝ

ΤΟΜΕΑΣ ΗΛΕΚΤΡΟΜΑΓΝΗΤΙΚΩΝ ΕΦΑΡΜΟΓΩΝ, ΗΛΕΚΤΡΟΟΟΠΤΙΚΗΣ ΚΑΙ ΗΛΕΚΤΡΟΝΙΚΩΝ ΥΛΙΚΩΝ

Προβλήματα Δυναμικής Φορτισμένων Σωματιδίων σε Θερμοπυρηνικό Πλάσμα

ΔΙΔΑΚΤΟΡΙΚΗ ΔΙΑΤΡΙΒΗ

ΠΑΝΑΓΙΩΤΗ Α. ΖΕΣΤΑΝΑΚΗ

ΤΡΙΜΕΛΗΣ ΣΥΜΒΟΥΛΕΥΤΙΚΗ ΕΠΙΤΡΟΠΗ:

1. Κ. Χιτζανίδης, Καθ. Ε.Μ.Π.(Επιβλέπων)
2. Ι. Ξανθάκης, Καθ. Ε.Μ.Π.
3. Ι. Βομβορίδης, ομοτ. Καθ. Ε.Μ.Π.

ΕΠΤΑΜΕΛΗΣ ΕΞΕΤΑΣΤΙΚΗ ΕΠΙΤΡΟΠΗ:

1. Κ. Χιτζανίδης, Καθ. Ε.Μ.Π.
2. Ι. Ξανθάκης, Καθ. Ε.Μ.Π.
3. Η. Γλύτσης, Καθ. Ε.Μ.Π.
4. Γ. Φικιώρης, Καθ. Ε.Μ.Π.
5. Ι. Ρουμελιώτης, Καθ. Ε.Μ.Π.
6. Κ. Πολιτόπουλος, Αναπλ. Καθ. Ε.Μ.Π.
7. Ι. Κομίνης, Επ. Καθ. Ε.Μ.Π.

Εγκρίθηκε από την επταμελή επιτροπή στις 9 Ιουλίου 2019

ΑΘΗΝΑ, Ιούλιος 2019

Στον δάσκαλό μου, Σωφρόνη–Ηλία Παπαδόπουλο

Παναγιώτης Ζεστανάκης,
Διδάκτωρ Ηλεκτρολόγος Μηχανικός και Μηχανικός Υπολογιστών Ε.Μ.Π.

Πρόλογος

Η παρούσα διατριβή εκπονήθηκε στο Εργαστήριο Πλάσματος, Ηλεκτρονικής Δέσμης & Μη Γραμμικής Οπτικής του Τομέα Ηλεκτρομαγνητικών Εφαρμογών, Ηλεκτροοοπτικής και Ηλεκτρονικών Υλικών της Σχολής Ηλεκτρολόγων Μηχανικών και Μηχανικών Υπολογιστών του Εθνικού Μετσόβιου Πολυτεχνείου. Ευχαριστώ τα μέλη της σχολής και του εργαστηρίου, που βοήθησαν στην εκπόνησή της.

ΠΑΝΑΓΙΩΤΗΣ Α. ΖΕΣΤΑΝΑΚΗΣ
Ιούλιος 2019

Περίληψη

Η μη γραμμική αλληλεπίδραση ιόντων σε μαγνητισμένο πλάσμα με την περιβάλλουσα υψίσυχνων ηλεκρομαγνητικών ρυθμών μελετάται διεξοδικά. Επιτυγχάνεται η έκφραση της Χαμιλτονιανής του γυρόκεντρου σε ισορροπία tokamak ως συνάρτηση δράσεων γωνιών. Με αυτόν τον τρόπο ανοίγει ο δρόμος για την εφαρμογή κανονικών θεωριών διαταραχών στη μελέτη της δυναμικής του γυρόκεντρου υπό την επίδραση μαγνητικών και ηλεκτρομαγνητικών διαταραχών.

Keywords	Λέξεις κλειδιά
plasma	πλάσμα
fusion	σύντηξη
Action Angle	δράση γωνία
chaos	χάος
guiding center	γυρόκεντρο
Hamiltonian dynamics	Χαμιλτονιανή δυναμική
Orbital Spectrum Analysis	Ανάλυση Τροχιακού Φάσματος
perturbation theory	θεωρία διαταραχών

Abstract

The nonlinear interaction between ions in magnetised plasmas and high frequency electromagnetic beat waves is studied. The Hamiltonian of the gyrocenter motion in tokamak equilibria is brought in an action angle form. This enables the application of canonical perturbation theories for the study of the gyrocenter dynamics in the presence of magnetic and electromagnetic perturbations.

Keywords	Λέξεις κλειδιά
plasma	πλάσμα
fusion	σύντηξη
Action Angle	δράση γωνία
chaos	χάος
guiding center	γυρόκεντρο
Hamiltonian dynamics	Χαμιλτονιανή δυναμική
Orbital Spectrum Analysis	Ανάλυση Τροχιακού Φάσματος
perturbation theory	θεωρία διαταραχών

Εκτεταμένη Περίληψη

Η θεωρία πλάσματος επιδέχεται τρεις διακριτές περιγραφές:

- Τροχιές μεμονωμένων σωματιδίων (single particle description). Η ανάλυση επικεντρώνεται στη δυναμική φορτισμένων σωματιδίων που απαρτίζουν το πλάσμα σε δεδομένο ηλεκτρομαγνητικό περιβάλλον.

- Κινητική θεωρία. Όπου τα συλλογικά φαινόμενα εξετάζονται με βάση την εξέλιξη συναρτήσεων κατανομής.

- Θεωρία ρευστού ή Μαγνητοϋδροδυναμική (MHD). Όπου οι συναρτήσεις κατανομής αναπαρίστανται από ένα πεπερασμένο αριθμό ροπών τους (συνηθέστερα από τις πρώτες δύο ή τρεις ροπές).

Η παρούσα εργασία εμπίπτει στην πρώτη από τις τρεις περιγραφές. Στην ισορροπία, τα σωματίδια που απαρτίζουν το μέσο κινούνται ανεξάρτητα το ένα από το άλλο και διατηρούν τα ολοκληρώματα της κίνησης που υπαγορεύονται από τις αντίστοιχες συμμετρίες. Η παραδοχή αυτή αιτιολογείται από τη διαφορά κατά τάξεις μεγέθους μεταξύ των χαρακτηριστικών χρόνων των φαινομένων που μας απασχολούν και των χρόνων μεταξύ των συγκρούσεων. Αν οι συγκρούσεις είναι ο κυρίαρχος μηχανισμός με τον οποίο τα μακροσκοπικά συστήματα έρχονται σε θερμοδυναμική ισορροπία, το ερώτημα του τι σημαίνει μακροσκοπική εξέλιξη ενός collisionless μέσου και πώς αυτή επιτυγχάνεται δεν έχει εύκολη απάντηση. Στην προσέγγιση που ακολουθούμε απουσιάζουν μεν οι συγκρούσεις, ωστόσο η δυναμική του κάθε σωματιδίου επηρεάζεται από τα υπόλοιπα διαμέσου ήπιων mean field διαταραχών, λόγω των ρυθμών που συντηρεί το πλάσμα. Διαταραχές επίσης ενδέχεται να προκύψουν και από καθαρά εξωτερικούς παράγοντες που χαλάνε τις συμμετρίες της αδιατάρακτης κίνησης. Η επίδραση αυτών των διαταραχών στη δυναμική του μεμονωμένου σωματιδίου σε μοντέλα που άπτονται της φυσικής πλάσματος σε tokamak και οι επιπτώσεις που αυτές ενδέχεται να έχουν στη συλλογική συμπεριφορά του μέσου είναι το ευρύτερο αντικείμενο αυτής της εργασίας.

Βασική παραδοχή της ανάλυσης είναι η ύπαρξη εξωτερικού μαγνητικού πεδίου στο πλάσμα. Υποθέτουμε ότι η ένταση του μαγνητικού πεδίου είναι αρκετά ισχυρή, ώστε να διαχωρίσει τη δυναμική σε δύο χωροχρονικές κλίμακες. Σαν αποτέλεσμα, αδιατάρακτη κίνηση των σωματιδίων απαρτίζεται από δύο διακριτές κινήσεις; τη γρήγορη κυκλοτρονική κίνηση, δηλαδή μια σπειροειδή ελικοειδή κίνηση γύρω από την εκάστοτε μαγνητική γραμμή, με σταθερή συχνότητα $\Omega_c = qB/m$ (κυκλοτρονική συχνότητα) και σταθερή ακτίνα ρ_L (ακτίνα Larmor), που υπερτίθεται στην κατά τάξεις μεγέθους πιο αργή ολίσθηση του κέντρου της κυκλοτρονικής κίνησης (γυρόκεντρου).

Η διαφορά κλίμακας έχει σημαντικές συνέπειες και για την επίδραση των διαταραχών στη δυναμική του σωματιδίου. Για διαταραχές με χαρακτηριστικούς χρόνους πολύ μεγαλύτερους από την περίοδο της κυκλοτρονικής κίνησης και μήκη πολύ μεγαλύτερα από την ακτίνα Larmor, μόνο η κίνηση του γυρόκεντρου ενδέχεται να επηρεαστεί σημαντικά από τη διαταραχή και, κατά τη μελέτη της διαταραγμένης δυναμικής, η κυκλοτρονική κίνηση μπορεί να αγνοηθεί. Παρομοίως, για μήκη και χρόνους της τάξης της κυκλοτρονικής κίνησης η ολίσθηση του γυρόκεντρου είναι αμελητέα και η αλληλεπίδραση μπορεί να θεωρηθεί ότι λαμβάνει χώρα σε περιβάλλον ομογενούς μαγνητικού πεδίου που έχει τα τοπικά χαρακτηριστικά του μαγνητικού πεδίου στη θέση του γυρόκεντρου. Τα Κεφάλαια 1 και 3 άπτονται της δεύτερης προσέγγισης, ενώ τα Κεφάλαια 2, 4 και 5 άπτονται της πρώτης

Στο Κεφάλαιο 1 εξετάζεται η δυναμική της κυκλοτρονικής κίνησης σε περιβάλλον ομογενούς μαγνητικού πεδίου υπό την επίδραση ενός υψίσυχνου ηλεκτροστατικού κύματος που διαδίδεται κάθετα στο μαγνητικό πεδίο. Το πρόβλημα αυτό μελετήθηκε διεξοδικά στα τέλη της δεκαετίας του 1970 και στις αρχές του 1980 και είναι ένα από τα παραδείγματα αναφοράς για περιπτώσεις ντετερμινιστικής δυναμικής που μεταπίπτει από ομαλή σε χαοτική κίνηση, όταν το πλάτος του κύματος αυξάνεται. Το κεφάλαιο αυτό λειτουργεί ως ιστορική αναδρομή στο πρόβλημα του φακέλλου δύο κυμάτων, που εξετάζεται στο Κεφάλαιο 3. Είναι επίσης μια εύκολη εισαγωγή στις μαθηματικές τεχνικές, τα μοτίβα και τους προβληματισμούς του κύριου μέρους της διατριβής.

Κάνοντας χρήσης της κανονικής θεωρίας διαταραχών του Deprit, εξετάζουμε την ύπαρξη ή μη ολοκληρωμάτων κίνησης και ομαλών τροχιών ΚΑΜ. Για μικρά πλάτη διαταραχών, οι διαταραγμένες τροχιές διατηρούν την ίδια τοπολογία με τις αδιατάρακτες τροχιές και τα ολοκληρώματα της κίνησης που υπολογίζονται με προσέγγιση πρώτης τάξης αναπαράγουν με ικανοποιητική ακρίβεια το ίχνος που αφήνουν οι διαταραγμένες τροχιές καθώς διέρχονται από μια τομή του φασικού χώρου

(τομή Poincare). Για μεγαλύτερα πλάτη, οι διαταραγμένες τροχιές εξακολουθούν να είναι ομαλές, αλλά η τοπολογία τους αλλάζει, λόγω της εμφάνισης συντονισμών. Οι συντονισμοί αυτοί είναι αποτέλεσμα μιας μικρής διόρθωσης της συχνότητας της αδιατάρακτης κίνησης κατά $\delta\Omega$, λόγω φαινομένων δεύτερης τάξεως. Η διόρθωση αυτή είναι αμελητέα για ιόντα με μικρές ταχύτητες και γίνεται σημαντική μόνο όταν ικανοποιείται η συνθήκη Cerenkov, δηλαδή μόνο όταν η ακτίνα Larmor είναι αρκετά μεγάλη ώστε η προβολή της ταχύτητας του σωματιδίου στον άξονα διάδοσης του κύματος να ξεπεράσει την φασική ταχύτητα του κύματος. Σε αυτήν την περίπτωση, οι καμπύλες ΚΑΜ αλλάζουν τοπολογία και, από ευθείες, σχηματίζουν αλυσίδες νησιών γύρω από τα κέντρα των συντονισμών.

Για ακόμη μεγαλύτερα πλάτη, οι καμπύλες ΚΑΜ καταστρέφονται εντελώς και η δυναμική γίνεται χαοτική. Τρεις συγγενείς μηχανισμοί είναι υπεύθυνοι για την εμφάνιση του χάους. Πρώτον, με την αύξηση του πλάτους της διαταραχής, αυξάνεται και η διόρθωση στην αδιατάρακτη συχνότητα, με αποτέλεσμα την εμφάνιση επιπλέον συντονισμών. Δεύτερον, το πλάτος των νησιών γύρω από τα κέντρα των συντονισμών μεγαλώνει. Τρίτον, εμφανίζονται συντονισμοί ανώτερης τάξης. Όπως προβλέπει το κριτήριο του Chirikov, όταν οι συντονισμοί επικαλύπτονται, η κίνηση γίνεται χαοτική.

Η εμφάνιση χαοτικών τροχιών είναι άρρηκτα συνδεδεμένη με μια ποιοτική αλλαγή στη συλλογική συμπεριφορά υπό την επίδραση της διαταραχής. Σε ένα μέσο από το οποίο απουσιάζουν συγκρούσεις, η ακτινοβολία μπορεί να μεταφέρει ενέργεια, είτε μέσω φαινομένων μείξης (απόσβεση Landau), είτε με καταστροφή των επιφανειών ΚΑΜ. Όταν οι επιφάνειες ΚΑΜ διατηρούνται, δεν είναι δυνατόν να υπάρξει μακροσκοπική μεταφορά, καθώς η κατανομή επιστρέφει στην αρχική της κατάσταση όταν σβήσει η διαταραχή. Για μέτρια πλάτη, η κλίση της συνάρτησης κατανομής μηδενίζεται στις περιοχές του φασικού χώρου όπου εμφανίζονται νησιά συντονισμού, εξαιτίας της μεταφοράς από περιστροφή γύρω από το κέντρο του συντονισμού. Η μεταβολή αυτή, λόγω μείξης, δεν είναι απόλυτα αναστρέψιμη και διατηρείται και μετά το πέρας της αλληλεπίδρασης. Ως συνέπεια, γίνεται μακροσκοπική μεταφορά ορμής και ενέργειας μεταξύ μέσου και ακτινοβολίας, η οποία όμως περιορίζεται από την έκταση των νησιών των συντονισμών. Αντίθετα, όταν κυριαρχεί η χαοτική κίνηση, η ανακατανομή – και, ως εκ τούτου, η μεταφορά – είναι περισσότερο αποτελεσματική, για το λόγο ότι τα σωματίδια είναι ελεύθερα να διαχυθούν σε σημαντικά μεγαλύτερες εκτάσεις του φασικού χώρου. Συμπερασματικά, ποιοτικές αλλαγές στη μονοσωματιδιακή δυναμική συνεπάγονται ανάλογες ποιοτικές διαφορές στη μακροσκοπική αλληλεπίδραση.

Στο Κεφάλαιο 2 εξετάζονται οι αξισυμμετρικές ισορροπίες πλάσματος σε συσκευές μαγνητικής συγκράτησης. Σε κατάσταση ισορροπίας, οι γραμμές του μαγνητικού πεδίου σε μια συσκευή tokamak αναπτύσσονται σε επιφάνειες εμφωλευμένων δισδιάστατων τόρων, που ενδέχεται να διαχωρίζονται από ένα ή περισσότερα separatrix. Η ιδιότητα αυτή οφείλεται στο γεγονός ότι, υπό προϋποθέσεις, οι μαγνητικές γραμμές δύνανται να αναπαρασταθούν από τις τροχιές ενός ολοκληρώσιμου χαμιλτονιανού δυναμικού συστήματος.

Η τοπολογία των μαγνητικών γραμμών είναι σε κάθε κλίμακα καθοριστική για τις ιδιότητες του πλάσματος που συγκρατείται και βρίσκεται σε ισορροπία μέσα στη συσκευή. Από μαγνητοϋδροδυναμική σκοπιά, όλες οι ποσότητες που χαρακτηρίζουν τη μαγνητική ισορροπία πρέπει να είναι σταθερές πάνω στις μαγνητικές επιφάνειες. Από κινητική σκοπιά, οι μεταβολές κατά μήκος των μαγνητικών επιφανειών είναι κατά τάξεις μεγέθους μικρότερες από αντίστοιχες μεταβολές κάθετα στις μαγνητικές επιφάνειες. Στη μονοσωματιδιακή περιγραφή, η δυναμική του γυρόκεντρου δίνεται από ένα ολοκληρώσιμο χαμιλτονιανό σύστημα με δύο βαθμούς ελευθερίας.

Οι συντεταγμένες ροής είναι γενικευμένα τοροειδή συστήματα συντεταγμένων στα οποία η ακτινική συντεταγμένη καθορίζει τη μαγνητική επιφάνεια, ενώ οι δύο ακτινικές συντεταγμένες δίνουν τη θέση του σημείου πάνω στη μαγνητική επιφάνεια. Το μεγάλο τους πλεονέκτημα είναι ότι η χρήση τους διευκολύνει σημαντικά τη διατύπωση των ιδιοτήτων αδιατάρακτων μαγνητικών ισορροπιών. Για παράδειγμα, μαγνητοϋδροδυναμικές ποσότητες, όπως η πίεση είναι συναρτήσεις μόνο της ακτινικής συντεταγμένης.

Οι συντεταγμένες ευθειών μαγνητικών γραμμών είναι ταυτόχρονα και συναρτήσεις δράσης – γωνίας του δυναμικού συστήματος των μαγνητικών γραμμών. Η ακτινική συντεταγμένη είναι η τοροειδής ροή που περικλείεται από τη μαγνητική επιφάνεια και η κανονική δράση του δυναμικού συστήματος. Η πολοειδής γωνία είναι η συζυγής γωνία της δράσης, ενώ η τοροειδής γωνία έχει την έννοια του χρόνου στον οποίο εξελίσσεται το δυναμικό σύστημα. Η Χαμιλτονιανή είναι ίση με την πολοειδή ροή που περικλείεται από την μαγνητική επιφάνεια.

Η κατηγορία συντεταγμένων ευθειών μαγνητικών γραμμών στην οποία η ροή του ρεύματος είναι επίσης ευθύγραμμη, ονομάζεται κατηγορία συντεταγμένων Boozer. Οι συντεταγμένες Boozer είναι δυνατόν να υπολογιστούν συναρτήσει των συντεταγμένων του εργαστηρίου, κάνοντας χρήση των ποσοτήτων που υπολογίζονται από ευρέως διαδεδομένους κώδικες που εξάγουν τη μαγνητική ισορροπία από πειραματικές μετρήσεις. Η χρήση τους διευκολύνει σημαντικά την έκφραση του δυναμικού συστήματος του γυρόκεντρου ως χαμιλτονιανού συστήματος.

Στο Κεφάλαιο 3 εξετάζεται η δυναμική της κυκλοτρονικής κίνησης σε περιβάλλον ομογενούς μαγνητικού πεδίου υπό την επίδραση δύο υψίσυχνων ηλεκτρομαγνητικών κυμάτων που διαδίδονται κάθετα στο μαγνητικό πεδίο. Σε σύγκριση με την αλληλεπίδραση με ένα μόνο κύμα, που μελετήθηκε στο Κεφάλαιο 1, η παρουσία ενός δεύτερου κύματος εισάγει έναν επιπλέον μηχανισμό δυνητικής ανταλλαγής ενέργειας. Πέρα από την αλληλεπίδραση με κάθε κύμα ξεχωριστά, τα σωματίδια μπορούνε να κερδίσουν ή να χάσουν ενέργεια, αλληλεπιδρώντας με το φάκελο που δημιουργείται από την υπέρθεση των δύο κυμάτων. Η αλληλεπίδραση μεταξύ ιόντων και φακέλου είναι μη γραμμική και τουλάχιστον δεύτερης τάξης ως προς το πλάτος της διαταραχής, ωστόσο, όταν η διαφορά μεταξύ των συχνοτήτων των δύο κυμάτων είναι ίση με την κυκλοτρονική συχνότητα, τότε ο φάκελος είναι σε συντονισμό με την αδιατάρακτη κίνηση των ιόντων και η μεταφορά ενέργειας ενδέχεται να είναι ισχυρή ακόμη και για μικρά πλάτη.

Στη μοντελοποίηση του προβλήματος εξετάζουμε την επίδραση πέντε ελεύθερων παραμέτρων; της κεντρικής συχνότητας, της ταχύτητας του φακέλου, της πόλωσης, του αποσυντονισμού της συχνότητας του φακέλου από την κυκλοτρονική συχνότητα και φυσικά του πλάτους της διαταραχής. Για μικρά πλάτη, η διαταραγμένη κίνηση των ιόντων αναλύεται σε δύο επιμέρους κινήσεις. Σε μια γρήγορη ταλάντωση μικρού πλάτους, λόγω της επίδρασης κάθε κύματος ξεχωριστά και σε μία αργή εξέλιξη του κέντρου της ταλάντωσης, λόγω της συνδυαστικής επίδρασης των κυμάτων μέσω του φακέλου. Το κέντρο της ταλάντωσης καθώς και η Χαμιλτονιανή που καθορίζει την εξέλιξή του υπολογίζεται σε δεύτερη τάξη με τεχνικές παρόμοιες με αυτές που χρησιμοποιήσαμε στο Κεφάλαιο 1.

Όταν η ταχύτητα του φακέλου έχει κατεύθυνση ίδια με τη φασική ταχύτητα των κυμάτων, ο φασικός χώρος χαμηλών ενεργειών, που στην περίπτωση του ενός μόνο κύματος παραμένει ανεπηρέαστος, λόγω του ενεργειακού κατωφλίου Cerenkov, μετασχηματίζεται δραστικά. Εμφανίζονται νησιά συντονισμού με ενεργειακό εύρος που εκτείνεται από σχεδόν μηδενικές ενέργειες μέχρι σχεδόν την ενέργεια κατωφλίου. Σωματίδια με πολύ χαμηλές αρχικές ενέργειες, υπό την επίδραση του φακέλου, περιστρέφονται γύρω από το κέντρο του νησιού και φτάνουν σε ενέργειες συγκρίσιμες με την ενέργεια Cerenkov. Εάν ο φάκελος διαδίδεται με κατεύθυνση αντίθετη από τη φασική ταχύτητα των δύο κυμάτων, εμφανίζονται και πάλι νησιά στον χώρο των χαμηλών ενεργειών, αλλά η έκτασή τους είναι σημαντικά περιορισμένη. Στην πρώτη περίπτωση, ο φάκελος δύναται να μεταφέρει σημαντικά ποσά ενέργειας σε μια κατανομή ιόντων, ενώ στη δεύτερη όχι.

Κύριο χαρακτηριστικό της διαταραγμένης κίνησης είναι η ύπαρξη ενός εκφυλισμένου συντονισμού μεταξύ αδιατάρακτης συχνότητας και της αλληλεπίδρασης δεύτερης τάξης. Επομένως, για μικρά πλάτη, είναι οι όροι δεύτερης τάξης εκείνοι που κυριαρχούν, ενώ η διόρθωση πρώτης τάξης είναι αμελητέα. Καθώς το πλάτος αυξάνει, τα φαινόμενα πρώτης τάξης γίνονται ισχυρότερα και η Χαμιλτονιανή του γυρόκεντρου λιγότερο ακριβής στην περιγραφή της πλήρους κίνησης.

Στην περιοχή του φασικού χώρου πέρα από το ενεργειακό κατώφλι αναπτύσσεται ένα δίκτυο νησιών συντονισμού του κέντρου ταλάντωσης. Όταν οι ταλαντώσεις πρώτης τάξης γίνουν αρκετά ισχυρές, τα νησιά αυτά καταστρέφονται και η περιοχή υψηλών ενεργειών γίνεται χαοτική. Για ευνοϊκές ταχύτητες φακέλου, σωματίδια που αποκτούν επαρκή ενέργεια, ώστε το κέντρο της ταλάντωσης να πλησιάσει το κατώφλι ενδέχεται να περάσουν στην χαοτική περιοχή, αν το πλάτος ταλάντωσης είναι αρκετά ισχυρό, και με αυτόν τον τρόπο να αποκτήσουν ακόμα μεγαλύτερες ενέργειες. Το ελάχιστο απαιτούμενο πλάτος της διαταραχής, καθώς και η έκταση της χαοτικής περιοχής, υπολογίζονται ημιαναλυτικά.

Η συχνότητα του φακέλου δεν χρειάζεται να είναι ακριβώς ίση με την κυκλοτρονική συχνότητα. Για μικρούς αποσυντονισμούς, η αλληλεπίδραση πρακτικά παραμένει ίδια με την αλληλεπίδραση τέλειου συντονισμού. Καθώς ο αποσυντονισμός μεγαλώνει, τα σωματίδια με μεγάλες ενέργειες παύουν να αλληλεπιδράνε με τον φάκελο. Όταν αυτό συμβαίνει για σωματίδια με ενέργεια συγκρίσιμη με την ενέργεια κατωφλίου, η αλληλεπίδραση καταστρέφεται. Ο μέγιστος επιτρεπόμενος αποσυντονισμός, ώστε να μην καταστρέφεται η αλληλεπίδραση, είναι κατά προσέγγιση αντιστρόφως ανάλογος της φέρουσας συχνότητας, που σημαίνει ότι για δεδομένο αποσυντονισμό υπάρχει μια μέγιστη φέρουσα συχνότητα πάνω από την οποία η αλληλεπίδραση είναι ασθενής.

Σε εφαρμογές που έχουν να κάνουν με μαγνητική συγκράτηση, η ολίσθηση του γυρόκεντρου αναπόφευκτα συνεπάγεται αποσυντονισμό, καθώς το αυτό διέρχεται από περιοχές με διαφορετική ένταση μαγνητικού πεδίου. Για τιμές παραμέτρων τυπικές για θερμοπυρηνικό πλάσμα σε συσκευή tokamak, ο μέγιστος αποσυντονισμός επιτυγχάνεται μέσα σε μόλις μια γυροπερίοδο, για φέρουσα συχνότητα μόλις δέκα φορές μεγαλύτερη της κυκλοτρονικής. Παράλληλα, ο χρόνος αλληλεπίδρασης, ο χρόνος δηλαδή που χρειάζεται ένα σωματίδιο με χαμηλή ενέργεια για να αποκτήσει ενέργεια συγκρίσιμη με την ενέργεια κατωφλίου, είναι πολύ μεγάλος και συχνά ξεπερνάει ακόμα και την περίοδο ολίσθησης του γυρόκεντρου. Ο συνολικός αποσυντονισμός που λαμβάνει χώρα κατά τη διάρκεια του χρόνου αλληλεπίδρασης είναι κατά τάξεις μεγέθους μεγαλύτερος του μέγιστου επιτρεπόμενου αποσυντονισμού.

Κατά συνέπεια, ο υπό μελέτη μηχανισμός δε φαίνεται να είναι ιδιαίτερα υποσχόμενος για πρακτικές εφαρμογές στη θερμοπυρηνική σύντηξη.

Στο Κεφάλαιο 4 αναπτύσσεται η μέθοδος ανάλυσης τροχιακού φάσματος για την μελέτη της δυναμικής του γυρόκεντρου σε μαγνητική ισορροπία tokamak. Η δυναμική του γυρόκεντρου σε μαγνητική ισορροπία tokamak παρουσιάζει μεγάλο ενδιαφέρον, τόσο από πρακτική σκοπιά, καθώς στην κίνηση του γυρόκεντρου οφείλονται οι συντονισμοί ιόντων υψηλής ενέργειας με μαγνητοϋδροδυναμικές διαταραχές που διεγείρονται στο πλάσμα, όσο και από θεωρητική σκοπιά. Αν και η μορφή της Χαμιλτονιανής του γυρόκεντρου είναι γνωστή από τη δεκαετία του 1980, δεν είχαν γίνει τα απαραίτητα βήματα ώστε η δυναμική να μπορεί να αναλυθεί με εφαρμογή της κανονικής θεωρίας διαταραχών, του δυνατότερου δηλαδή εργαλείου που διαθέτουμε για την ανάλυση των διαταραχών ολοκληρώσιμων χαμιλτονιανών προβλημάτων.

Το πρώτο βήμα της κανονικής θεωρίας διαταραχών είναι η εξεύρεση ενός κανονικού μετασχηματισμού των συντεταγμένων του φασικού χώρου σε κανονικές συντεταγμένες δράσεων γωνιών, έτσι ώστε η αδιατάρακτη Χαμιλτονιανή να είναι συνάρτηση των δράσεων αποκλειστικά. Παραδοσιακά η κανονική θεωρία διαταραχών εφαρμόζεται σε προβλήματα όπου η αδιατάρακτη Χαμιλτονιανή είναι είτε εξ αρχής εκπεφρασμένη σαν συνάρτηση των δράσεων, είτε είναι αρκετά απλή ώστε να μπορεί εύκολα να εκφραστεί σε τέτοια μορφή αναλυτικά.

Σε ισορροπίες με αξονική συμμετρία, όταν η δυναμική εκφράζεται σε συντεταγμένες Boozer, η Χαμιλτονιανή του γυρόκεντρου είναι ανεξάρτητη από την τοροειδή γωνία. Επομένως, η κανονική τοροειδής ορμή είναι σταθερή και ίση με την τοροειδή δράση και το σύστημα είναι πρακτικά ένα δυναμικό σύστημα ενός μόνο βαθμού ελευθερίας και ως εκ τούτου ολοκληρώσιμο. Αν και η Χαμιλτονιανή του γυρόκτεντρου είναι ολοκληρώσιμη, σε καμία περίπτωση δεν έχει απλή μορφή. Συχνά δε οι παράμετροί της είναι γνωστές μόνο αριθμητικά. Επομένως είναι πρακτικά αδύνατον να εκφραστεί αναλυτικά σαν συνάρτηση των δράσεων, όπως απαιτεί η κανονική θεωρία διαταραχών. Η προϋπόθεση αυτή ικανοποιείται με την ανάπτυξη του αριθμητικού κανονικού μετασχηματισμού του φασικού χώρου σε δράσεις γωνίες.

Ο αριθμητικός μετασχηματισμός σε δράσεις γωνίες υπολογίζεται ξεχωριστά σε κάθε επίπεδο του φασικού χώρου με σταθερή τοροειδή ορμή, με ολοκλήρωση κατάλληλων ποσοτήτων κατά μήκος των τροχιών. Ωστόσο, δεν υπάρχει συνεχής μετασχηματισμός που να καλύπτει ολόκληρο το επίπεδο. Αντίθετα, ο μετασχηματισμός ένας μετασχηματισμός σε δράσεις γωνίες είναι συνεχής μόνο για χωρία που δεν εμπεριέχουν separatrix. Επομένως, προκειμένου να καλυφθεί ολόκληρο το επίπεδο, είναι

απαραίτητο να υπολογιστεί ένα σύνολο ξεχωριστών μετασχηματισμών, ένας για κάθε μία περιοχή που καθορίζεται από κάποιο separatrix. Τις περιοχές ορίζονται από τα separatrices σε κάποιο επίπεδο με σταθερή F τις ονομάζουμε ηπείρους. Το σύνολο των μετασχηματισμών σε δράσεις γωνίες για κάθε ήπειρο αποτελεί έναν άτλαντα.

Η μελέτη των συντονισμών είναι απαραίτητη για την πρόβλεψη της συμπεριφοράς ενός δυναμικού συστήματος παρουσία διαταραχών. Καθώς ο συντονισμός είναι μη τοπικό φαινόμενο, αλλά εξαρτάται από ολόκληρη την τροχιά, η μελέτη των συντονισμών διευκολύνεται σε μεγάλο βαθμό, όταν η δυναμική διατυπώνεται σε σύστημα δράσεων – γωνιών, επειδή σε αυτήν την περίπτωση η συνθήκη συντονισμού παίρνει αλγεβρική μορφή. Ο ορισμός σημαντικών αλλά εν γένει δύσκολα μοντελοποιήσιμων μεγεθών, όπως για παράδειγμα η απόσταση ή η έκταση των συντονισμών είναι τετριμμένος όταν λαμβάνει χώρα στον χώρο των δράσεων. Τα εύρη των συντονισμών εξαρτώνται από τη μορφή της διαταραχής, αλλά τα κέντρα τους καθορίζονται σε πρώτη προσέγγιση από τα χαρακτηριστικά του αδιατάρακτου προβλήματος αποκλειστικά. Περιοχές στο χώρο των δράσεων που είναι πυκνές σε συντονισμούς είναι εν γένει εκείνες στις οποίες θα πρωτοεμφανιστεί χάος, παρουσία κάποιας διαταραχής. Το εύρος του κάθε συντονισμού είναι ανάλογο με την τετραγωνική ρίζα του πλάτους της αντίστοιχης αρμονικής της διαταραχής. Όταν τα πλάτη των συντονισμών επικαλύπτονται, εμφανίζεται χάος στην περιοχή εμβέλειας των δύο συντονισμών. Κατ΄ επέκταση, αλυσίδες αλληλοεπικαλυπτόμενων συντονισμών συνεπάγονται χαοτική διάχυση στην περιοχή του φασικού χώρου που αυτές καλύπτουν. Αναλύσεις τέτοιου τύπου μας επιτρέπουν να προβλέψουμε ενδεχόμενη απώλεια σωματιδίων από το tokamak παρουσία μαγνητικών διαταραχών.

Η ανάλυση τροχιακού φάσματος είναι σημαντική όχι μόνο για τη μονοσωματιδιακή κίνηση, αλλά και για τη μοντελοποίηση της συλλογικής συμπεριφοράς. Απουσία διαταραχών, κάθε συνάρτηση κατανομής σε ισορροπία μπορεί να εκφραστεί σαν συνάρτηση δύο ανεξάρτητων διατηρήσιμων ποσοτήτων (και της μαγνητικής ροπής). Κάθε τέτοια δυάδα είναι έγκυρη, αλλά για τους σκοπούς της διαταρακτικής ανάλυσης, η δυάδα των δράσεων είναι η περισσότερο χρήσιμη. Σε περίπτωση ισχυρού χάους, όταν οι περισσότερες καμπύλες ΚΑΜ έχουν καταστραφεί, η εξέλιξη της συνάρτησης κατανομής περιγράφεται από μια εξίσωση τύπου Focker–Plank. Ο τελεστής διάχυσης υπολογίζεται συναρτήσει των αρμονικών πλατών της διαταραχής. Το γεγονός ότι ο τελεστής διάχυσης εκφράζεται ρητά ως συνάρτηση των δράσεων είναι ένα σημαντικό πλεονέκτημα της μεθόδου.

Στο Κεφάλαιο 5 εξετάζουμε από μαθηματική σκοπιά τη μέθοδο ανάλυσης τροχιακού φάσματος. Η αδιατάρακτη Χαμιλτονιανή του γυρόκεντρου ανήκει στην οι-

κογένεια των Χαμιλτονιανών δύο βαθμών ελευθερίας με μία αγνοήσιμη θέση, που έχουν τη μορφή

$$H = H(p, q; F),$$

όπου F η συζυγής κανονική ορμή της αγνοήσιμης θέσης. Στην περίπτωση της Χαμιλτονιανής του γυρόκεντρου, η F είναι ίση με την κανονική τοροειδή ορμή. Όλες οι Χαμιλτονιανές αυτής της οικογένειας είναι ολοκληρώσιμες, αλλά, όπως και στην περίπτωση της Χαμιλτονιανής του γυρόκεντρου, είναι σχεδόν πάντα απαραίτητος ο αριθμητικός υπολογισμός ενός μετασχηματισμού σε δράσεις γωνίες, ώστε αυτές να εκφραστούν σαν συνάρτηση των δράσεων

$$K = K(J, F).$$

Όμως, ο υπολογισμός του μετασχηματισμού σε δράσεις γωνίες δεν λύνει όλα τα προβλήματα. Απαιτείται επιπλέον η κατασκευή μοντέλων για τη μορφή της νέας Χαμιλτονιανής $K(J, F)$ από δείγματα από τριάδες (J, F, K), υπολογισμένες με αριθμητική ολοκλήρωση κατά μήκους των τροχιών. Απαραίτητη προϋπόθεση είναι ο διαχωρισμός των δειγμάτων ανά ήπειρο, επομένως απαιτείται γνώση και μοντελοποίηση των κρίσιμων σημείων της Χαμιλτονιανής και του σχήματος των separatrices σε κάθε τομή με σταθερή F. Κάθε άλλο παρά τετριμμένη απαίτηση, αλλά απαραίτητο να ικανοποιηθεί για τις ανάγκες της ανάλυσης τροχιακού φάσματος.

Για της ανάγκες της κανονικής θεωρίας διαταραχών, τα μοντέλα μας θα πρέπει να μπορούν να υπολογίσουν και τις παραγώγους της Χαμιλτονιανής. Για παράδειγμα, η εκτίμηση του εύρους του συντονισμού απαιτεί τη γνώση του Χεσσιανού πίνακα (του πίνακα δευτέρων παραγώγων) της νέας Χαμιλτονιανής ως προς τις δράσεις. Για αυτόν τον υπολογισμό, η ύπαρξη περισσότερων της μίας ηπείρου σε κάθε τομή συνεπάγεται μια σημαντική δυσκολία. Τα δείγματα διαδοχικών τομών, όχι μόνο θα πρέπει να διαχωριστούν ανά ηπείρους, αλλά και οι ίδιες οι ήπειροι γειτονικών τομών να κατηγοριοποιηθούν ανά οικογένειες ισοδυναμίας. Με άλλα λόγια απαιτείται η μοντελοποίηση του τοπολογικού σκελετού του αδιατάρακτου φασικού χώρου. Επιπλέον, αυτή θα πρέπει να γίνεται αποδοτικά και αυτόματα, χωρίς καμία εκ των προτέρων υπόθεση για τον αριθμό, το σχήμα και την θέση των ηπείρων.

Η μοντελοποίηση του τοπολογικού σκελετού είναι ένα ιδιαίτερα απαιτητικό πρόβλημα. Μπορεί ωστόσο να παρακαμφθεί, κάνοντας χρήση αποκλειστικά τοπικών χαρακτηριστικών. Ο μετασχηματισμός σε δράσεις γωνίες υπολογίζεται με ολοκλήρωση κατά μήκους των προβολών των τροχιών σε τομές με σταθερή F και εμφανίζει εξάρτηση από την διατηρήσιμη δράση F, λόγω της μεταβολής του δρόμου ολο-

κλήρωσης σε διαδοχικές τομές. Ωστόσο δεν είναι ιδιαίτερα δύσκολο να μεταφέρει κανείς αυτήν την εξάρτηση εντός του ολοκληρώματος, κρατώντας το δρόμο ολοκλήρωσης σταθερό και αλλάζοντας κατάλληλα την υπό ολοκλήρωση ποσότητα. Με αυτόν τον τρόπο υπολογίζεται ολοκληρωτικά, όχι μόνο ο ίδιος ο μετασχηματισμός, αλλά και η παράγωγός του ως προς F.

Εντελώς ανάλογα υπολογίζονται και οι πρώτες παράγωγοι κάθε ρητού ολοκληρώματος της κίνησης, δηλαδή κάθε ποσότητας που εκφράζεται ρητά σαν ολοκλήρωμα κατά μήκους μιας κλειστής τροχιάς κάποιας διαφορικής μορφής. Με επαγωγή, όλες οι παράγωγοι κάθε ρητού ολοκληρώματος της κίνησης είναι δυνατόν να εκφραστούν σαν ρητά ολοκληρώματα της κίνησης. Με ανάλογο τρόπο, τα στοιχεία του Χεσσιανού πίνακα της νέας Χαμιλτονιανής εκφράζονται σαν ρητά ολοκληρώματα της κίνησης και υπολογίζονται παράλληλα με τον ίδιο τον μετασχηματισμό, χωρίς αναφορά σε τοπολογικά χαρακτηριστικά των τροχιών. Τέλος, η μέθοδος δοκιμάζεται με την εφαρμογή της στη διαταρακτική ανάλυση του γενικευμένου εκκρεμούς.

Contents

List of Figures

List of Tables

Glossary

Action Angle	δράση γωνία
action quantity	ποσότητα δράσης
Boozer coordinates	συντεταγμένες Boozer
bracket operator	παρενθετικός τελεστής
chaos	χάος
degeneracy, accidental	περιστασιακός εκφυλισμός
degeneracy, intrinsic	εγγενής εκφυλισμός
equilibrium	ισορροπία
explicit integral of motion	ρητό ολοκλήρωμα της κίνησης
extended pendulum	εκτεταμένο εκκρεμές
flux function	συνάρτηση ροής
flux surface	επιφάνεια ροής
guiding center	γυρόκεντρο
Hamiltonian	Χαμιλτονιανή
Landau damping	απόσβεση Λαντάου
lower hybrid	κατώτερος υβριδικός
magnetic axis	μαγνητικός άξονας
magnetic coordinates	μαγνητικές συντεταγμένες
magnetic moment	μαγνητική ροπή
Orbital Spectrum Analysis	Ανάλυση Τροχιακού Φάσματος
oscillation center	κέντρο ταλάντωσης
perturbation theory	θεωρία διαταραχών
Poincare surface	επιφάνεια Πουανκαρέ
resonance	συντονισμός

Chapter 1

Electrostatic Wave perpendicular to a Uniform Magnetic Field

The single ion dynamics in a uniform magnetic field under the influence of a perpendicularly propagating electrostatic wave has been one of the paradigms of deterministic dynamics that undergoes transition from regular to chaotic motion with increasing perturbation strength. The motivation for studying it in the context of thermonuclear fusion has been the application of lower hybrid waves for plasma heating, by means of *collisionless* ion energization. This short chapter will serve both as an introduction to the beating wave problem discussed in Chapter 3 and as a demonstration of some of the mathematical tools we will be employing in the rest of this thesis.

1.1 Modelling and analysis

Here we will follow the analysis Karney et al. (Karney, 1978, Karney and Bers, 1977). For typical fusion plasmas (see tab. 1.1) the plasma and cyclotron frequencies of electrons and protons are related by:

$$\omega_{pi} \gg \Omega_{ci},$$

and

$$\omega_{pe} \approx \Omega_{ce}.$$

It follows from the cold plasma dispersion relation (Stix, 1992) that the lower hybrid waves in the plasma core propagate almost perpendicularly to the magnetic field (Kikuchi et al., 2012), with frequency $\omega \gg \Omega_{ci}$ and almost electrostatic polarization (Brambilla, 1998); see

quantity	symbol	value
average electron density	n	$1 \times 10^{15}\,\mathrm{cm}^{-3}$
average electron temperature	T	10 keV
electron cyclotron frequency	$\Omega_{\mathrm{ce}}(B = 1\,\mathrm{T})$	176 GHz
proton cyclotron frequency	$\Omega_{\mathrm{cp}}(B = 1\,\mathrm{T})$	95.8 MHz
proton bounce frequency	$\omega_{\mathrm{bp}}(B = 1\,\mathrm{T})$	100 kHz
electron plasma frequency	ω_{pe}	2 THz
proton plasma frequency	ω_{pp}	40 GHz
proton Larmor radius	ρ_{Lp}	1 cm

Table 1.1 Characteristic scales of magnitude for typical fusion plasmas

also subsection 3.3.2. In a Tokamak, the magnetic field inhomogeneity is characterized by

$$\nabla B \sim \frac{B}{R_0},$$

with R_0 the major radius of the Tokamak. Since the typical Larmor radius of the ions is much smaller than R_0 and the drift frequencies of the guiding center motion are much smaller than the cyclotron frequency, i.e.

$$\begin{aligned} \rho &\ll R_0, \\ \omega_{\mathrm{drift}} \approx \Omega_c \frac{\rho}{L_{\mathrm{drift}}} &\ll \Omega_c, \end{aligned}$$

where L_{drift} is the characteristic length of the drift motion, it is reasonable to model the magnetic field as a homogeneous field in the $\mathbf{z}$ direction

$$\mathbf{B} = B_0\mathbf{z}, \quad \mathbf{A} = B_0 x\mathbf{y}$$

and the lower hybrid wave as an electrostatic wave propagating in the $\mathbf{y}$ direction

$$\mathbf{E} = E_0\mathbf{y}\cos(ky - \omega t) \quad \Phi = -E_0/k\sin(ky - \omega t).$$

The Hamiltonian of the perpendicular motion of the particle is

$$\begin{aligned} H &= \frac{1}{2m}(\mathbf{p} - q\mathbf{A})^2 + q\Phi \\ &= \frac{1}{2m}((p_y - qB_0x)^2 + p_x^2) + q\Phi \end{aligned}$$

Normalizing

- time to $\Omega_c^{-1} = \dfrac{m}{qB}$
- length to k^{-1}
- momentum to $\dfrac{m\Omega}{k}$
- energy to $\dfrac{m\Omega^2}{k^2}$

the normalized single particle Hamiltonian becomes

$$\begin{aligned} h &= \frac{k^2}{2m^2\Omega^2}\left[(\frac{m\Omega}{k}p_y - \frac{qB_0}{k}x)^2 + \left(\frac{m\Omega}{k}\right)^2 p_x^2\right] - \frac{kqE_0}{m\Omega^2}\sin(kk^{-1}y - \omega/\Omega_c t) \\ &= \frac{1}{2}\left[(p_y - x)^2 + p_x^2\right] - \epsilon\sin(y - \nu t) \end{aligned}$$

where

$$\nu = \omega/\Omega_c$$

is the wave to cyclotron frequency ratio, which is assumed to be a *large non integer number* in general and

$$\epsilon = \frac{kqE_0}{m\Omega^2}.$$

is the effective amplitude of the wave, which can function as the ordering parameter. Then the Hamiltonian is naturally arranged in orders of ϵ as the first order polynomial

$$h = h_0 + \epsilon h_1,$$

where h_0 is the unperturbed Hamiltonian and h_1 is the (first order) perturbation.

It so happens that h_0 be integrable. The canonical transform to the *guiding center variables* (μ, ϕ) and (p_g, y_g) is generated by the mixed generating function (Goldstein, 1956)

$$G(x, y, p_g, \phi) = y p_g + \frac{1}{2}(x - p_g)^2 \cot\phi, \tag{1.1}$$

from which we have

$$\begin{aligned}
p_x &= \frac{\partial G}{\partial x} = (x - p_g)\cot\phi, \\
p_y &= \frac{\partial G}{\partial y} = p_g, \\
y_g &= \frac{\partial G}{\partial p_g} = y - (x - p_g)\cot\phi = y - p_x, \\
\mu &= \frac{\partial G}{\partial \phi} = \frac{1}{2}(x - p_g)^2 \sin^{-2}\phi,
\end{aligned}$$

which, by appropriate sign and angle conventions, gives

$$p_x = \sqrt{2\mu}\cos\phi \tag{1.2}$$

$$x = p_g + \sqrt{2\mu}\cos\phi \tag{1.3}$$

$$p_y = p_g \tag{1.4}$$

$$y = y_g + \sqrt{2\mu}\sin\phi \tag{1.5}$$

$$\tag{1.6}$$

The unperturbed Hamiltonian in the guiding center variables is

$$h_0(\mu, \phi, p_g, y_g) = \mu, \tag{1.7}$$

from which it follows that the guiding center variables are also the *Action Angle coordinates* (Goldstein, 1956, Jose and Saletan, 1998) of h_0. The Action μ is the *magnetic moment* of the particle and the Angle ϕ the gyro-angle of the gyration motion. Note that both the variables of the (p_g, y_g) Action Angle pair are ignorable in the unperturbed Hamiltonian h_0. The full Hamiltonian becomes

$$h = \mu - \epsilon \sin(p_g + \sqrt{2\mu}\sin\phi - \nu t). \tag{1.8}$$

This can be further simplified by taking into account that the canonical momentum p_g is a constant of motion. The time evolution of the canonical position y_g conjugate to p_g is

determined by the time evolution of the (μ, ϕ) pair by

$$\frac{dy_g}{dt} = \frac{\partial h}{\partial p_g} = -\epsilon \cos(p_g + \sqrt{2\mu} \sin\phi - \nu t). \tag{1.9}$$

Since the two degrees of motion are decoupled and the (p_g, y_g) couple does not contribute to the particle energization, we can, for our purposes, resort to the reduced Hamiltonian

$$h(\mu, \phi, t) = \mu - \epsilon \sin(\rho \sin\phi - \nu t), \tag{1.10}$$

where $\rho = \sqrt{2\mu}$ is the Larmor radius and we wave taken $p_g = 0$ by an appropriate phase shift of the wave.

1.2 Analyzing near integrable dynamics: Perturbation theories

In order to construct the first order integral of motion of the perturbed system will follow Deprit perturbation theory (Deprit, 1969), a theory in the family of Lie transform methods. We will only summarize the main concepts of Deprit perturbation theory here. Excellent descriptions and tutorials can be found elsewhere (Cary, 1981, Lichtenberg and Lieberman, 1992).

1.2.1 Interlude: Lie Pertubration Theory

The objective of canonical perturbation theories is to find a continuous family of near identity transforms that map points $\mathbf{z}$ in the original phase space U to points $\bar{\mathbf{z}}$ in a transformed phase space V

$$\Phi_\epsilon : \mathbf{z} \in U \rightarrow \bar{\mathbf{z}} \in V,$$

so that

$$\Phi_{\epsilon=0} : \mathbf{z} \rightarrow \mathbf{z}$$

be the identity map, with the intent that the dynamics on the new phase space V is less complicated. Canonical perturbation theories rely on the conjecture that *all quantities can be expressed as power series of one or more ordering parameters* and that *equality of power series implies equality of the individual terms*.

Traditional perturbation techniques focus on calculating the terms of a canonical transform *generating function*(Goldstein, 1956)

$$S = \sum_n \epsilon^n S_n.$$

Each step of the process adds an extra term to the power series of S. The generating functions are necessarily of mixed form, e.g. $S(\mathbf{q}, \mathbf{P}, t)$, functions of the old positions and the new momenta, or any such combination. Subsequently, they give rise to transforms that are also expressed in mixed form and have to be inverted in every step of the process. As a consequence, the algebraic complexity increases significantly in each step to such an extent that carrying out the process to order higher than ϵ^2 may be impracticable, or disheartening at best (Lichtenberg and Lieberman, 1992).

Lie perturbation theories overcome the problem of mixed variables. The do so by calculating the transform indirectly. In Lie perturbation theories the focus is not on transforms between phase spaces per se, but on transforms of *functions on the phase space*. Instead of seeking to calculate Φ_ϵ directly, Lie perturbation techniques calculate the operator $T = \ \Phi$, the *pullback* operator associated with Φ_ϵ (Flanders, 1989). The operator T maps functions $g : V \to \mathbf{R}$ to functions $f = Tg : U \to \mathbf{R}$, so that $f(x) = g(\bar{\mathbf{z}}(\mathbf{z}))$, i.e

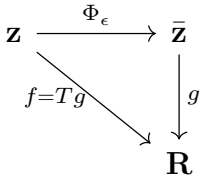

and is formally defined by means of a generating function $w(\mathbf{z}, t; \epsilon)$, so that

$$T = \exp[-\int_0^\epsilon L(\epsilon')d\epsilon'],$$

with L being the Poisson bracket operator defined by

$$Lf = [w, f] \equiv \frac{\partial w}{\partial q_i}\frac{\partial f}{\partial p_i} - \frac{\partial f}{\partial q_i}\frac{\partial w}{\partial p_i}.$$

Deprit Perturbation Theory

Up to now the discussion has been kept rather general. No rules have been given about how the transform T is related to the problem at hand. *Deprit perturbation theory* is one of many possible recipes for specifying T and w incrementally. First, as is customary, we assume

that all objects can be expanded as power series in the perturbation parameter ϵ:

$$w = \sum_{n=0}^{\infty} \epsilon^n w_{n+1}, \tag{1.11}$$

$$L = \sum_{n=0}^{\infty} \epsilon^n L_{n+1}, \tag{1.12}$$

$$T = \sum_{n=0}^{\infty} \epsilon^n T_n, \tag{1.13}$$

$$H = \sum_{n=0}^{\infty} \epsilon^n H_n, \tag{1.14}$$

$$K = \sum_{n=0}^{\infty} \epsilon^n K_n, \tag{1.15}$$

where K is the Hamiltonian in the new phase space V, given by

$$K = T^{-1}H + T^{-1}\int_0^{\epsilon} T(\epsilon')\frac{\partial w(\epsilon')}{\partial t}d\epsilon'.$$

Up to first order the Lie transform is given by

$$\begin{aligned} T_0 &= 1, \\ T_1 &= -L_1, \\ T_2 &= -\frac{1}{2}L_2 + \frac{1}{2}L_1^2, \\ &\vdots \end{aligned}$$

and its inverse by

$$\begin{aligned} T_0^{-1} &= 1, \\ T_1^{-1} &= L_1, \\ T_2^{-1} &= \frac{1}{2}L_2 + \frac{1}{2}L_1^2 \\ &\vdots \end{aligned}$$

The components of the generating function w must satisfy a series of p.d.es

$$\frac{\partial w_1}{\partial t} + [w_1, H_0] = K_1 - H_1 \tag{1.16}$$

$$\frac{\partial w_2}{\partial t} + [w_2, H_0] = 2(K_2 - H_2) - L_1(K_1 + H_1) \tag{1.17}$$

$$\vdots \tag{1.18}$$

All equations above are of the type of inhomogeneous Liouville equation

$$\frac{\partial f}{\partial t} + [f, H_0] = g,$$

with solution

$$f(t) = \int_{t_0}^{t} d\tau S_0^{-1}(t, \tau) g(\tau),$$

with S_0 being the time evolution operator under the unperturbed Hamiltonian H_0.

Each term in the sequence depends only on those that precede it, so that in principle, the terms w_n can be computed iteratively to arbitrarily high order. In each step i, the i-th order term of the new Hamiltonian K_i is unspecified and we are free to choose it as we like. We typically choose K_i to be *as simple as possible*, provided that our choice does not break the ordering scheme. Ideally, we want to take $K_i = 0$ in every step. As we will see, this is not always possible, such as in the case of resonances, where the choice $K_i = 0$ introduces the problem of *small denominators* and the perturbation scheme fails.

1.2.2 First order effects

We begin by Fourier expanding eq. 1.10 by means of the well-known Bessel series (Abramowitz and Stegun, 1970)

$$h = \mu - \epsilon \sum_{n=-\infty}^{\infty} \mathrm{J}_n(\rho) \sin(n\phi - \nu t) \tag{1.19}$$

Although it is perfectly valid to proceed with a time dependent Hamiltonian like the one above, it is conceptually easier to work with an equivalent autonomous Hamiltonian in the extended phase space. Let us introduce the canonical pair (I, χ) and the extended autonomous Hamiltonian

$$H = \mu + \nu I - \epsilon \sum_{n=-\infty}^{\infty} \mathrm{J}_n(\rho) \sin(n\phi - \chi). \tag{1.20}$$

Note that χ is trivially integrated in time as

$$\chi(t) = \nu t.$$

To proceed with the perturbation analysis, we assume there exist a time independent generating function that w can be expanded as a power series in ϵ. The first order component w_1 is given by the equation

$$\begin{aligned}[w_1, H_0] = -H_1 &= \sum_{n=-\infty}^{\infty} \mathrm{J}_n(\rho) \sin(n\phi - \chi) \\ &= -\frac{i}{2} \sum_{n=-\infty}^{\infty} \mathrm{J}_n(\rho) e^{i(n\phi-\chi)} + \text{c.c.},\end{aligned}$$

where we have taken K_1 to be zero. Expanding

$$w_1 = \sum_{n=-\infty}^{\infty} w_{1,n} e^{i(n\phi-\chi)} + \text{c.c.},$$

we get

$$w_{1,n} = -\frac{\mathrm{J}_n(\rho)}{2(n-\nu)}.$$

and

$$\begin{aligned}w_1 &= -\sum_{n=-\infty}^{\infty} \frac{\mathrm{J}_n(\rho)}{2(n-\nu)} e^{i(n\phi-\chi)} + \text{c.c.} \\ &= -\sum_{n=-\infty}^{\infty} \frac{\mathrm{J}_n(\rho)}{(n-\nu)} \cos(n\phi - \chi).\end{aligned}$$

Obviously, if the wave to cyclotron frequency ratio ν where integer or near integer, we would already be in trouble.

The new magnetic moment can be computed to first order by

$$\begin{aligned}\bar{\mu} = T\mu &= \mu - \epsilon L_1 \mu = \mu - \epsilon[w_1, \mu] \\ &= \mu - \epsilon \frac{\partial w_1}{\partial \phi} = \mu - \epsilon \sum_{n=-\infty}^{\infty} n \frac{\mathrm{J}_n(\rho)}{(n-\nu)} \sin(n\phi - \chi)\end{aligned}$$

For small perturbation amplitudes, the curves of conserved first order invariants accurately reproduce the particle orbits, as can be verified by comparing the Poincare plot on the

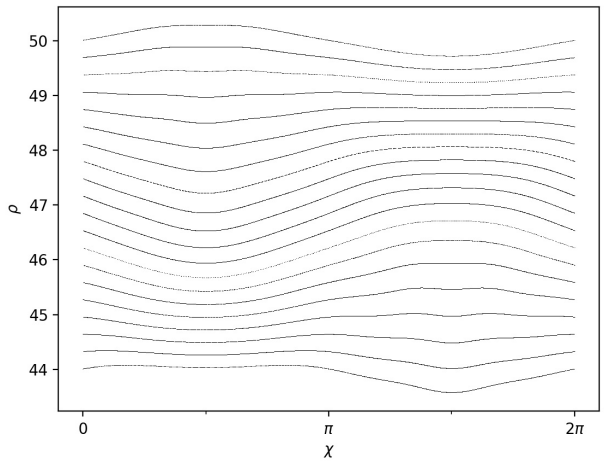

Figure 1.1 Poincare plot on $\phi = 0$, for $\epsilon = 1.2, \nu = 30.23$.

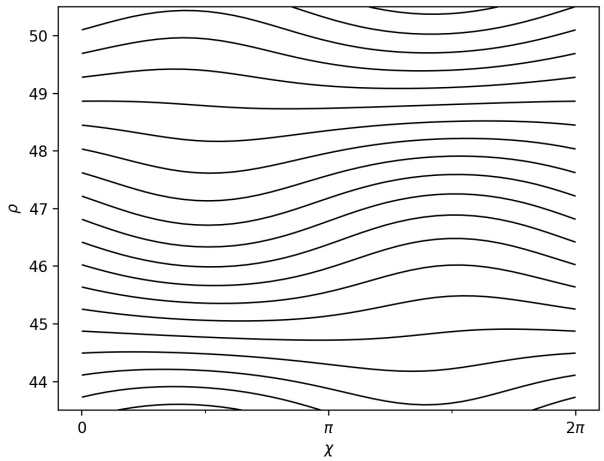

Figure 1.2 Contour plot of the first order invariant $\bar{\mu} = T\mu$ for $\epsilon = 1.2, \nu = 30.23$.

Poincare surface $\phi = 0$ for $\nu = 30.23$ and $\epsilon = 1.2$ (fig. 1.1) and the contour plot of $\bar{\mu} = T\mu$ for the same parameter values (fig. 1.2).

1.2.3 Second Order Effects

For larger amplitudes, the perturbation scheme begins to fail, although the mechanism by which it does so may not be too obvious. Hopefully, it will become clear when we carry the perturbation analysis to the next order.

The second order component of w is given by the Liouville equation:

$$\frac{\partial w_2}{\partial t} + [w_2, H_0] = 2(K_2) - L_1 H_1. \tag{1.21}$$

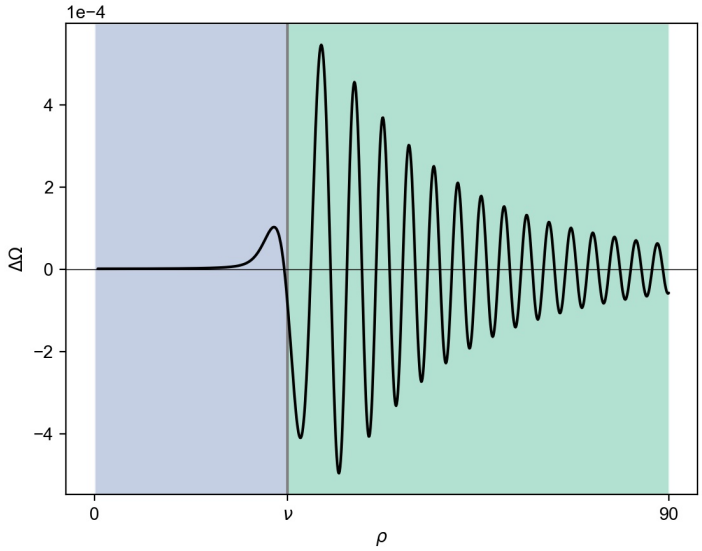

Figure 1.3 Second order frequency correction $\Delta\Omega$ for $\nu = 30.23$. The correction is almost zero for small Larmor radii, and takes on significant value, only for $\rho \gtrapprox \nu$, where its diagram resembles a weakly decaying oscillation curve. The second order islands will first appear at the local extrema of this curve.

Again, we would like to take $K_2 = 0$, as we did with K_1, but unfortunately we can not. If we did, the constant terms on left hand side of eq. 1.21 would lead to a blowup of w_2, which would destroy the ordering. To avoid this, we are forced to take

$$K_2 = \frac{1}{2}\langle L_1 H_1 \rangle = \frac{1}{2}\langle [w_1, H_1] \rangle = -\frac{1}{2}\sum_{n=0}^{\infty} \frac{n}{n-\nu} \frac{\mathrm{J}_n(\rho)\,\mathrm{J}_n'(\rho)}{\rho}, \tag{1.22}$$

where $\langle ... \rangle$ denotes the non oscillating part of the enclosed quantity. The new Hamiltonian K is up to second order

$$K = \mu + \nu I - \epsilon^2 \frac{1}{2} \sum_{n=0}^{\infty} \frac{n}{n-\nu} \frac{\mathrm{J}_n(\rho)\,\mathrm{J}_n'(\rho)}{\rho}. \tag{1.23}$$

In the transformed phase space the canonical momenta μ and I are invariant up to second order, but the frequencies have changed. The interaction with the wave has introduced a second order correction to the average gyrofrequency, so that

$$\frac{d\phi}{dt} = 1 + \epsilon^2 \Delta\Omega,$$

where the correction $\Delta\Omega$ is given by

$$\Delta\Omega = -\frac{1}{2} \frac{\partial}{\partial I} \sum_{n=0}^{\infty} \frac{n}{n-\nu} \frac{\mathrm{J}_n(\rho)\,\mathrm{J}_n'(\rho)}{\rho}. \tag{1.24}$$

The correction $\Delta\Omega$ is rather small, as can be seen in fig. 1.3. It is almost zero for small Larmor radii, and takes on significant value, only for $\rho \gtrapprox \nu$, where its diagram resembles a weakly decaying oscillation curve, but then it never becomes greater than 0.5%. There is a surprisingly simple physical argument to explain this behaviour. In order for the cyclotron frequency to be significantly modified, the *Cerenkov condtidion* should be satisfied in the course of a single gyration. This should require that the projection of the particle velocity $v_\perp$ along the direction of the wave propagation become equal to the phase velocity v_{ph} at least once for every full turn around the axis of rotation. Temporarily letting go of the normalizations, we have on one hand

$$v_\perp = \Omega\rho$$

and on the other

$$v_{\text{ph}} = \frac{\omega}{k}.$$

Therefore the requirement that the particle catches up with the wave implies

$$v_\perp \gtrapprox v_{\text{ph}},$$

or

$$k\rho \gtrapprox \frac{\omega}{\Omega} = \nu,$$

which explains why there is a threshold in ρ. Additionally, considering that as the normalized radius becomes much larger than ν, the energy of the particle increases quadratically, it is reasonable that the relative effect of the interaction with the wave should decline for increasing Larmor radii, which explains the slow decay in $\Delta\Omega$, for high values of ρ.

This small frequency correction is enough to modify the topology of the invariant curves, even for relatively small perturbation amplitudes. This can have a dramatic effect on the qualitative features of the perturbed phase space, as can be seen for example in fig. 1.4. To demonstrate this, let us from now on, without loss of generality, limit the discussion to $\nu = 30.23$, which we have chosen so that its fractional part be far from any low order rational number, such as e.g. $1/4$, or $2/5$. Let us first reexamine the first order Hamiltonian H_1, which we copy here for convenience.

$$H_1 = -\sum_{n=-\infty}^{\infty} \mathrm{J}_n(\rho)\sin(n\phi - \chi). \tag{1.25}$$

In this series above there are two 'slow' angles, namely $\phi_1 = 30\phi - \chi$ and $\phi_2 = 31\phi - \chi$. They are slow in the sense that their unperturbed frequencies are close to the cyclotron frequency, but because of the way we have chosen the wave frequency, they are safely away from any low order resonance with the cyclotron frequency.

For moderate amplitudes, however, the frequency correction can bring these angles in resonance with the base frequency. This changes the topology of the *Kolmogorov, Arnold, Moser (KAM) curves*, the solid curves on the Poincare surface, which are associated with the existence of integrals of motion. This means that islands form around the fixed points, bounded by *separatrices*,i.e. the limiting curves on the Poincare surface that separate areas of different topology. Due to the oscillating character of $\Delta\Omega$ multiple chains for different resonance orders form, see . 1.4

We can predict the amplitude of first appearance and location of such resonances of order s/p, where s, p are small integers, by requiring that

$$\begin{aligned} 30\Delta\Omega - 0.23 &= \frac{s}{p}, && \text{for } \phi_1, \text{and} \\ 31\Delta\Omega - 0.23 &= \frac{s}{p} - 1, && \text{for } \phi_2. \end{aligned}$$

We can also predict the shape of the curves on the Poincare surface along which the resonant islands will occur. This is achieved by mapping any solutions $\bar{\rho}_{\text{res}}$ of the equations above to the original phase space through

$$\rho_{\text{res}} = T^{-1}\bar{\rho}_{\text{res}}.$$

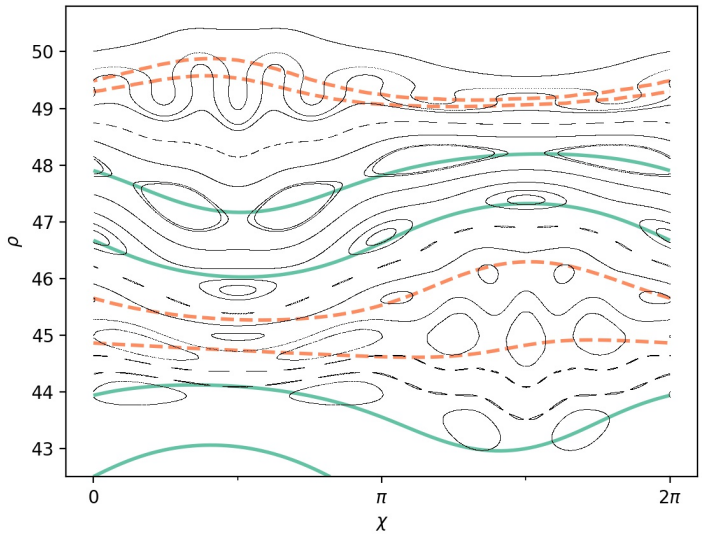

Figure 1.4 Poincare plot and prediction of the location of resonance islands, for $\nu = 30.23$ and $\epsilon = 1.8$. The interaction with the wave modifies the base frequencies of the particle so that second order resonances appear. Solid green lines: Predicted locations for the $3/4$ resonance with ϕ_2. Dashed orange lines: Similarly, for the $4/5$ resonance. The mapping of the estimated resonance locations onto the Poincare surface has been carried out by using the first order approximation of the inverse Lie transform.

Of course, we do not use the exact T^{-1}, which we do not know, but the first order approximation of it that we have already calculated perturbatively. The perfectionist could in principle approximate T^{-1} to any order they like, carrying out the same amount of steps in the perturbation analysis, but we find that the first order approximation suffices for the purposes of this chapter.

In fig. 1.4 we get the chance to compare the estimated location of the resonance chains to the actual location of the islands on the Poincare plots for $\nu = 30.23$ and $\epsilon = 1.8$. Five or six resonance chains form, three for the $3/4$ resonance of ϕ_2 with the base frequency and two or three for the $4/5$ resonance. The corresponding approximations are depicted with solid green lines for the $3/4$ resonance and dashed orange lines, for the $4/5$ resonance. The essential features of the perturbed phase space are reproduced with great accuracy, even by first order approximation.

1.3 Onset of chaotic behaviour.

The features of the moderately perturbed phase space, as depicted in fig. 1.4 may be qualitatively different from the weakly perturbed phase space, fig. 1.1, but the motion is still regular: The trace of each separate orbit on the Poincare plot lies on one or more one-dimensional curves. However, as the amplitude of the perturbation increases, the situation changes. The integrals of motion get broken and there appear orbits whose trace covers densely a finite area on the Poicare map. This is the signature of *chaotic motion* .

Three related but distinct mechanisms are at work to cause this effect. First, as the perturbation amplitude grows, so does the effect of $\Delta\Omega$, which means that resonances that where previously absent are allowed to form chains of islands on the Poincare surface. Second, the width of the already existing islands grows, due to the fact that the resonances become stronger. Third, higher order effects come into play, that may introduce even more chains or modify the characteristics of the already existing ones. Obviously, this cannot go on ad infinitum. There is only so much room for resonant islands before they begin to overlap. When this happens, the integrals of motion break and the motion becomes chaotic. This criterion for estimating the onset of chaotic motion, namely *overlap of resonant islands* is called *Chirikov criterion*.

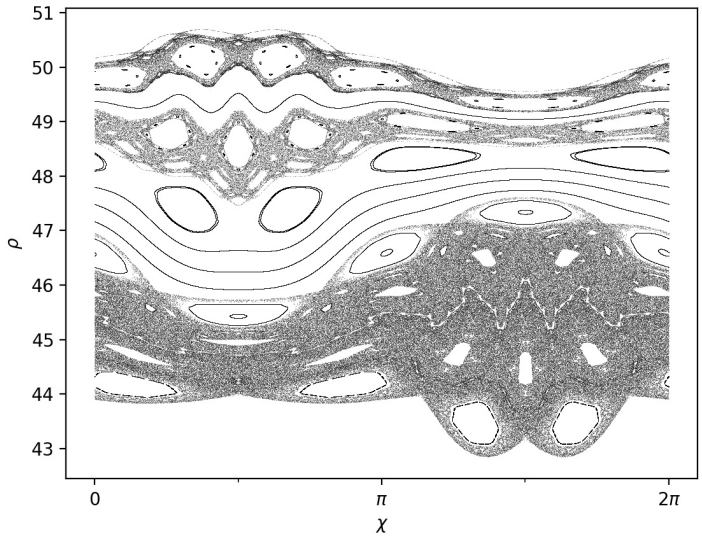

Figure 1.5 Poincare plot and prediction of the location of resonance islands, for $\nu = 30.23$ and $\epsilon = 2.2$. Part of phase space has become chaotic, due to resonance overlap. The primary resonance chains that appeared in fig. 1.4 are also present here along with new ones that did not appear before. Satellite islands around the primary once also form.

The case of $\epsilon = 2.2$, as depicted in fig. 1.5 is an excellent demonstration of the effects of these mechanisms. This figure is a reproduction of a figure that was first published by Karney et al. (Karney, 1978, Karney and Bers, 1977), but with much more detail than the original. Much can be said about this rich and beautiful structure, but most would be out of scope for this chapter. Notice that the resonance chains that appeared in fig. 1.4 are also present here. Around them there is a sea of chaotic orbits, except for the upper $3/4$ chain, which was a bit more isolated from its neighbours to begin with. Resonance chains of other ratios that where previously either absent or too narrow to be detected can also be seen perforating the stochastic sea, running parallel to the $3/4$ and $4/5$ chains. Around the islands of the primary resonances, satellite islands form; a higher order effect.

For $\epsilon = 3.8$ most of the part of phase space we have focussed on has become chaotic. As is expected, with increasing amplitude the fraction of phase space that still supports KAM curves shrinks, but never completely disappears (Markus and Meyer, 1974). As is demonstrated in fig. 1.6, there exist two wide disjoined chaotic bands, separated by a narrow band of regular motion, where there still persists a modified integral of motion $\bar{\mu}$. Orbits inside the chaotic bands are allowed to cover densely all available phase space.

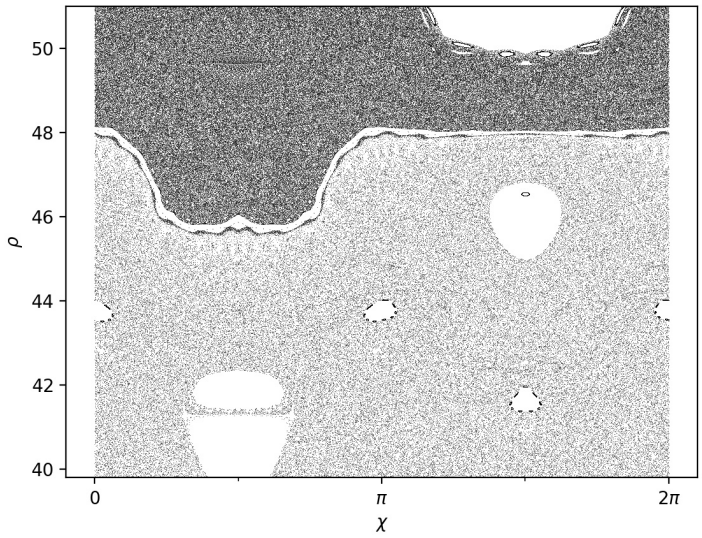

Figure 1.6 Poincare plot and prediction of the location of resonance islands, for $\nu = 30.23$ and $\epsilon = 2.2$. Part of phase space has become chaotic, due to resonance overlap. The primary resonance chains that appeared in fig. 1.4 are also present here along with new ones that did not appear before. Satellite islands around the primary once also form.

There is deep connection between the onset of chaotic behaviour and underlying physics of the interaction that causes it. Consider for example a particle distribution representing a

collisionless plasma. The only way a wave can exchange significant energy with a such a medium is either by means of phase mixing (i.e. *Landau damping*), or by destruction of KAM surfaces[1]. With no change in the KAM surface topology, such as in the low amplitude domain, there can be no net transfer, since only small fluctuations around the equilibrium state are induced, and the particle distribution returns to its original state once the wave source turns off and the interaction stops. In the moderate amplitude regime, phase mixing effects inside the islands that form around the resonances flatten out the distribution function, which forms plateaus on the location of the resonant islands (White, 2012, 2013, White et al., 2010). This results in a net exchange between wave and plasma, but the amount of this exchange is limited by the widths of the islands. When chaotic motion dominates, the redistribution can be much more effective, since the particles are able to diffuse on much wider parts of phase space. In conclusion, qualitative changes in single particle dynamics imply qualitative changes in wave – plasma interaction.

1.4 Conclusions and Discussion

The interaction of a gyrating ion in a homogeneous magnetic field with a perpendicular high frequency electrostatic wave, such as the lower hybrid wave, is a problem with rich physics. Depending on the amplitude of the wave, there are three qualitatively distinct regimes of interaction, weak, medium and strong, that correspond to different topologies of the single particle phase space. In order for a particle to exchange net energy with the wave, the Cerenkov condition must be satisfied along the particle orbit. This puts a lower threshold on the energy of the particles that can be energized by the wave. For realistic conditions, the phase velocity of the lower hybrid wave is significantly larger that the thermal velocity of the ions, meaning that only the tail of the ion distribution can be thermalized.

This chapter served both as an introduction to the beating wave problem, which we address in a later chapter, as well as a short tutorial to some of the mathematical techniques we are going to be using in the rest of this thesis. It also gave us the opportunity to introduce and discuss important concepts such as KAM curves, resonance chains and resonance overlap, as well as the onset of chaos. These concepts are the recurring themes that bring together the different chapters of this thesis.

[1]For an interesting discussion about whether or not KAM surface destruction and Landau Damping are indeed unrelated and if Landau Damping is in fact a collisionless process, see (Mouhot and Villani, 2011)

Chapter 2

Flux Coordinates in Tokamak Equilibria

When a Tokamak is in *equilibrium*, the magnetic field lines inside it have a very special property; each of them can be embedded in a smooth 2D surface, which has the topology of a two dimensional torus. In general, the magnetic field lines cover densely and therefore can be said to define these surfaces, which we call *flux surfaces*, for obvious reasons. Since the magnetic lines can never cross one another, the magnetic surfaces are arranged in families of embedded tori (see fig. 2.1). There are two kinds of limiting surfaces in this configuration; first, if the family of embedded tori, is simply connected, there is the degenerate case where the magnetic field line lies on a 1D curve, so that the flux surface is no a surface at all, but rather a line, the innermost element in the set of the embedded tori, which we call *magnetic axis*. Second, the case when two such surfaces share a common line of contact, which must be a limiting curve for the magnetic field lines, because of the no cross constraint. Such surfaces separate disjoined families of embedded flux surfaces and are called *separatrices* (see fig. 2.2). The trace of the lines of contact on a *Poincare surface* , i.e two dimensional cross section, is an unstable stationary point, or an *X-point*. The trace of the magnetic axis is a stable stationary point, or an *O-point*.

It is no coincidence that the picture we described above is also a signature of integrable Hamiltonian systems. As we will see, the magnetic field lines are indeed Hamiltonian. The topology of the magnetic field has a profound effect on the coexisting plasma in multiple scales. In the fluid/MHD picture, all equilibrium quantities must be constant on the magnetic surfaces. In the kinetic description, gradients along the surfaces and gradients across the surfaces differ by scales of magnitude. In the single particle drift picture, the unperturbed guiding center dynamical system is an integrable Hamiltonian system with two degrees of motion (see Chapter 4).

Unless there is good reason to do otherwise, any reasonable mathematical modelling of Tokamak plasmas should provide ways to express these properties of plasma equilibria in a

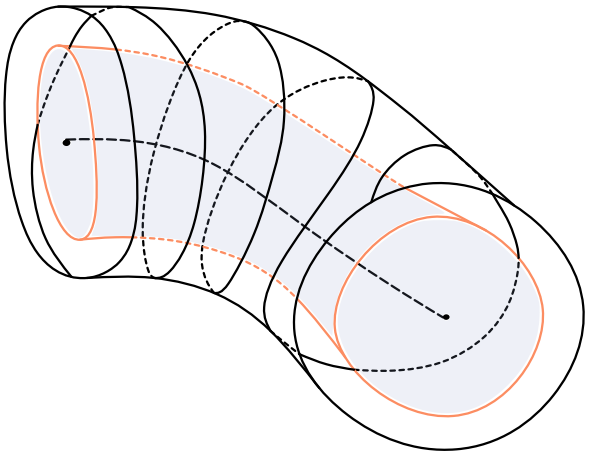

Figure 2.1 general toroidal topology

trivial manner. For example, an MHD quantity, such as the pressure, which is necessarily constant on a given magnetic surface, should be a function of *a single* variable. For this reason, it is sensible make use of coordinate systems adapted to the magnetic field topology. Such systems are known as *magnetic surface coordinates*, or *magnetic coordinate representation* and a wide variety of those have been used in literature. To meet the demands of the toroidal topology, we will use one radial coordinate ρ, which is constant on each magnetic surface, as well as two angular coordinates θ and ϕ. On the degenerate innermost surface, ϕ parametrizes the magnetic axis curve, while θ is undefined. We assume that the triad

$$\mathbf{e}^{\rho} = \nabla\rho, \quad \mathbf{e}^{\theta} = \nabla\theta, \quad \mathbf{e}^{\phi} = \nabla\phi \tag{2.1}$$

forms a right handed *contravariant basis*. The associated *covariant basis* is

$$\mathbf{e}_{\rho} = \partial_{\rho}\mathbf{r}, \qquad \mathbf{e}_{\theta} = \partial_{\theta}\mathbf{r}, \qquad \mathbf{e}_{\phi} = \partial_{\phi}\mathbf{r}, \tag{2.2}$$

Of course the angular coordinates θ, ϕ are not "true" coordinates, in the sense that the one-forms $d\theta$ and $d\phi$ are not closed and, whenever we make use of the functions $\theta(\mathbf{r})$ and $\phi(\mathbf{r})$, it is to be understood that they are defined only locally[1].

By construction,

$$\mathbf{e}^{i} \cdot \mathbf{e}_{j} = \delta^{i}_{j}, \qquad \mathbf{e}^{i} = \frac{1}{\mathcal{J}}\varepsilon_{i,j,k}\mathbf{e}_{j} \times \mathbf{e}_{k}, \qquad \mathbf{e}_{i} = \mathcal{J}\varepsilon_{i,j,k}\mathbf{e}^{j} \times \mathbf{e}^{k}, \tag{2.3}$$

[1]For an interesting example of how a physicist may run into trouble, when naively neglecting the local nature of the angular coordinates, see (Peierls, 1979, Peierls and Urbano, 1968).

with $\varepsilon_{i,j,k}$ the Levi-Civita symbol and

$$\mathcal{J} = \mathbf{e}_\rho \cdot \left(\mathbf{e}_\theta \times \mathbf{e}_\phi\right) = \frac{1}{\mathbf{e}^\rho \cdot \left(\mathbf{e}^\theta \times \mathbf{e}^\phi\right)} \tag{2.4}$$

the Jacobian.

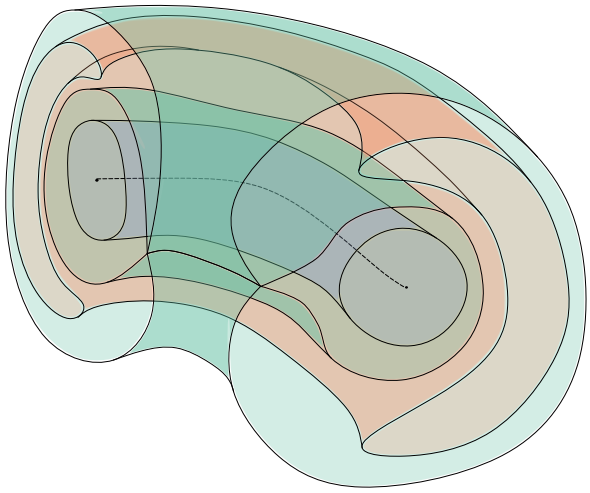

Figure 2.2 toroidal surfaces with separatrix

The magnetic field is associated with a vector potential $\mathbf{A}$ so that

$$\mathbf{B} = \nabla \times \mathbf{A}. \tag{2.5}$$

Write

$$\mathbf{A} = A_\rho \nabla\rho + A_\theta \nabla\theta + A_\phi \nabla\phi \tag{2.6}$$

so that

$$\mathbf{B} = \nabla A_\rho \times \nabla\rho + \nabla A_\theta \times \nabla\theta + \nabla A_\phi \times \nabla\phi. \tag{2.7}$$

For the radial coordinate ρ, it is possible to find a function G so that $\partial_\rho G = A_\rho$. This is not always possible for for the angular coordinates, since $d\theta$ and $d\phi$ are not closed. We can therefore eliminate the radial component of the vector potential by means of the gauge transform $\mathbf{A}' \rightarrow \mathbf{A} - \nabla G$. Then

$$\begin{aligned} \mathbf{A}' &= \left(A_\theta - \partial_\theta G\right) \nabla\theta + \left(A_\phi - \partial_\phi G\right) \nabla\phi \\ &= \psi \nabla\theta - \psi_p \nabla\phi \end{aligned} \tag{2.8}$$

And

$$\mathbf{B} = \nabla\psi \times \nabla\theta - \nabla\psi_p \times \nabla\phi. \tag{2.9}$$

Eq. 2.9 is known as the *contravariant representation* of the magnetic field.

2.1 Boozer Coordinates

In the above, the discussion has been kept rather general and we have made no use of the prescribed toroidal topology of the magnetic field. Accordingly no justification for the contravariant representation of the magnetic field has been given and we have jet to assign any physical meaning to the individual terms of eq. 2.9. In this section we show that the existence of invariant tori for the magnetic field lines implies that the contravariant representation can take the form

$$\mathbf{B} = \nabla\psi(\rho) \times \nabla\theta - \nabla\psi_p(\psi) \times \nabla\phi. \tag{2.10}$$

meaning that both ψ and ψ_p are *flux functions*. When this is the case, ψ is the normalized toroidal flow and ψ_p the normalized poloidal flow inside the flux surface.

2.1.1 The Hamiltonian nature of the magnetic lines

Let the following two assumptions hold:

1. The map $(\rho, \theta, \phi) \to (\psi, \theta, \phi)$ is a diffeomorphism, so that the flux surface coordinate ρ can be replaced by ψ,

2. The poloidal component of the magnetic field $\mathbf{B} \cdot \nabla\phi$ is everywhere non zero.

Assumption 1 means that we can use the triad (ψ, θ, ϕ) as a coordinate system. Then, the magnetic field line equations are given by

$$\begin{aligned}
\frac{d\psi}{d\phi} &= \frac{\mathbf{B}\cdot\nabla\psi}{\mathbf{B}\cdot\nabla\phi} = -\frac{\nabla\psi\cdot\left(\nabla\psi_p\times\nabla\phi\right)}{\nabla\phi\cdot(\nabla\psi\times\nabla\theta)} \\
&= -\mathcal{J}_{(\psi,\theta,\phi)}\nabla\psi_p\cdot(\nabla\phi\times\nabla\psi) = -\nabla\psi_p\cdot\left(\mathcal{J}_{(\psi,\theta,\phi)}\mathbf{e}^{\phi}\times\mathbf{e}^{\psi}\right) \\
&= -\nabla\psi_p\cdot\mathbf{e}_\theta = -\nabla\psi_p\cdot\partial_\theta\mathbf{r} = -\frac{\partial\psi_p}{\partial\theta},
\end{aligned} \tag{2.11}$$

And

$$\begin{aligned}\frac{d\theta}{d\phi} &= \frac{\mathbf{B}\cdot\nabla\theta}{\mathbf{B}\cdot\nabla\phi} = -\frac{\nabla\theta\cdot\left(\nabla\psi_p\times\nabla\phi\right)}{\nabla\phi\cdot\left(\nabla\psi\times\nabla\theta\right)} \\ &= -\mathcal{J}_{(\psi,\theta,\phi)}\nabla\psi_p\cdot\left(\nabla\phi\times\nabla\theta\right) = \nabla\psi_p\cdot\left(\mathcal{J}_{(\psi,\theta,\phi)}\mathbf{e}^{\theta}\times\mathbf{e}^{\phi}\right) \\ &= \nabla\psi_p\cdot\mathbf{e}_{\psi} = \frac{\partial\psi_p}{\partial\psi}.\end{aligned} \tag{2.12}$$

It follows that the magnetic field lines describe a Hamiltonian flow for the canonical pair (θ,ψ) with the Hamiltonian $H=\psi_p(\theta,\psi,\phi)$ and ϕ being the time.

Interlude:Variational Approach

Carry and Littlejohn have given us an alternative, perhaps more satisfying, interpretation of the Hamiltonian nature of the magnetic field (Cary and Littlejohn, 1983). They wave pointed out that for some given vector potential $\mathbf{A}$, the magnetic field lines are reproduced by the Lagrangian:

$$L = \mathbf{A}\left(\mathbf{r}\right)\cdot\frac{d\mathbf{r}}{d\tau}d\tau.$$

This is easily confirmed, considering that the variational principle for the action integral

$$\delta\int\mathbf{A}\left(\mathbf{r}\right)\cdot\frac{d\mathbf{r}}{d\tau} = 0, \tag{2.13}$$

yields the Euler–Lagrange equations:

$$\left(\nabla\times\mathbf{A}\right)\times\frac{d\mathbf{r}}{d\tau} = 0, \tag{2.14}$$

so that the parametric line $\mathbf{r}(\tau)$ is parallel to the magnetic field.

If we assume that the toroidal field is never zero, so that the magnetic field line can locally be parametrized by ϕ and use the representation:

$$\mathbf{A} = \psi\nabla\theta - \psi_p\nabla\phi, \tag{2.15}$$

as we did before, the variational principle becomes

$$\begin{aligned}
&\delta \int \mathbf{A}\left(\mathbf{r}\right) \cdot \frac{d\mathbf{r}}{d\phi}\, d\phi = 0 \Rightarrow \\
&\delta \int \mathbf{A}\left(\mathbf{r}\right) \cdot \left(\mathbf{e}_\rho \dot{\rho} + \mathbf{e}_\theta \dot{\theta} + \mathbf{e}_\phi\right)\, d\phi = 0 \Rightarrow \\
&\delta \int \left(\psi \mathbf{e}^\theta - \psi_p \mathbf{e}^\phi\right) \cdot \left(\mathbf{e}_\rho \dot{\rho} + \mathbf{e}_\theta \dot{\theta} + \mathbf{e}_\phi\right)\, d\phi = 0 \Rightarrow \\
&\delta \int \left(\psi \frac{d\theta}{d\phi} - \psi_p\right)\, d\phi = 0
\end{aligned} \tag{2.16}$$

Notice the similarity of eq. 2.16 with the Hamiltonian dynamics variational principle, namely

$$\delta \int \left[\mathbf{p}\frac{d\mathbf{q}}{dt} - h(\mathbf{q}, \mathbf{p}, t)\right]\, dt = 0. \tag{2.17}$$

One can define ψ as the canonical momentum conjugate to the canonical angle θ and ψ_p as the Hamiltonian. There is only one problem. The poloidal flux ψ_p must be expressed as a function of ψ, θ and ϕ. There should therefore exist a diffeomorphism from (ρ, θ, ϕ) to (ψ, θ, ϕ) for the Hamiltonian description to make sense. This is the diffeomorphism condition we postulated in the beginning of this section. In the Hamiltonian dynamics literature it is known as the Hessian condition (Jose and Saletan, 1998).

An interesting consequence of eq. 2.9 is that the magnetic field is independent of any variation of ψ_p with respect to ϕ, so that we can substitute $\psi_p(\rho, \theta, \phi)$ with $< \psi_p >_\phi$, its average over ϕ. Thus, the Hamiltonian H can be brought in *autonomous*, i.e. time independent form and is therefore conserved and the dynamic system for the magnetic field lines is integrable. In other words, the assumption that ϕ is a time-like variable implies the existence of flux surfaces. This is a direct consequence of the Coulomb law for the magnetic field.

Integrability means that – at least locally – there is some transform to *Action Angle variables* $\bar{\psi}, \bar{\theta}$. These are straight field line coordinates, so that

$$\begin{aligned}
&\psi_p = \psi_p(\bar{\psi}), \\
&\frac{d\bar{\psi}}{d\phi} = 0, \\
&\frac{d\bar{\theta}}{d\phi} = \frac{\partial \psi_p}{\partial \bar{\psi}} = \frac{1}{q(\psi)}.
\end{aligned}$$

For the remainder of this thesis, whenever there exist flux surfaces, we will make use of Action Angle flux coordinates exclusively, so that we can drop the barred notation and the

reader can safely assume that the flux coordinates $(\psi, \theta, \psi_p, \phi)$ to be Action Angle coordinates, unless otherwise stated.

The covariant representation of the magnetic field in Action Angle variables takes the form

$$\mathbf{B} = \nabla\psi \times [\nabla\theta - \frac{1}{q(\psi)}\nabla\phi], \tag{2.18}$$

so that

$$\mathbf{B} \cdot \nabla\psi = 0.$$

The flux function $q(\psi)$ represents the number of toroidal turns per poloidal turn. MHD stability criteria impose restrictions for the allowed values of q in realistic Tokamak equilibria. Suppression of the Kink instability, for example, requires $q > 1$ (Zohm, 2014). For this reason q is known as the *safety factor*.

The Physical interpretation of flux Coordinates

Since ψ_p is a flux function, we have

$$\begin{aligned} &\mathbf{B} \cdot \nabla\psi_p = 0 \Rightarrow \nabla\psi_p \cdot (\nabla\psi \times \nabla\theta) = 0 \\ &\Rightarrow \nabla\psi_p \cdot \frac{\mathbf{e}_\phi}{\mathcal{J}_{(\psi,\theta,\phi)}} = 0 \Rightarrow \partial_\phi\psi_p = 0, \end{aligned} \tag{2.19}$$

which re-states the known fact that the Hamiltonian is conserved, if it is explicitly independent of time. The requirement that ψ is also a flux function means that

$$\begin{aligned} &\mathbf{B} \cdot \nabla\psi = 0 \Rightarrow -\nabla\psi_p \cdot (\nabla\phi \times \nabla\psi) = 0 \\ &\Rightarrow \partial_\theta\psi_p = 0. \end{aligned} \tag{2.20}$$

Therefore, the Hamiltonian ψ_p is only a function of ψ, so that ψ is a function of the action. In fact ψ *is* the action, since

$$J = \frac{1}{2\pi}\oint \psi d\theta = \psi. \tag{2.21}$$

It follows that $\dot{\theta} = \partial_\phi\psi_p = 0$ and that (θ, ψ) is the angle–action pair. Apart from a dynamical meaning, ψ also has a significant interpretation in terms of the magnetic field quantities alone; it is proportional to the toroidal magnetic flux enclosed by the corresponding magnetic field surface. To demonstrate this, let us calculate the magnetic flux flowing through a tube defined

by $\psi = \psi_S$. Since $\mathbf{B} \cdot \nabla\psi = 0$, we have

$$\Psi_t = \iint_S \mathbf{B} \cdot \mathbf{dS}, \tag{2.22}$$

where S is the surface depicted in fig. 2.3a) , with $\phi =$ const. and $\mathbf{dS}$ parallel to the toroidal vector $\mathbf{e}^\phi$.

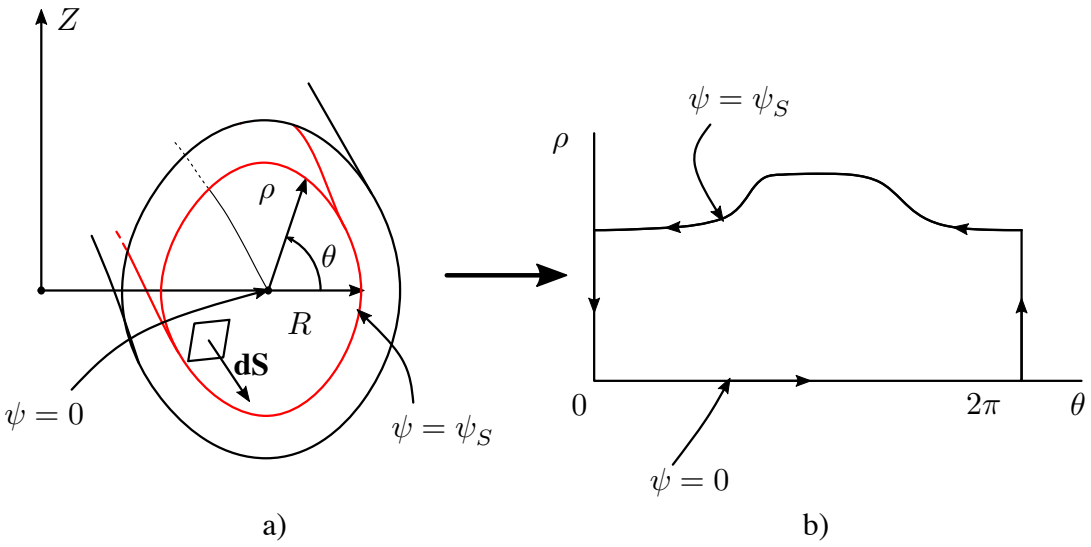

Figure 2.3 a) The flux tube $\psi = \psi_S$ encloses a surface S perpendicular to the toroidal direction $\mathbf{e}^\phi$. b) When calculating the toroidal flux Ψ_t through S, the surface integral transforms to a closed path integral in the θ, ρ plane.

Therefore

$$\begin{aligned}
\Psi_t &= \iint_S \mathbf{B} \cdot \mathbf{dS} = \iint_S \mathbf{B} \cdot \boldsymbol{d\rho} \times \boldsymbol{d\theta} = \iint_S \mathbf{B} \cdot \left(\mathbf{e}_\rho \times \mathbf{e}_\theta\right) d\rho d\theta \\
&= \iint_S \mathcal{J}\mathbf{B} \cdot \nabla\phi \, d\rho d\theta = \iint_S \mathcal{J} \left(\nabla\psi \times \nabla\theta\right) \cdot \nabla\phi \, d\rho d\theta \\
&= \iint_S \mathbf{e}_\rho \cdot \nabla\psi \, d\rho d\theta = \iint_S \partial_\rho \psi \, d\rho d\theta.
\end{aligned} \tag{2.23}$$

Making use of Green's theorem, which we quote here, for convenience

$$\iint_D \partial_x Q - \partial_y D \, dxdy = \int_{\partial D} P \, dx + Q \, dy,$$

we get (by substituting $P = -\psi$ and $Q = 0$)

$$\Psi_t = -\int\limits_{\partial S} \psi \, d\theta = 2\pi\psi_S - 2\pi \, \psi|_{r=0} \,, \tag{2.24}$$

where the integration path ∂S is shown on fig. 2.3b). By choosing $\psi|_{\rho=0} = 0$,

$$\psi = \frac{1}{2\pi}\Psi_t, \tag{2.25}$$

so that ψ is the normalized toroidal flux enclosed in a flux tube around the magnetic axis.

Similarly, the poloidal flux through the surface S' bounded by $\psi_p = 0$ and $\psi_p = \psi_{p,S'}$, with $\theta = \text{const.}$ and $\mathbf{dS}'$ parallel to the poloidal vector $\mathbf{e}^\theta$ is given by

$$\begin{aligned}
\Psi_p &= \iint\limits_{S'} \mathbf{B} \cdot \mathbf{dS} = \iint\limits_{S'} \mathbf{B} \cdot \boldsymbol{d\phi} \times \boldsymbol{d\rho} \\
&= \iint\limits_{S'} \mathcal{J}\mathbf{B} \cdot \nabla\theta \, d\rho d\phi = \iint\limits_{S'} -\mathcal{J} \left(\nabla\psi_p \times \nabla\phi\right) \cdot \nabla\theta \, d\rho d\phi \\
&= \iint\limits_{S'} -\mathcal{J}\nabla\psi_p \cdot (\nabla\phi \times \nabla\theta) \; d\rho d\phi = \iint\limits_{S'} \nabla\psi_p \cdot \mathbf{e}_\rho \, d\rho d\phi \\
&= \iint\limits_{S'} \partial_\rho\psi_p \, d\rho d\phi = -\int\limits_{\partial S'} \psi_p \, d\theta = 2\pi\psi_p,
\end{aligned} \tag{2.26}$$

where again we have chosen $\psi_p\big|_{\rho=0} = 0$. It becomes clear that ψ_p is the normalized poloidal flux.

2.1.2 Boozer Coordinates: A particular pair of Action Angle variables

There is more than one Acton Angle representation for the magnetic field. As can easily be confirmed, the contravariant representation

$$\mathbf{B} = \nabla\psi(\rho) \times \nabla\theta - \nabla\psi_p(\psi) \times \nabla\phi.$$

remains invariant under the transform

$$\begin{aligned}
\phi' &= \phi + q\lambda, \\
\theta' &= \theta + \lambda,
\end{aligned}$$

so does the Hamiltonian character of the magnetic field lines. Here λ is chosen so that the transform is a diffeomorphism, but is otherwise undefined. This leaves a freedom of choice in the straight field line representation.

In general, the covariant representation for the magnetic field is

$$\mathbf{B} = g\nabla\phi + I\nabla\theta + \delta\nabla\psi,$$

where

$$g = \frac{I_{\text{pol}}(\psi)}{2\pi} + \frac{\partial\sigma}{\partial\phi}, \tag{2.27}$$

$$I = \frac{I_{\text{tor}}(\psi)}{2\pi} + \frac{\partial\sigma}{\partial\theta}, \tag{2.28}$$

where $I_{\text{pol}}(\psi)$ is the normalized poloidal current outside the flux surface, $I_{\text{tor}}(\psi)$ the normalized toroidal current inside the flux surface and σ an unspecified function (D'haeseleer et al., 1991). By appropriate choice of λ, the covariant representation can be brought in a form in which the covariant poloidal and toroidal components of the magnetic field are flux functions, i.e constant on any flux surface:

$$\mathbf{B} = g(\psi)\nabla\phi' + I(\psi)\nabla\theta' + \delta\nabla\psi. \tag{2.29}$$

The flux coordinates (ψ, θ', ϕ') are a particular choice of straight field line coordinates flux coordinates known as *Boozer Coordinates* (Boozer, 1980, 1981).

In Boozer coordinates the Jacobian is related to the magnetic field amplitude by

$$\mathcal{J} = \frac{h(\psi)}{B^2},$$

where

$$h(\psi) = (I + gq)/q,$$

a flux function. When studying the drift dynamics of the guiding center in Tokamaks, this property of Boozer coordinates is especially important, because it facilitates writing the equations of motion in Hamiltonian form (White and Chance, 1984). We should point out however, that Boozer coordinates, although a popular and convenient choice, are by no means the only available choice, see for example (Meiss and Hazeltine, 1990, White and Zakharov, 2003). For the remainder of this thesis we will drop the primed notation for the Boozer coordinates and, unless otherwise stated, we will assume $(\psi, \theta, \psi_p, \phi)$ to be already in Boozer form.

2.1.3 Axisymmetric Equilibria

Ideal Tokamaks are devices which support *axisymmetric equilibria*, i.e plasma equilibria that are symmetric around the vertical axis (Mukhovatov and Shafranov, 1971, Wesson, 2004, White, 2013, Zohm, 2014). In axisymmetric equilibria the force balance condition[1] [2]

$$\nabla p = \mathbf{j} \times \mathbf{B}, \tag{2.30}$$

yields the *Grad-Shafranov (GS)* equation

$$R\frac{\partial}{\partial R}\left(\frac{1}{R}\frac{\partial \psi_p}{\partial R}\right) + \frac{\partial^2 \psi_p}{\partial Z^2} = -\partial_\psi p - g\partial_\psi g \tag{2.31}$$

where we make use of the right handed pseudo-toroidal coordinate system (R, Z, ϕ), fig 2.4, with Z the axis of symmetry and ϕ the ignorable toroidal angle. Here both the scalar pressure p and the poloidal current g are flux functions[3].

In the right handed toroidal coordinate system (R, Z, ϕ), fig. 2.4, Z is the axis of symmetry and ϕ the ignorable toroidal angle.

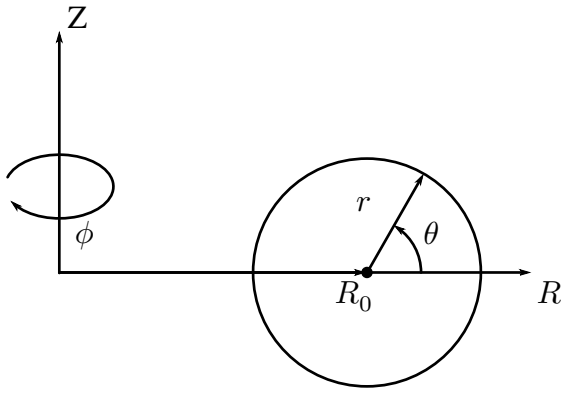

Figure 2.4 pseudo toroidal coordinates

[1]The equilibrium condition is equivalent to the force balance condition, if the plasma inertia term is negligible with respect to the pressure gradient force:

$$\nabla p \gg \rho \mathbf{v} \cdot \nabla \mathbf{v} \Rightarrow \sqrt{\frac{p}{\rho}} \gg v,$$

which means that the plasma flow must be much smaller than the speed of sound. This is usually assumed to hold, (White, 2013, Zohm, 2014), but this assumption is not always valid, e.g. see (Guazzotto and Betti, 2005, McClements and Hole, 2010) and references within.

[2]For typical Tokamak plasmas, the gravitational force is at least 10 orders of magnitude smaller than the Lorentz force and can safely be neglected (J. P. Goedbloed, 2008).

[3]That g must be a flux function is a consequence of axisymmetry and eq. 2.27 and eq. 2.28, which require that $\partial_\theta g = \partial_\phi I$.

Efficient Grad-Shafranov solvers that reconstruct the equilibrium by minimizing the error between the calculated flux, pressure and current profiles and the field measurements date back more than 30 years (Hutchinson, 2005, Lao et al., 1985) and it can safely be assumed that numerical approximations for $\psi_p(R, Z)$, $g(\psi)$ and $q(\psi)$ are readily available.

Reconstructing the Boozer Coordinates from solutions of the GS equation

Due to axisymmetry, the toroidal Boozer angle ζ is related to ϕ through

$$\zeta = \phi - \nu(\psi, \theta),$$

with ν a yet to be determined function. Since

$$(\nabla\psi \times \nabla\theta) \cdot \zeta = (\nabla\psi \times \nabla\theta) \cdot \phi,$$

the transformation $\phi \to \zeta$ leaves the Jacobian invariant White (2013).

The solution of the Grad-Shafranov equation fully defines the magnetic field. The poloidal components of the magnetic field can be calculated by taking the dot product of the contravariant representation

$$\mathbf{B} = \nabla\psi \times \nabla\theta - \nabla\psi_p \times \nabla\zeta = \nabla\psi \times \nabla\theta - \frac{1}{R}\nabla\psi_p \times \hat{\phi} + \nabla\psi_p \times \nabla\nu$$

with the corresponding unit vectors, so that

$$B_R = \mathbf{B} \cdot \mathbf{R} = -\frac{1}{R}\frac{\partial\psi_p}{\partial Z},$$
$$B_Z = \mathbf{B} \cdot \mathbf{Z} = \frac{1}{R}\frac{\partial\psi_p}{\partial R}.$$

Similarly, the toroidal component can be calculated similarly by taking the dot product of $\hat{\phi}$ with the covariant representation

$$\mathbf{B} = \frac{g}{R}\hat{\phi} - g\nabla\nu + I\nabla\theta + \delta\nabla\psi,$$

so that

$$B_\phi = \mathbf{B} \cdot \hat{\phi} = \frac{g}{R}.$$

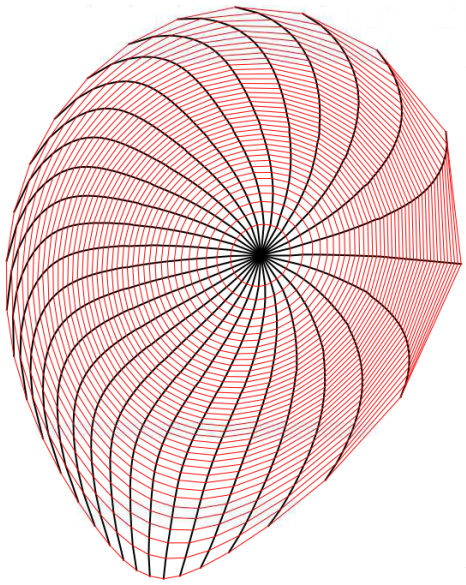

Figure 2.5 Boozer Coordinates for an AUG equilibrium, shot 33147, at t=1.0

We are now ready to reconstruct the Boozer coordinates. On one hand we have

$$\mathbf{B} \cdot \nabla\theta = \frac{1}{\mathcal{J}_p} = \frac{1}{q(\psi_p)\mathcal{J}},$$

where $\mathcal{J}_p = \left(\nabla\psi_p \cdot (\nabla\theta \times \nabla\phi)\right)^{-1}$ is the poloidal Jacobian. On the other, differentiation along the magnetic field line is given by

$$\mathbf{B} \cdot \nabla = B_p\partial_p + B_t\partial_t,$$

where ∂_t is the derivative along the toroidal direction and ∂_p the derivative along the poloidal direction. Applying the above operator to θ, we get

$$\mathbf{B} \cdot \nabla\theta = B_p\partial_{l_p}\theta,$$

or

$$\theta = \int \frac{1}{\mathcal{J}_p B_p} dl_p,$$

with the integration taking place along the poloidal cross section of the magnetic surface. In Boozer coordinates, the poloidal Jacobian has the form

$$\mathcal{J}_p = q\mathcal{J} = q\frac{h(\psi)}{B^2},$$

so that

$$\theta = \frac{1}{qh} \int \frac{B^2}{B_p} dl_p,$$

The flux function $h(\psi)$ is determined by requirement that the angle coordinate θ spans from 0 to 2π:

$$h = \frac{1}{2\pi} \frac{1}{q} \oint B^2 / B_p dl_p$$

thus, the toroidal current flux I can be calculated through

$$B^2 \mathcal{J} \; = \; (I + gq) / q \Rightarrow I \; = \; B^2 \mathcal{J} q - gq \; = \; h - gq$$

.

Finally, the function ν is given by the straight field line condition

$$\frac{\mathbf{B} \cdot \nabla \zeta}{\mathbf{B} \cdot \nabla \theta} = q,$$

After substitution, we get

$$\frac{\partial \nu}{\partial \theta} = \frac{gq\mathcal{J}}{R^2} - q,$$

which determines ν up to an added arbitrary flux function, which can be taken equal to zero. The Boozer coordinates for an equilibrium in the ASDEX Upgrade tokamak are depicted in fig. 2.5. The calculations where carried out using the GS solution calculated by the CLISTE code (Carthy, 1999).

Chapter 3

Heating of ions by high frequency electromagnetic waves in magnetized plasmas.

In fusion type plasmas, electrostatic waves, like the lower hybrid wave, cannot access the core of the plasma as easily as high harmonic fast waves or electron cyclotron waves; these are primarily electromagnetic waves. As was established in Chapter 1, single waves can exchange energy only with high energy ions. However, low energy particles may interact with the envelope formed by the interference of two such waves, provided that the frequency of the envelope is comparable to the gyrofrequency of the particles.

In this chapter, previous studies on heating of ions by two or more electrostatic waves that propagate directly across the confining magnetic field are extended to *electromagnetic waves*. The nonlinear wave-particle interaction is studied analytically using a two time-scale canonical perturbation theory. The theory reveals the effects of various parameters on the gain in energy by the ions – parameters such as the amplitudes and polarizations of the waves, the ratio of the wave frequencies to the cyclotron frequency, the difference in the frequency of the two waves, and the wave numbers associated with the waves.

3.1 Introduction

The interaction of electromagnetic waves with charged particles in magnetized plasmas manifests itself in a variety of environments, such as space and astrophysical plasmas, particle accelerators, and laboratory plasmas. Of particular interest are conditions in which net momentum or energy exchange takes place between the particles and the waves. In fusion plas-

mas, externally launched electromagnetic waves are used to heat the plasma and to drive plasma currents for enhanced confinement (Fisch, 1987, Kikuchi and Azumi, 2012). Conversely, in microwave sources the kinetic energy of energetic particles is transferred to waves in order to generate and amplify electromagnetic radiation (Chu, 2004).

The interaction of a single electrostatic wave with ions in a uniform magnetic field has been a paradigm for studying nonlinear wave-particle interactions (Fukuyama et al., 1977, Karney, 1978, Karney and Bers, 1977, Lichtenberg and Liebermann, 1983, Smith and Kaufman, 1975, Taylor and Laing, 1975). We analyzed the non resonant case of this interaction in Chapter 1. The wave incident on the ions was assumed to be of the lower hybrid type, a quasi – electrostatic mode that propagates almost perpendicularly to the magnetic field, whose wave frequency is typically a large multiplicand of the ion cyclotron frequency. The tree regimes of weak, medium and strong wave particle interaction apply on particles that satisfy the Cherenkov condition, i.e. particles with

$$v_{\perp} \gtrapprox v_{\text{ph}},$$

with v_{ph} being the phase velocity of the wave, so that there exist a lower energy threshold for efficient wave particle interaction to take place. For typical plasma parameters, this means that only the tail of a Maxwellian ion distribution function can be affected by a monochromatic non resonant lower hybrid wave. On the other hand, in case of resonance, i.e when the wave frequency is an integer multiple of the ion cyclotron frequency, a "stochastic web" is formed in the dynamical phase space of the ions and the energy threshold is significantly lower (Benisti et al., 1997). Ions within the stochastic web can gain energy for small wave amplitudes; however, the volume of phase space that is affected is limited, and the gain in energy occurs over very long times (Benisti et al., 1997).

The aforementioned picture changes dramatically when ions interact with two non resonant electrostatic waves whose frequencies differ by an integer multiple (≤ 3) of the ion cyclotron frequency, so that the beating envelope of the waves is in resonance with the unperturbed particle motion (Bénisti et al., 1998a,b, Ram et al., 1998, Spektor and Choueiri, 2004). The low energy ions, can interact with the beating envelope of the two waves and through this interaction may gain sufficient energy so as to cross the Cherenkov threshold. This interaction is nonlinear and, at least, of second order in the wave amplitudes. For electrostatic waves propagating obliquely to the magnetic field, similar energy exchange takes place provided that the wave numbers parallel to the magnetic field are equal for the two waves (Strozzi et al., 2003).

Although the frequency of the envelope of waves does not have to be in exact resonance with the ion cyclotron frequency, the acceptable tolerances are very small. In spite of the fact

that this remark has already been made in passing by other authors, (Bénisti et al., 1998a, Strozzi et al., 2003), we believe not enough emphasis has been given on how strict limitations this implies for realistic applications.

In previous studies, the stochhasticity threshold and the upper bound of the stochastic region for beating electrostatic waves with equal (Benisti et al., 1997, Bénisti et al., 1998a,b, Ram et al., 1998, Spektor and Choueiri, 2004) or almost equal (Jorns and Choueiri, 2013) wavenumbers were estimated through the Chirikov criterion. The important question of collective ion behaviour due to beating electrostatic waves was raised in (Jorns and Choueiri, 2011) and an attempt to tackle it was made by estimating ensemble averages of the energy exchange. Due to the non linear character of the beat wave interaction, third or higher order perturbation terms, which are challenging to calculate, are necessary for such an estimation. In order to circumvent this difficulty, the authors modified expressions for the single wave interaction, with the introduction of unknown pre-factors and scaling functions that they fit to numerical data (Jorns and Choueiri, 2011, 2013). Although mathematically convenient, these modifications do not have an clear physical meaning.

In this work we extend previous studies along two main directions. First, we consider beating *electromagnetic* waves. This enables us to examine the effect of the polarization on both single and collective ion dynamics, which can be significant. Second, we follow a novel approach for studying the evolution of the ion velocity distribution function through functional mapping equations. The effects of finite envelope phase velocity and finite deviation from resonance, effects that had not been given enough attention before, are thoroughly studied. Finally, we estimate the stochasticity threshold following a different –more satisfying in our opinion –approach, without applying the Chirikov criterion. Excellent agreement between numerical and analytical results is achieved, without the need of unknown prefactors that need to be fitted to numerical results (Jorns and Choueiri, 2013).

3.2 The single particle Hamiltonian

Let us consider an ion of mass m and charge q moving in a uniform magnetic field along the z–direction and two X waves propagating along the x-direction, each having an electrostatic component E_x and an electromagnetic component E_y. The frequencies of the two waves, ω_1 and ω_2, are assumed to be much larger than the gyrofrequency $\Omega = qB_0/m$. The beat frequency $\Delta\omega = \omega_1 - \omega_2$ is assumed to be equal or approximately equal to Ω. Consequently, there exists a second order resonance between the unperturbed motion and the envelope formed by the waves, leading to energy transfer from the waves to the ions. The time scale

separation due to the fact that the carrier frequencies are much larger than any other frequency involved, i.e. $\omega_i \gg \Omega$ and $\omega_i \gg \Delta\omega$ will be a central point of our analysis.

The ellipticity of the wave polarization α is given by

$$\frac{E_x}{E_y} \equiv \frac{i}{\alpha}, \tag{3.1}$$

and is assumed to be the same for both waves. This assumption requires that

$$\frac{\partial \alpha}{\partial \omega}\Delta\omega \ll \alpha.$$

This condition is mode dependent and should be checked a posteriori.

For convenience, let us normalize the physical quantities with respect to characteristic scales, just as we did in sec. 1.1 :

- Time is normalized to Ω^{-1}
- lengths to $k_0^{-1} = \left(\frac{k_1 + k_2}{2}\right)^{-1}$, k_i being the wave vectors of each wave,
- velocities to $\frac{\Omega}{k_0}$,
- momenta to $\frac{m\Omega}{k_0}$,
- and energies to $\frac{m\Omega^2}{k_0^2}$.

Adopting the Wheyl gauge $\Phi = 0$, the electromagnetic field is described solely by the vector potential

$$\mathbf{A} = \mathbf{A}_0 + \mathbf{A}_1,$$

where

$$\mathbf{A}_0 = \hat{\mathbf{y}} B_0 x \tag{3.2}$$

stands for the uniform magnetostatic field along the z axis and $\mathbf{A}_1$ for the electromagnetic waves. We take $\mathbf{A}_1$ to correspond to two elliptically polarized electromagnetic waves propagating perpendicularly to the magnetic field, along the $\hat{\mathbf{x}}$ axis. The wave fields have an electrostatic component $\mathbf{A}_1|_{ES}$ along $\hat{\mathbf{x}}$ an electromangetic component $\mathbf{A}_1|_{EM}$ perpendicular to $\mathbf{A}_1|_{ES}$. The electrostatic component is given by

$$\mathbf{A}_1|_{ES} = -\frac{E_0}{2}\left[\frac{1}{\omega_1}\exp\left[i\left(k_1 x - \omega_1 t\right)\right] + \frac{1}{\omega_2}\exp\left[i\left(k_2 x - \omega_2 t\right)\right]\right]\hat{\mathbf{x}} \; + \; \text{c.c.} \tag{3.3}$$

where c.c. denotes the complex conjugate of the preceding expression. The ellipticity of the polarization α determines the electromagnetic component of the waves:

$$\mathbf{A}_1|_{EM} = -i\alpha\, \hat{\mathbf{z}} \times \mathbf{A}_1|_{ES}\,, \tag{3.4}$$

or

$$\mathbf{A}_1|_{EM} = i\alpha \frac{E_0}{2}\left[\frac{1}{\omega_1}\exp\left[i\left(k_1 x - \omega_1 t\right)\right] + \frac{1}{\omega_2}\exp\left[i\left(k_2 x - \omega_2 t\right)\right]\right]\hat{\mathbf{y}} \;+\; \text{c.c.} \tag{3.5}$$

The Hamiltonian of the particle in the presence of the vector potential $\mathbf{A}$ is

$$H \;=\; \frac{1}{2m}\left(\mathbf{p} - q\mathbf{A}_0 - q\mathbf{A}_1\right)^2 \tag{3.6}$$

For $\mathbf{A}_1 = 0$, this is equal to the Hamiltonian for the motion in this uniform magnetic field:

$$H_0 \;=\; \frac{1}{2m}\left[p_x^2 + \left(p_y - qB_0 x\right)^2\right], \tag{3.7}$$

or, in normalized units

$$H_0 \;=\; \frac{1}{2}\left[p_x^2 + \left[p_y - x\right]^2\right], \tag{3.8}$$

We will refer to H_0 as the unperturbed Hamiltonian and the corresponding motion of the ion as the unperturbed motion. The full Hamiltonian is

$$\begin{aligned} H =& \frac{1}{2}\left[p_x + \epsilon\left(\frac{1}{\nu_1}\cos(\phi_1) + \frac{1}{\nu_2}\cos(\phi_2)\right)\right]^2 \\ &+ \frac{1}{2}\left[p_y - x + \alpha\epsilon\left(\frac{1}{\nu_1}\sin(\phi_1) + \frac{1}{\nu_2}\sin(\phi_2)\right)\right]^2, \end{aligned} \tag{3.9}$$

where

$$\kappa_i = k_i/k_0$$

are the normalized wavenumbers,

$$\nu_i = \omega_i/\Omega$$

are the normalized wave frequencies,

$$\phi_i \;=\; \kappa_i p_g + \kappa_i \rho \sin\psi - \nu_i t$$

are the phases of the waves at the partilce location, with

$$\rho = \sqrt{2\mu}$$

the Larmor radius of the ion and

$$\epsilon = k_0 q E_0/(m\Omega^2)$$

the effective perturbation strength, which will later serve as an ordering parameter.

Before applying any canonical perturbation technique to analyze the particle dynamics, we need to express the Hamiltonian in the Action Angle variables of the unperturbed gyromotion, i.e. the guiding centre variables $[(\psi,\mu),(y_g,p_g)]$,using the generating function of eq. 1.1

$$G_c\left(x,y,p_g,\psi\right) \;=\; xp_g + \frac{1}{2}\left(x-p_g\right)^2\cot\psi. \tag{3.10}$$

The old phase space variables are related to the guiding centre variables as follows

$$\begin{aligned} p_x &= \sqrt{2\mu}\cos\psi \\ x &= p_g + \sqrt{2\mu}\sin\psi \\ y &= y_g + \sqrt{2\mu}\sin\psi \\ p_y &= p_g, \end{aligned}$$

where the Action of the unperturbed motion μ is the magnetic moment of the ion.

In guiding center coordinates, the single particle Hamiltonian $H_c = h_0+h_1+h_2$, ordered in powers of ϵ, takes the following form:

$$h_0 = \mu, \tag{3.11}$$

$$h_1 = \epsilon\rho\cos\psi\left(\frac{1}{\nu_1}\cos\phi_1+\frac{1}{\nu_2}\cos\phi_2\right) - \alpha\,\epsilon\rho\sin\psi\left(\frac{1}{\nu_1}\sin\phi_1+\frac{1}{\nu_2}\sin\phi_2\right), \tag{3.12}$$

$$h_2 = \frac{1}{2}\epsilon^2\left(\frac{1}{\nu_1}\cos\phi_1+\frac{1}{\nu_2}\cos\phi_2\right)^2 + \frac{1}{2}\alpha^2\epsilon^2\left(\frac{1}{\nu_1}\sin\phi_1+\frac{1}{\nu_2}\sin\phi_2\right)^2, \tag{3.13}$$

Note that the canonical position y_g, the y coordinate of the gyrocenter, does not appear in the Hamiltonian. Therefore, its conjugate momentum p_g is a constant of the motion. The only effect p_g has on the dynamics is to add a constant phase shift θ to the phases of the waves ϕ_i as seen by the particle. From now on, in order to simplify the notation, we replace p_g by the phase shift θ.

For the purpose of perturbation analysis, it is useful to express the perturbations h_1 and h_2 as Fourier series in ψ. For the first order perturbation we have

$$\begin{aligned} h_1 =& \epsilon\, e^{i(\kappa_1\theta-\nu_1 t)}\frac{\rho}{4\nu_1}\sum_{n=-\infty}^{\infty}\left[(1+\alpha)\,\mathrm{J}_{n-1}\left(\kappa_1\rho\right)+(1-\alpha)\,\mathrm{J}_{n+1}\left(\kappa_1\rho\right)\right]e^{in\psi} \\ &+\epsilon\, e^{i(\kappa_2\theta-\nu_2 t)}\frac{\rho}{4\nu_2}\sum_{n=-\infty}^{\infty}\left[(1+\alpha)\,\mathrm{J}_{n-1}\left(\kappa_2\rho\right)+(1-\alpha)\,\mathrm{J}_{n+1}\left(\kappa_2\rho\right)\right]e^{in\psi} \\ &+\text{c.c.}, \end{aligned} \tag{3.14}$$

and for the second order perturbation

$$\begin{aligned} h_2 =& \frac{\epsilon^2\left(1-\alpha^2\right)}{8\nu_1^2}e^{i(2\kappa_1\theta-2\nu_1 t)}\sum_{n=-\infty}^{\infty}\mathrm{J}_n\left(2\kappa_1\rho\right)e^{in\psi} \\ &+\frac{\epsilon^2\left(1-\alpha^2\right)}{8\nu_2^2}e^{i(2\kappa_2\theta-2\nu_2 t)}\sum_{n=-\infty}^{\infty}\mathrm{J}_n\left(2\kappa_2\rho\right)e^{in\psi} \\ &+\frac{\epsilon^2\left(1+\alpha^2\right)}{4\nu_1\nu_2}e^{i(\Delta\kappa\theta-\Delta\nu t)}\sum_{n=-\infty}^{\infty}\mathrm{J}_n\left(\Delta\kappa\rho\right)e^{in\psi} \\ &+\frac{\epsilon^2\left(1-\alpha^2\right)}{4\nu_1\nu_2}e^{i(2\kappa_0\theta-2\nu t)}\sum_{n=-\infty}^{\infty}\mathrm{J}_n\left(2\kappa_0\rho\right)e^{in\psi} \\ &+\text{c.c.}, \end{aligned} \tag{3.15}$$

where J_n is the Bessel function of the first kind of rank n, ν is the carrier frequency $(\nu_1+\nu_2)/2$, $\Delta\nu=\nu_1-\nu_2$, $\Delta\kappa=\kappa_1-\kappa_2$, and $\kappa_0=\left(\kappa_1+\kappa_2\right)/2$.

3.3 Oscillation Center Dynamics

Two distinct time scales can be immediately identified in the beat envelope interaction. The fast wave frequencies on one hand and the slow gyrofrequency, which is comparable to the slow beat envelope frequency on the other. The simultaneous presence of these timescales implies that, for small enough perturbation amplitudes, it should be meaningful to separate the perturbed motion in a similar manner. Conceptually, we expect the particle to perform a fast oscillating motion, due to the linear interaction with each wave independently, superimposed on a much slower drift of some *oscillation center*, due to the slow nonlinear interaction with the beat envelope. This is confirmed by the Poincare plot of fig. 3.1, of which more later.

Instead of rushing to give a precise definition of the fast and slow motions and then struggle to find the appropriate equations to describe them, we can delegate both actions to

our perturbation scheme. To accomplish this, we seek to approximate a canonical transform operator T which maps the original phase space to a new phase space where the new Hamiltonian K includes only slowly varying terms. Following the steps we took in Chapter 1 we will apply Deprit's perturbation method (Cary, 1981, Deprit, 1969, Lichtenberg and Lieberman, 1983) to determine T up to second order in ϵ. All terms absorbed in T are attributed to the fast motion. The oscillation center motion is *defined* as motion dictated by the new Hamiltonian K, which we will appropriately call *oscillation center Hamiltonian*.

3.3.1 Approximating the second order Invariant

The perturbation scheme applied here differs from the one we used in Chapter 1 in two aspects. First, the resonances with the envelope create extra secular terms, which must be taken into account. Second, in keeping with the spirit of a similar analysis on the ponderomotive force from the non resonant envelope of an electromagnetic wavepacket (Cary and Kaufman, 1981), we chose to integrate all Liouville equations that arise on a semi–infinite, rather than an infinite domain. This choice is dictated by our resolution to look for a perturbation scheme that explicitly separates the timescales. Explicit time dependence in the constructed canonical transform will account for the fast linear oscillations around the oscillation center due to each of the waves independently.

Let us begin by considering some yet to be defined operator T which maps a phase space point z in the original phase space to a point Z in a new phase space

$$Z \;=\; Tz. \tag{3.16}$$

T is determined by a generating function $w = w_0 + w_1 + w_2$, where w_i is of order ϵ^i ($i = 0, 1, 2$). The leading term w_0 is the generator of the identity transformation. Since w depends on time, the evolution of Z is governed by a new Hamiltonian K which, to second order in ϵ, is $K = K_0 + K_1 + K_2$ with

$$K_0 = h_0 \tag{3.17}$$

$$K_1 = h_1 + \frac{\partial w_1}{\partial t} + \{w_1, h_0\} \tag{3.18}$$

$$K_2 = h_2 + \frac{1}{2}\left[\frac{\partial w_2}{\partial t} + \{w_2, h_0\}\right] + \frac{1}{2}\{w_1, h_1 + K_1\}. \tag{3.19}$$

Again, we try to choose w_1 and w_2 so that K is as simple as possible; Ideally we would like $K_1 = K_2 = 0$.

The first order generating function w_1 satisfies the inhomogeneous Liouville equation

$$\frac{\partial}{\partial t} w_1 + \{w_1, h_0\} \;=\; K_1 - h_1, \tag{3.20}$$

with solution

$$w_1 \;=\; \int_{t_0}^{t} d\tau \; S_0^{-1}\left(t,\tau\right) g(\tau), \tag{3.21}$$

where S_0 is the evolution operator for the unperturbed Hamiltonian, and $g = K_1 - h_1$ is the right hand side of Eq. (3.20). In other words, we integrate g along the unperturbed orbits given by h_0. Since h_0 is time independent and $S_0(t,\tau)$ maps $\psi \to \psi + (t-\tau)$, the evolution operator can be written as $S_0^{-1}\left(t,\tau\right) = S_0\left(\tau - t\right)$. We choose $K_1 = 0$ and, assuming that the wave fields are turned on adiabatically, set $t_0 = -\infty$, so that

$$w_1 \;=\; -\int_{-\infty}^{0} d\tau \; S_0\left(\tau\right) h_1\left(\tau + t\right), \tag{3.22}$$

or

$$\begin{aligned} w_1 \;= & \, i\epsilon \; e^{i(\kappa_1\theta - \nu_1 t)} \frac{\rho}{4\nu_1} \sum_{n=-\infty}^{\infty} \frac{\left(1+\alpha\right) \mathrm{J}_{n-1}\left(\kappa_1\rho\right) + \left(1-\alpha\right) \mathrm{J}_{n+1}\left(\kappa_1\rho\right)}{n - \nu_1} e^{in\psi} \\ & + i\epsilon \; e^{i(\kappa_2\theta - \nu_2 t)} \frac{\rho}{4\nu_2} \sum_{n=-\infty}^{\infty} \frac{\left(1+\alpha\right) \mathrm{J}_{n-1}\left(\kappa_2\rho\right) + \left(1-\alpha\right) \mathrm{J}_{n+1}\left(\kappa_2\rho\right)}{n - \nu_2} e^{in\psi} \\ & + \text{c.c.} \end{aligned} \tag{3.23}$$

The denominators appearing in the terms above are not singular, since we have assumed that ν_i's are not integers.

The Liouville equation for w_2 is

$$\frac{\partial}{\partial t} w_2 + \{w_2, h_0\} \;=\; 2(K_2 - h_2) - \{w_1, h_1\}. \tag{3.24}$$

The Poisson bracket between w_1 and h_1 contains terms with frequencies equal to the beating frequency of the two waves. These secular terms remain constant along the unperturbed orbits and their integral would diverge, unless they are absorbed into K_2, which we must choose in such way that it cancels them out. Thus,

$$K_2 = \left\langle h_2 + \frac{1}{2}\left\{w_1, h_1\right\} \right\rangle_0, \tag{3.25}$$

where $\langle\rangle_0$ denotes averaging along the unperturbed orbits. Then Eq. (3.24) becomes

$$\frac{\partial}{\partial t}w_2 + \{w_2, h_0\} \;=\; \langle -2h_2 - \{w_1, h_1\}\rangle_1 \,, \tag{3.26}$$

where $\langle ...\rangle_1$ denotes the oscillating part of the enclosed expression. We solve Eq. (3.26) using the same procedure used for solving Eq. (3.20).

The new Hamiltonian K up to second order in ϵ is

$$K \;=\; \mu + \epsilon^2 K_2\left(\psi, \mu\right), \tag{3.27}$$

where K_2 has the form

$$K_2 \;=\; K_{2,0}\left(\mu\right) + K_{2,1}\left(\mu\right)\exp\left[i\left(\psi - t\right)\right] + \text{c.c.}. \tag{3.28}$$

The expressions for $K_{2,1}$ and $K_{2,0}$ are lengthy and do not elucidate any physics. The only practical way of calculating them is by means of a symbolic computation package. No insight could be possibly gained by viewing them in print form –the author never attempted to do so –hence, they are not included in this thesis. We can eliminate the time dependence by setting $\bar{\psi} = \psi - t$, obtaining:

$$\bar{K} = \epsilon^2\left[\, K_{2,0}\left(\mu\right) + K_{2,1}\left(\mu\right)\exp\left[i\left(\bar{\psi}\right)\right]\right] + \text{c.c.}. \tag{3.29}$$

$\bar{K}$ is independent of time and, to order ϵ^2, a constant of the motion.

The perturbation scheme yields a separation of timescales into fast and slow occurs through T and $\bar{K}$, respectively. The canonical transform T applied to $\bar{K}$,

$$J \equiv T\bar{K}, \tag{3.30}$$

provides a fuzzy quasi constant of motion in the original phase space variables. By construction, T is a time dependent near identity canonical transformation to the new phase space variables, which accounts for the fast motion due to the off–resonant carrier frequency of the waves. Consequently, the old and the new canonical variables can be said to oscillate around one another. Since the time evolution of the new phase space, governed by the Hamiltonian $\bar{K}$, is by construction slow, the old phase space variables z can be thought as performing fast small amplitude oscillations around the slow phase space variables Z. The new phase space is the oscillation centre phase space and the Hamiltonian $\bar{K}$ the oscillation centre Hamiltonian that describes the averaged slow evolution of the oscillation centre of an ion.

For small enough perturbation amplitudes, K provides an accurate description of the overall dynamics of ions. This applies for moderate amplitudes as well, provided that the particle does not cross the Cherenkov threshold. Since K is a function of μ and $\bar{\psi}$, we can plot contours of constant K in the two-dimensional $\mu - \bar{\psi}$ phase space. These curves represent the orbits of the oscillation centers of the ions. They interpolate smoothly the traces left by the complete orbits on the Poincare surface $\mu - \bar{\psi}$ for $t = 2n\pi$. Figure 3.1 shows the contours of constant K superimposed on the Poincaré surface-of-section obtained from numerical integration of the equations of motion. The surface-of-section points almost lie along the contour lines; the difference is due to small oscillations of the ions around their oscillation centers.

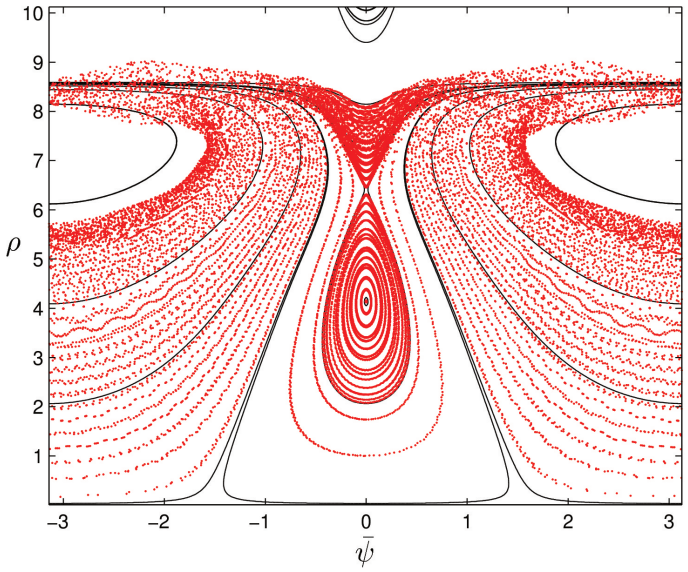

Figure 3.1 Contour plot (solid lines) for $\epsilon = 0.3$, $\alpha = 2$, $\nu = 10.123$ and $\delta\kappa = 0.0436$ and the corresponding Poincare plot (dots). Particles with low initial energy follow the oscillation center curves and are coherently energized up to $\rho \approx 8.5$, where a separatrix is located. There are also particles trapped around the elliptical points. The amplitude of the fast oscillations becomes large near the separatrix, giving the false impression of chaotic motion.

The dynamics depicted in Fig. 3.1 is representative of a class of interactions with similar patterns, which occur for a wide range of wave parameters and will be referred to as favourable interaction. When favourable interaction takes place, practically all of the low energy phase space is significantly affected by the beat wave. A common characteristic is the appearance of one or more elliptical, around which form islands that extend from $\rho \approx 0$ up to a separatrix, which lies near $\rho \approx \nu$. Low energy particles can thus be coherently energized to energies close to the Cerenkov energy threshold. If, as is assumed in similar

studies (Jorns and Choueiri, 2011), the bulk of the initial distribution function of the ions is located at the phase space area with small values of ρ, phase mixing effects will lead to a net energy exchange and the distribution function will spread significantly across phase space. Although the Poincare plot in Fig. 3.1 appears fuzzy, the motion of the particles is coherent. The apparent fuzziness in the orbits, which is more pronounced near the separatrix, is due to the fast oscillations around the oscillation centre. If the amplitude of the perturbation is large enough, ions which happen to have been gained energy near the Cerenkov energy threshold, may cross the separatrix and be stochastically energized to even higher energies. The onset of chaotic motion of ions will be discussed in section 3.5 below.

We shall refer to those cases where only the high energy tail of the distribution function is affected as unfavourable cases(see Fig. 3.3a)). In such cases the interaction is qualitatively similar to the single wave interaction studied in Chapter 1.

3.3.2 The effect of the envelope phase velocity on the energy exchange

The envelope phase velocity $\delta\nu/\delta\kappa$ plays a significant role in the qualitative behaviour of the ion dynamics, as can be seen in Fig. 3.3. In general, when the envelope phase velocity is in the opposite direction of the wave phase velocity the interaction is unfavourable; a velocity threshold for ion energisation is introduced as in the case of ion interaction with a single wave and most of the low energy phase space is only slightly affected by the presence of waves, as in Fig. 3.3 a). On the other hand, a large positive envelope phase velocity leads to strong energization of the low energy ions, but there are still particles that are trapped around an elliptic point that appears in the middle of the low energy phase space (Fig. 3.3 b)). This is similar to the phase space structure that emerges for infinite envelope phase velocity ($\Delta k = 0$) that has been regarded as representative of all beat wave interactions in previous studies (Jorns and Choueiri, 2011, Spektor and Choueiri, 2004). The strongest energy exchange takes place when the envelope phase velocity is approximately equal to the wave phase velocity (Fig. 3.3 c)); the envelope is propagating at the same speed as the carrier wave and there are no trapped particles. Similar behaviour has been observed for beating electrostatic waves (Ram et al., 1998) as well as localized electrostatic wave packets (Kominis et al., 2012).

Envelope phase velocity that is opposite to carrier phase velocity is not unrealistic. For example, *lower hybrid beating waves* with fixed $k_{\|}$ fall under this category, and thus cannot transfer significant energy to low energy ions. This is because the envelope phase velocity

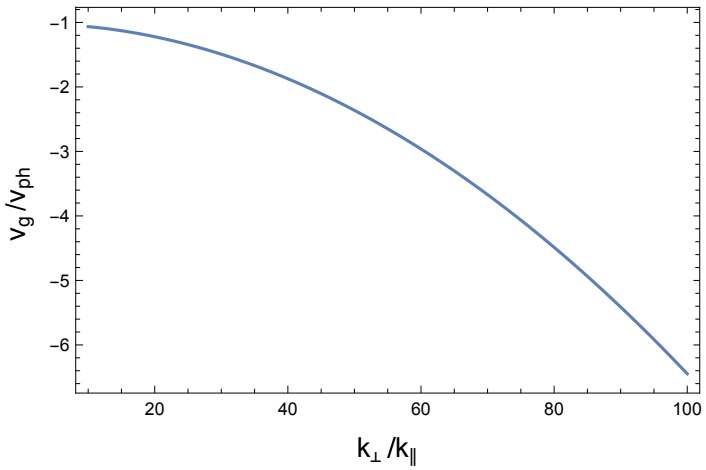

Figure 3.2 The relation between v_g and v_{ph}, when $\Delta k_{\parallel} = 0$.

is determined by the cold plasma dispersion relation, which, in the lower hybrid range, is

$$\omega \approx \omega_{\text{LH}} \left(1 + \frac{k_{\parallel}^2}{k^2} \frac{m_i}{m_e} \right) \tag{3.31}$$

were

$$\omega_{\text{LH}}^2 \approx \frac{\omega_{\text{pi}}^2}{1 + \omega_{\text{pe}}^2 / \Omega_{\text{ce}}^2} \tag{3.32}$$

is the lower hybrid frequency, when $\omega_{\text{pi}} \gg \Omega_{\text{ci}}$.

According to eq. 3.31, the wave vector is indeed almost perpendicular to the magnetic field, while the group velocity is almost parallel to the magnetic field (Brambilla, 1998). It is not unusual for $k_{\parallel}$ to be fixed by some external condition, e.g. an antenna (Porkolab et al., 2012), so that $\Delta k_{\parallel} = 0$. Then

$$\Delta k_{\perp} = \left(\frac{\partial \omega}{\partial k_{\perp}} \right)^{-1} \Delta \omega, \tag{3.33}$$

and the perpendicular envelope group velocity $v_g \equiv \Delta k_{\perp} / \Delta \omega$ is related to the perpendicular phase velocity v_{ph} via

$$v_g \approx -v_{\text{ph}} \left(\frac{k_{\perp}^2}{k_{\parallel}^2} \frac{m_e}{m_i} + 1 \right), \tag{3.34}$$

so that the envelope phase velocity is comparable in magnitude and opposite in sing with the carrier phase frequency fig. 3.2. This falls under the domain of unfavourable energization, depicted in Fig. 3.3 a).

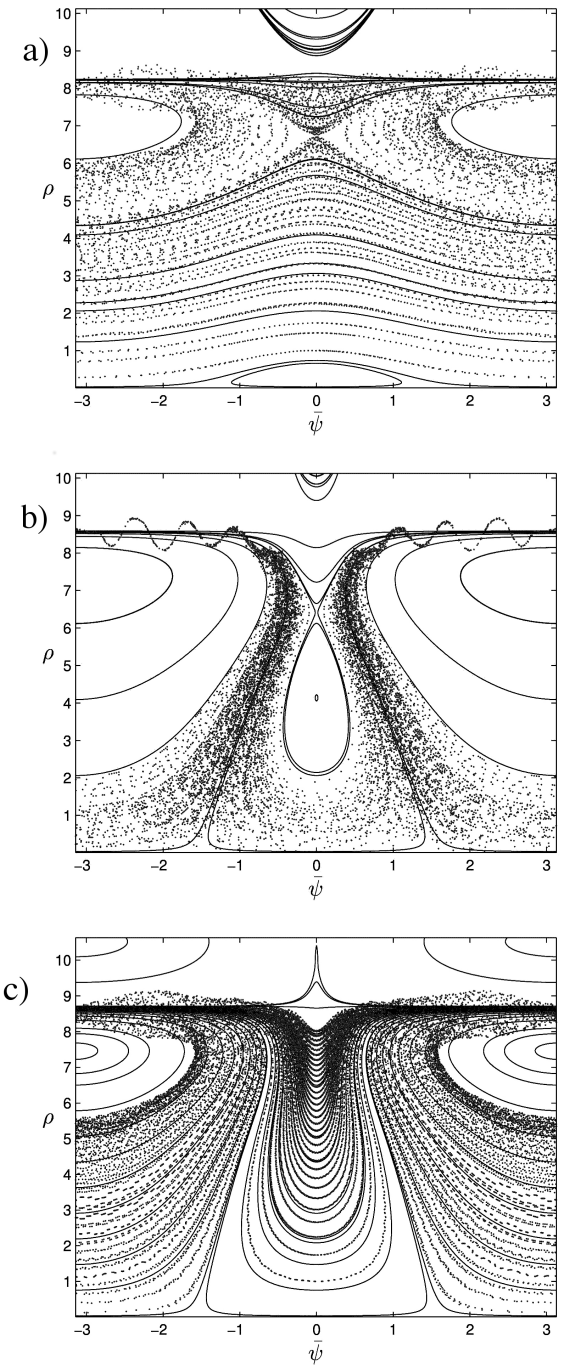

Figure 3.3 The effect of the envelope phase velocity on the topology of the phase space. Contour plots (solid lines) and Poincare surfaces (dots). a) the envelope phase velocity is in opposite direction to the phase velocity ($\epsilon = 0.3, \alpha = 2, \nu = 10.123$ and $\delta\kappa = -0.0436$). The low energy particles cannot exchange energy with the waves. b)the envelope phase velocity is 2.25 times the phase velocity ($\epsilon = 0.3, \alpha = 2, \nu = 10.123$ and $\delta\kappa = 0.0436$).The interaction is strong but there are still particles trapped around the elliptic point. c) the envelope phase velocity is almost equal to the phase velocity ($\epsilon = 0.3, \alpha = 2, \nu = 10.123$ and $\delta\kappa = 0.0861$). More particle orbits get squeezed near the separatrix.

3.3.3 Detuning Tolerance

Suppose there is a mismatch δ between the beat frequency and the gyrofrequency, so that

$$\delta\nu = 1 + \delta.$$

Then, the new Hamiltonian K takes on the form[1]

$$K \;=\; \mu + \epsilon^2 \left[K_{2,0}\left(\mu,\delta\right) + K_{2,1}\left(\mu,\delta\right)\exp\left[i\left(\psi - (1+\delta)t\right)\right]\right] + \text{c.c.}. \tag{3.35}$$

If we now eliminate the time dependence by setting $\bar{\psi} = (1+\delta)t$, we get

$$\bar{K} = -\delta\mu + \epsilon^2 \left[\; K_{2,0}\left(\mu,\delta\right) + K_{2,1}\left(\mu,\delta\right)\exp\left[i\left(\bar{\psi}\right)\right]\right] + \text{c.c.} \tag{3.36}$$

For large enough values of δ, the term $-\delta\mu$ dominates and μ is approximately a constant of motion. In this context, we could have made the choice $K_2 = 0$ in the first place, without violating the perturbation ordering.

For small values of δ, where the interaction is expected to be significant, we have

$$K_{2,i}\big|_{\delta} \sim K_{2,i}\big|_{\delta=0}.$$

The most prominent difference with exact resonance is the appearance of the leading term $-\delta\mu$. Since this term is a function of μ and independent of $\bar{\psi}$, it eventually dominates for large enough values of μ, i.e. for large enough energies. Given that, K_2 is a bounded function, while $\delta\mu = \delta\rho^2/2$ is not, the detuning restricts the phase space region over which islands can appear. An interaction that is favourable, when the envelope is in exact resonance with the unperturbed particle motion easily be rendered unfavourable by introducing a small detuning, if the detuning term dominates for energies smaller or equal to the Cerenkov energy threshold.

As a consequence, the maximum detuning tolerance scales as

$$\delta_{\text{tol}} \sim \nu^{-2}.$$

Obviously, the scaling constant is a function of the beat phase velocity and the ellipticity of the wave polarization α, but rigorously calculating it would be a formidable task.

[1]For $\delta = 0$, secular terms appear on the right hand side of eq. 3.26, whose integrals along the unperturbed orbits diverge. These terms need to be cancelled out by K_2. For $\delta \neq 0$, these terms are no longer constant along the unperturbed orbits, but they still need to be cancelled out by K_2. This is because their integrals,

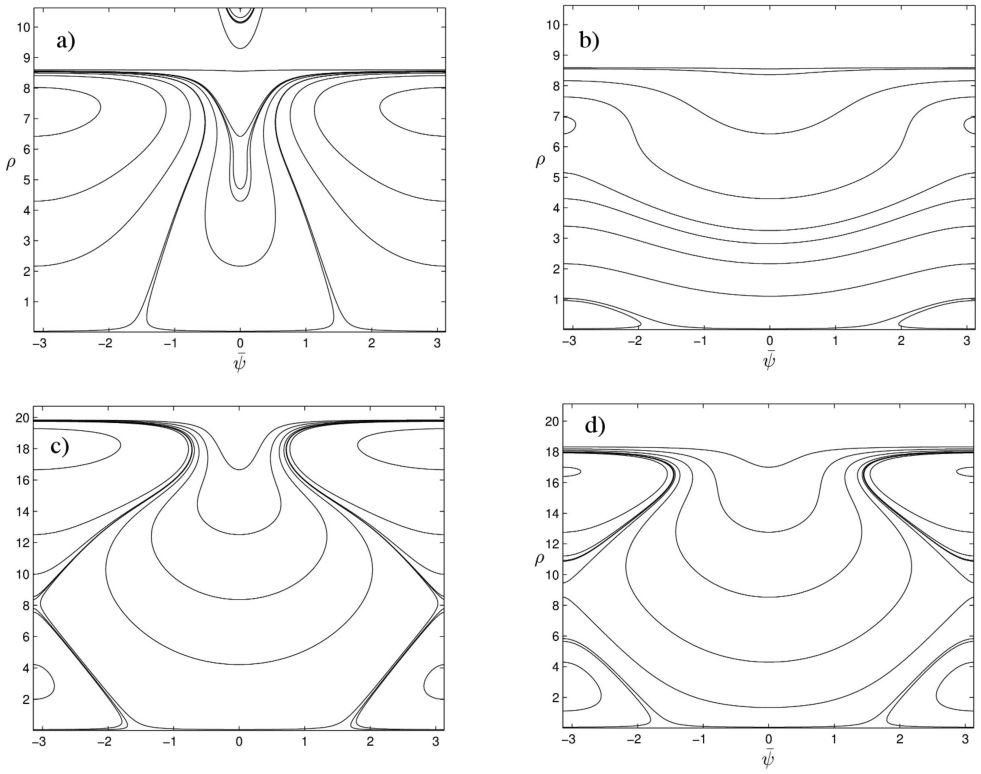

Figure 3.4 The effect of the detuning on the topology of the phase space. Contour plots for $\epsilon = 0.3$, $\alpha = 2, \delta\kappa = 0.0436$ and different values of the carrier frequency and the detuning. a) For $\nu = 10.123$, and $\delta = 8 \cdot 10^{-6}$ the detuning has little or no effect. b) When the detuning is increased to $\delta = 3 \cdot 10^{-4}$, the energization of the low energy particles is destroyed. Similar results are obtained by increasing the carrier frequency: c) $\delta = 8 \cdot 10^{-6}$ and $\nu = 19.723$ some of the low energy particles are trapped while others can still access the $\rho \approx \nu$ separatrix. d) A small increase in carrier frequency $\nu = 20.123$ leads to the appearance of an extra separatrix, that prevents the energization of the low energy particles.

The contour plots depicted in Fig. 3.4 are indicative of the effect of detuning on the topology of phase space. Cases a) and b) demonstrate interaction destruction by means of dominance of the leading detuning term. For $\nu \approx 10$, the detuning tolerance is empirically estimated to be $\delta_{\text{tol}} \sim 10^{-4}$. When δ exceeds this value, the interaction becomes unfavourable.

Based on the scaling law, the detuning tolerance when the carrier frequency doubles should be approximately equal to $2.5 \cdot 10^{-5}$. However, the scaling law overestimates the detuning tolerance, since dominance of the leading term at the Cerenkov level is not the only way the detuning can destroy the wave envelope interaction. This is also achieved though the structural dependence of K_2 on the detuning δ, as demonstrated in fig. (3.4c) and

although finite, are proportional to δ^{-1}. Including them in w_2, for small values of δ, would imply violating the perturbation ordering.

fig. (3.4d), for which $\nu \approx 20$ and $\delta = 8 \cdot 10^{-6}$, safely within the predicted tolerance limits. For $\nu = 19.723$ (Fig. (3.4c)) ions with very small initial energies can still be energized up to $\rho \approx \nu$. But, for $\nu = 20.123$, as shown in Fig. (3.4d), the energy gain by the ions is quite limited as an extra separatrix appears in the low energy domain of phase space.

To get a feeling of the effect of these tolerances for realistic problems, we should compare δ_{tol} with the detuning experienced in a single gyration, due to the slow gyrocenter motion though areas of varying magnetic field amplitude inside a tokamak. The total detuning experienced over a bounce period is

$$\delta_{\text{b}} \sim \left.\frac{\Delta B}{B}\right|_{\text{bounce}} \sim \frac{r}{R}, \tag{3.37}$$

where r is the minor radius and R the major radius of the tokamak. The total detuning experienced over a single gyration is therefore

$$\delta_{\text{c}} \sim \frac{\omega_b}{\Omega_c}\delta_{\text{b}} \tag{3.38}$$

and, in order for the assumed time scale separation to hold, it must be much smaller than the detuning tolerance, i.e. it is required that

$$\delta_{\text{c}} \ll \delta_{\text{tol}}$$

However, for typical tokamak plasmas (see tab. 1.1) we have

$$\frac{\omega_b}{\Omega_c} \sim 10^{-3}$$

and the aspect ratio is typically of the order

$$\frac{r}{R} \sim 10^{-1},$$

so that

$$\delta_{\text{c}} \sim 10^{-4} \approx \delta_{\text{tol}}.$$

It follows that the detuning experienced over a single period is typically comparable to – or even larger than – the typical detuning tolerance for the beating interaction to be effective. Most particles in a tokamak will quickly drift away from resonance before they can interact with the beat envelope.

3.4 Distribution function evolution

So far we have used the oscillation center Hamiltonian K to extract information about the qualitative features of the beat envelope interaction and in particular whether the interaction favourable or not. In this section we calculate the time evolution of the ion distribution function under the influence of the beat waves.

Let us begin by considering a generic Hamiltonian H, whose exact evolution operator cannot be easily calculated. Suppose additionally that it is possible to construct an approximate canonical transformation $T\left(t,t_0\right)$ to a new phase space $Z=T\,z$, which is governed by the simpler Hamiltonian K, whose related evolution operator S_K is easy to calculate. The distribution function g of the new phase space is related to the distribution function f of the old phase space by

$$f\left(z,t\right)\;=\;g\left(Z,t\right)\;=\;T\left(t,t_0\right)\;g\left(z,t\right) \tag{3.39}$$

The time evolution of g is given by

$$g(z,t)\;=\;S_K^{-1}(t,t_0)\,g(z,t_0). \tag{3.40}$$

Therefore,

$$f\left(z,t\right)\;=\;T\left(t,t_0\right)\;S_K^{-1}\left(t,t_0\right)\;T^{-1}\left(t_0,t_0\right)\;f\left(z,t_0\right). \tag{3.41}$$

For our purposes the formula above is not very useful as it is. Even though K is simpler than H, it is still much too complicated for us to determine S_K in closed form. We can bypass this difficulty by integrating on a finite time domain of length Δt (Kominis et al., 2010). Then, for small enough Δt, the integrals do not diverge and no terms need to be absorbed by K. We can now choose $K\;=\;h_0$ and $S_K\;=\;S_0$. The canonical transform T is accurate to the same order as Δt. This means that, in general, the evolution of the distribution function needs to be calculated iteratively,

$$f\left(z,2\Delta t\right)\;=\;T\left(2\Delta t,\Delta t\right)\;S_K^{-1}\left(2\Delta t,\Delta t\right)\;T\left(\Delta t,0\right)\;S_K^{-1}\left(\Delta t,0\right)f\left(z,0\right), \tag{3.42}$$

where we have assumed that $T\left(t,t\right)$ is the identity operator. In principle, this is equivalent to

$$f\left(z,2\Delta t\right)\;=\;T\left(2\Delta t,0\right)\;S_K^{-1}\left(2\Delta t,0\right)\;f\left(z,0\right), \tag{3.43}$$

but not quite so, since T is only evaluated approximately. Moreover, if $2\Delta t$ is outside the accuracy limits, the second form fails to give any correct result. However, one can simplify eq. 3.42, provided that the following assumptions hold: (1) K is time independent. Therefore, $S_K^{-1}\left(t+\Delta t,t\right)\;=\;S_K(-\Delta t)$. (2) The nonsecular terms of the generator of

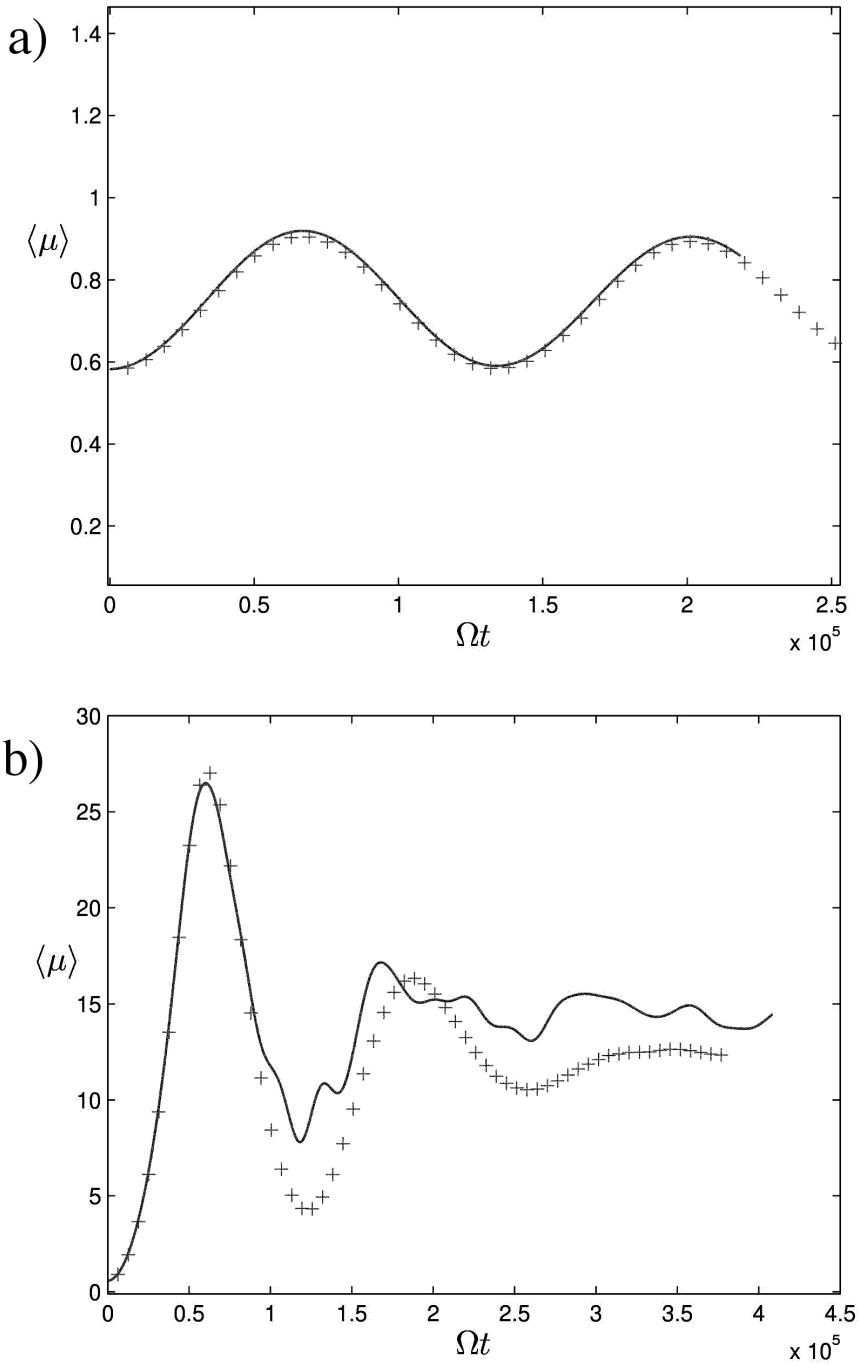

Figure 3.5 Mapping (solid line) and simulation (crosses) of the average energy evolution for one unfavourable and one favourable case corresponding to the parameters of Fig. 3.3 a) and b). a) Unfavourable energization. There is a small oscillation in the average energy due to the elliptical point in the low energy domain of the phase space. b) The energy peaks and then relaxes at a constant value due to phase mixing.

T commute with the secular ones up to the same order in which T is calculated. Then $T \approx T_{\text{nonsec}}\, T_{\text{sec}} \approx T_{\text{sec}}\, T_{\text{nonsec}}$. In this case, and if both Eq. 3.42 and Eq. 3.43 hold, we have:

$$T\left(2\Delta t, \Delta t\right)\; S_K\left(-\Delta t\right)\; T\left(\Delta t, 0\right) \;=\; T\left(2\Delta t, 0\right)\; S_K\left(-\Delta t\right) \tag{3.44}$$

Obviously, T_{sec} requires Δt to be small, but T_{nonsec} does not. So, under the aforementioned assumptions we have

$$\begin{aligned} T_{\text{sec}}(2\Delta t, \Delta t)\, T_{\text{nonsec}}(2\Delta t, \Delta t)\, S_K(-\Delta t)\, T_{\text{nonsec}}(\Delta t, 0)\, T_{\text{sec}}(\Delta t, 0) = \\ T_{\text{sec}}(2\Delta t, \Delta t)\, T_{\text{nonsec}}(2\Delta t, 0)\, S_K(-\Delta t)\, T_{\text{sec}}(\Delta t, 0) \;= \\ T_{\text{nonsec}}(2\Delta t, 0)\, T_{\text{sec}}(2\Delta t, \Delta t)\, S_K(-\Delta t)\, T_{\text{sec}}(\Delta t, 0) \end{aligned}$$

That is, only T_{sec} has to be applied iteratively, while the contribution from the nonsecular terms is given by one single mapping which is commuted to the right hand side of the expression. By induction, when the calculation of the evolution over greater time intervals is to be carried out, T_{nonsec} can be commuted all the way to the right and applied only once, so that

$$f\left(z, N\Delta t\right) \;= T_{\text{nonsec}}(N\Delta t, 0)\; S_{\text{sec}}(N\Delta t, 0) f\left(z, 0\right), \tag{3.45}$$

with

$$S_{\text{sec}}(N\Delta t, 0) = T_{\text{sec}}(N\Delta t, \left(N-1\right)\Delta t)\; S_K(-\Delta t) \ldots T_{\text{sec}}(\Delta t, 0) S_K(-\Delta t). \tag{3.46}$$

We have tested this mapping by applying it to an initial distribution function of the form $f_{\text{init}} \;=\; \text{sech}\left(2\mu\right)$ and letting it evolve under the influence of beat waves with the same parameters as the ones we have used in fig. 3.3. The results are depicted in Fig. 3.5. The first subfigure corresponds to the unfavourable case of fig. 3.3a). By choice, almost all of the particles are initially located at the area around $\rho \approx 0$, where an elliptic point exists. As expected from the phase space structure and verified by Fig. 3.5a), no significant energy transfer to the particles takes place. The results of the mapping fit perfectly those obtained by numerically integrating particle orbits.

The favourable case, fig. 3.5b) is much more interesting for various reasons. The particles that are initially located near $\rho \approx 0$ move along the lines dictated by the oscillation centre Hamiltonian, acquiring significant amounts of energy. At $\Omega t \approx 6 \cdot 10^4$ the average energy peaks, since most of the particles are to be found near the separatrix at this time. As can be seen in Fig. 3.3b), the 2nd order oscillation centre Hamiltonian fails to accurately describe the motion near the separatrix. A separatrix does indeed exist, its average height being the same as the one predicted by the 2nd order Hamiltonian, but its shape is curled due

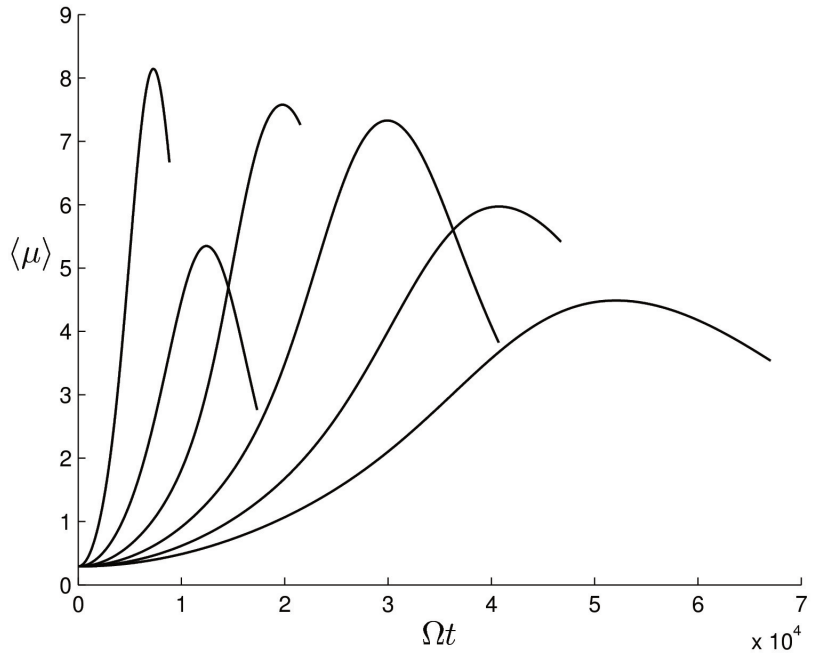

Figure 3.6 Average energy vs time for 7 different xmode IC waves spanning the range from $\nu = 5.123$ to 18.470. The time needed for the energy to reach the maximum increases with increasing carrier frequency. For high frequencies the detuning comes into play, impeding the energization of the ions.

to fourth order effects. Due to phase mixing effects, the average energy relaxes at a constant value which is about half the maximum value, but still about 20 times higher than the original one. The application of the evolution mapping reproduces qualitatively the same picture as the one described above, but fails to accurately predict the phase mixing effect. This is in part due to the limitation of the second order analysis near the separatrix. However, the peak time, the peak value, the relaxation time, as well as the relaxation value are all calculated with good precision. The accuracy of the mapping is not limited only by higher order effects. As with any scheme that cannot account for mixing, the roughness of the distribution increases with time and eventually the mapping becomes unstable.

Finally, we have studied the evolution of the ion distribution function under the influence of *beating X– mode ion cyclotron (IC)* waves, which satisfy the cold plasma dispersion relation (Stix, 1992). We choose a deuterium plasma with $n_e \approx 10^{14}\text{cm}^{-3}$ and $B \approx 4T$. We choose 7 different carrier frequencies spanning the range from $\nu = 5.123$ to 18.470. We also assume a detuning $\delta = 8 \cdot 10^{-6}$ in all cases. Meaningful comparisons require that the same normalization is used in all cases, so we have kept the normalisation that corresponds to the wave vector of the carrier with the lowest frequency. We have also scaled the effective perturbation amplitude ϵ, so that the amplitude of the electric field is equal in all cases. As

depicted in Fig. 3.6, the time needed for the energy to reach the maximum increases with increasing carrier frequency. For high frequencies the detuning comes into play, impeding the energization of the ions.

3.5 Onset of chaotic behaviour

We have demonstrated that the oscillation centre Hamiltonian is very efficient in reproducing the slow motion of the oscillation centre of the particle. This applies when the perturbation amplitude is sufficiently small, so that the perturbation scheme is well ordered and the perturbation analysis holds. However, as it is typical for dynamical systems, when the perturbation amplitude increases, the topology of the phase space changes, as parts of it become chaotic and it becomes possible for particles to orbit through previously separated phase space regions.

Onset of chaotic behaviour under the interaction with a single non resonant electrostatic wave was reviewed in Chapter 1. Karney et al.(Karney, 1978, Karney and Bers, 1977) have shown that chaotic motion takes place in the region above $\rho_{min} \approx \nu - \sqrt{\epsilon}$, ν and ϵ being the normalised frequency and the normalised amplitude of the wave respectively. The mechanism that gives rise to chaotic motion is the overlapping of the first order islands that appear in this region and become broader with increasing ϵ. For Larmor radii near ρ_{min} the minimum required wave amplitude for stochastic motion scales like $\epsilon \sim \nu^{2/3}$. This is closely related to particle trapping by an electrostatic wave in the absence of a magnetic field, which takes place near $\rho = \nu$. Karney's criterion suggests that for stochastic motion to take place, the particle should stay in the trapping region for at least one trapping bounce period, which is equivalent to the Cerenkov condition. The chaotic region is also bounded from above. For amplitudes much larger than the threshold value, the upper boundary scales like $\rho_{\max} \sim \epsilon^{2/3}$.

The case of a single near– or on–resonance electrostatic wave is qualitatively different. Due to *intrinsic degeneracy*, the first order islands appear in all or almost in all the phase space, depending on whether there is exact or approximate resonance, no matter how small the perturbation amplitude is. The chaotic motion is not due to resonance overlap between the first order islands, but a result of resonance overlap between the higher order islands that emerge in between the first order ones(Fukuyama et al., 1977). The energy threshold for chaotic motion is significantly lower than the Cerenkov energy threshold that applies to the non resonant interaction (Benisti et al., 1997).

The beating wave motion differs from the cases discussed above in the sense that there is a resonance between the intrinsically degenerate unperturbed Hamiltonian and the second order interaction. Therefore, somewhat counter intuitively, for small perturbation amplitudes

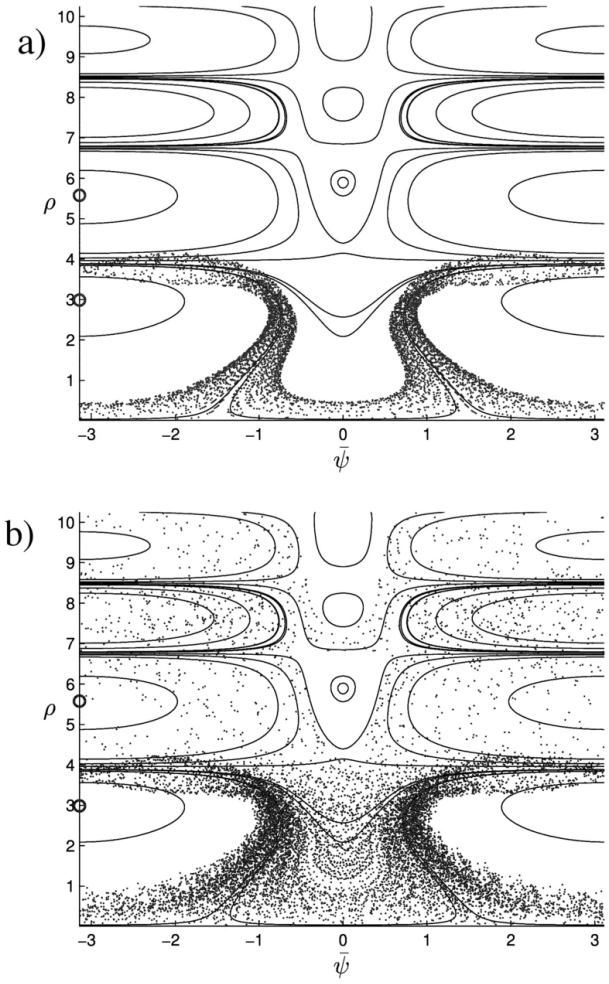

Figure 3.7 Oscillation centre phase space plots and Poincare plots for $\alpha = 0.8$, $\nu = 5.123$, $\delta\kappa = 0.0861$, $\delta = 0$ and different perturbation values. a) $\epsilon = 0.3$ and the motion is coherent. b)$\epsilon = 0.35$ and stochastic diffusion through the separatrix boundary takes place.

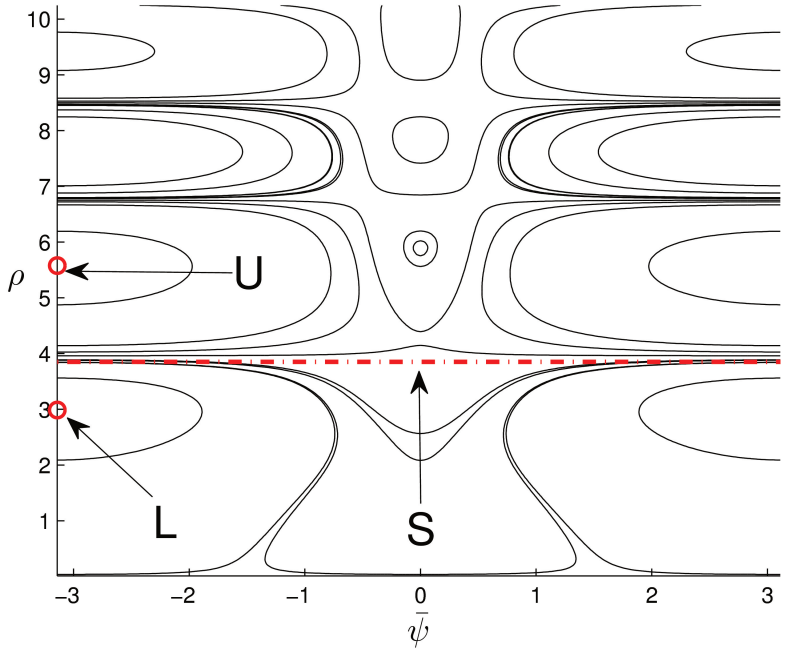

Figure 3.8 Contour plot for $\alpha = 0.8$, $\nu = 5.123$ and $\delta\kappa = 0.0861$. The separatrix S acts as a barrier for the coherent energization of low energy particles. For sufficiently strong perturbation amplitudes though, the particles can cross the barrier by stochastically diffusing from the lower island L, to the upper island U and into the chaotic region.

the particle motion is governed by the *second order oscillation centre Hamiltonian*, while the *first order* interaction is negligible. As the perturbation amplitude increases, the fast first order oscillatory motion kicks in, rendering the oscillation centre Hamiltonian less accurate and destroying the second order invariants, giving rise to chaotic behaviour. In a recent paper, Jorns and Choueiri (Jorns and Choueiri, 2013) analyse the stochastic motion under the influence of beating electrostatic wave. Their analysis is based on the conjecture that the stochasticity criterion has a functional form given by $\{K_2, \psi\}$ times an unknown prefactor, which they fit to numerical data. In this section we give an alternative interpretation. We argue that the origin of sotcastization has a simple physical explanation, namely separatrix crossing due to the fast first order oscillations around the oscillation centre.

In favourable cases, particles with very small Larmor radii can be energized up to energies close to the Cerenkov threshold $\rho \approx \nu$, where a separatrix lies, blocking the passage to higher energy areas of the phase space. In the area above the separatrix there is a web structure of a multitude of oscillation centre islands. For large enough perturbation amplitudes, these islands can be destroyed, forming a chaotic sea in the area above the separatrix (see Fig. 3.7). Particles whose oscillation center orbit passes near the separatrix can also access the chaotic sea. This is demonstrated in Fig. 3.7, where a small increase in the perturbation amplitude gives rise to a transition from coherent to stochastic motion. For favourable beat wave interactions, there is no minimum energy threshold for chaotic motion.

For an orbit to become chaotic, two conditions must be satisfied. First, the oscillation centre orbit must bring it to energies close to the Cerenkov energy threshold. Second, the amplitude of the first order oscillations must be large enough for the particle to overcome the Cerenkov energy threshold so that it can efficiently exchange energy with each wave separately. When the fast oscillations near the separatrix are violent enough, the perturbation scheme fails and the distinction between oscillation centre motion and oscillatory motion is no longer possible. Obviously, there must be a minimum beat wave amplitude for which separatrix crossing may occur.

A quantitative criterion for the minimum beat wave amplitude can be constructed, if one allows oneself to be creative. We postulate that the factor that determines whether or not the particle orbit remains bound to the oscillation centre orbit lies is the relation of the oscillation amplitude to the distance of the two elliptical points marked with L and U in Fig. 3.8, that are located below and above the separatrix S respectively. Chaotic diffusion takes place when the ratio of the fast oscillation amplitude to the resonance distance exceeds some minimum value. Then, a particle whose oscillation centre moves around the lower island L, can be picked up by the upper island U and cross into the chaotic sea region.

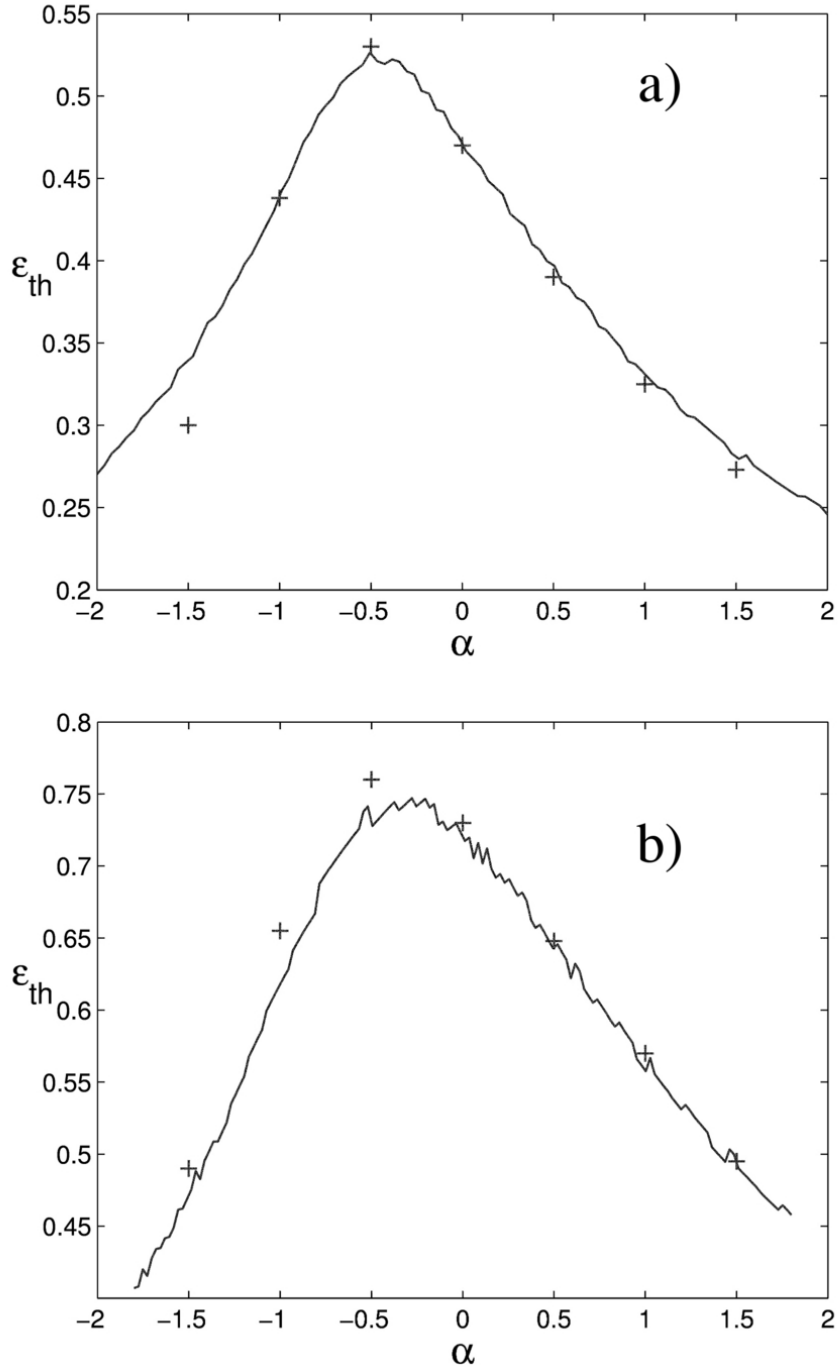

Figure 3.9 Threshold values for the perturbation amplitude required for stochastic diffusion into the chaotic sea as a function of the polarization parameter α for $\delta\kappa = 0.0861$ and $\delta = 0$. a) $\nu = 5.123$, b)$\nu = 10.123$. The analytical results (solid lines), show remarkable agreement with the numerical experiments (crosses).

A reasonable measure for the intensity of the fast oscillations at the oscillation centre area between the two resonance points L and U is the rms fast oscillation amplitude with respect to time, averaged over ϕ,

$$\{\rho\}_{\text{rms}} = \langle |\{w_1, \rho\}| \rangle_{\phi, \rho=\rho_m} . \tag{3.47}$$

Let us also define the index of stochasticity I_{st} as the ratio

$$I_{\text{st}} = \frac{\{\rho\}_{\text{rms}}}{\Delta\rho_{L,U}}, \tag{3.48}$$

where $\{\rho\}_{\text{rms}}$ is calculated at the separatrix level, which is approximately the mid level between the resonances,

$$\rho_m \equiv \frac{\rho_U + \rho_L}{2}.$$

Numerical analysis for various values of ϵ and the rest of the parameters the same as in Fig. 3.7 indicate that stochastic diffusion takes place for $I_{\text{st}} \geq 0.0862$. From this we can compute the corresponding minimum perturbation amplitude ϵ_{th}. If our postulate is valid, the same value of I_{st} must successfully determine the amplitude threshold for other wave parameters. This is indeed the case. Results obtained for various parameter values are depicted in Fig. 3.9 and show very good agreement with those obtained from simulations.

The chaotic region does not extend to infinity but it has an upper boundary at $\rho = \rho_{\text{max}}$. Although it is difficult to give a simple analytic calculation of its numerical value, we can instead derive the power law with which ρ_{max} scales as a function of ϵ. The same mechanism as before applies here, i.e. separatrix crossing becomes possible, when the fast oscillation amplitude is comparable to the island separation.

In general, island separation is approximately a constant function of ρ for large Larmor radii. This should not come as surprise, because the island location is determined by the local extrema of the oscillation center Hamiltonian K. K is composed of a series of terms of the form $\mathrm{J}_n(k\rho)\,\mathrm{J}_{-n+1}(k\rho)$ and we know that the Bessel function of the first kind behaves asymptotically as (Abramowitz and Stegun, 1970)

$$\mathrm{J}_n(z) \sim (2/\pi z)^{-1/2} \cos\left(z - \frac{1}{2}n\pi - \frac{1}{4}\pi\right), \tag{3.49}$$

which means it has approximately evenly distributed extrema. The island separation should be compared with the oscillating part of the Larmor radius $\{\rho\}$, which up to first order is given by

$$\{\rho\} = \{w_1, \rho\} \sim \frac{w_1}{\rho}. \tag{3.50}$$

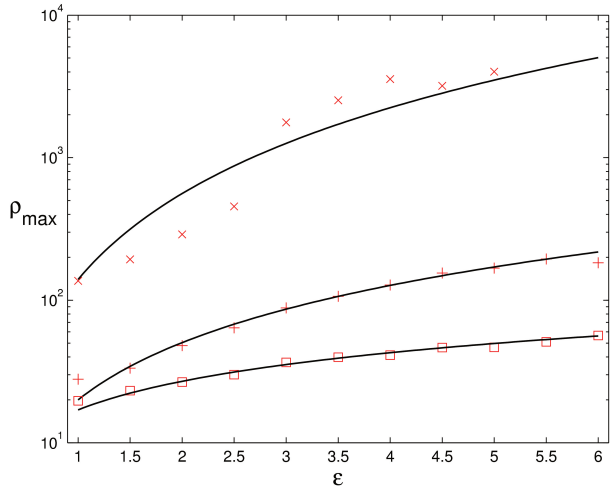

Figure 3.10 The upper boundary of the stochastic region as a function of ϵ for three different values of α. Squares: Numerical results for $\alpha = 0$. ρ_{max} goes as $\epsilon^{2/3}$. Plus signs: Numerical results for $\alpha = -0.5$. ρ_{max} goes as $\epsilon^{4/3}$. Crosses: Numerical results for $\alpha = 2$. ρ_{max} goes as ϵ^2. Solid lines: Fitted curves to the numerical data.

The way $\{\rho\}$ scales for large values of ρ depends strongly on the ellipticity α and can be easily computed for the two limiting cases of a purely electrostatic beating wave with $\alpha = 0$ or a transverse one with $\alpha \gg 1$. By inspection of Eq. (3.23), making use of the recurrence relations for the Bessel functions (Abramowitz and Stegun, 1970), it is seen that the numerators that appear in the series that compose w_1 are proportional to $\epsilon\rho^{-1/2}\,\mathrm{J}_n\,(k_i\rho)$ in the former case and $\epsilon\rho^{1/2}\,\mathrm{J}'_n\,(k_i\rho)$ in the latter. Thus, by virtue of the asymptotic form of the Bessel functions Eq. (3.49) and their derivatives (Abramowitz and Stegun, 1970), we expect the oscillating part of the Larmor radius to behave asymptotically as

$$\{\rho\} \sim \frac{\epsilon}{\rho^{3/2}}, \tag{3.51}$$

for $\alpha = 0$ and

$$\{\rho\} \sim \frac{\epsilon}{\rho^{1/2}}, \tag{3.52}$$

for $\alpha \gg 1$.

The stochasticity criterion requires $\{\rho\}$ to be compared with the island separation, which is approximately constant. This gives us a power law for the upper boundary of the stochastic region of the form $\rho_{\text{max}} \sim \epsilon^{2/3}$ for electrostatic beating waves and $\rho_{\text{max}} \sim \epsilon^2$ for transverse ones. Note that the former is of the same form as Karney's result for the single wave interaction. For intermediate values of α we expect the power law to take on values in the interval $[2/3, 2]$. This is confirmed by numerical simulations, the results of which are presented in

Fig. 3.10 for three different values of the polarization ellipticityα. For $\alpha = -0.5$ we get a $4/3$ power law. Note that the square law turns up for ellipticity values as low as $\alpha \approx 2$.

3.6 Conclusions.

In idealized uniformly magnetized plasmas, two high frequency electromagnetic waves can effectively heat low energy ions, when the frequency difference between the two waves is close to the ion cyclotron frequency. For small amplitude waves, low energy ions can gain energy through coherent motion provided the envelope propagates in the same direction as the phase velocity of each of the waves. However, if the envelope propagation is in opposite direction to the single wave propagation, which is the case for e.g. low hybrid waves with fixed parallel wavelengths, the energy gain is limited. For adequately high amplitudes of the waves, ions that acquire velocities close to the Cerenkov velocity, can access the chaotic region of the dynamical phase space where they extract much higher energies from the waves.

The conditions for efficient energy exchange between waves and ions have been determined by means Deprit's perturbation theory (see Chapter 1). The amplitude threshold for the onset of chaotic motion has also been determined semi-analytically, along with a scaling law for the maximum energy that can be acquired though beat envelope interaction. The validity of our calculations has been confirmed by comparison with simulations of the complete dynamical equations.

Chapter 4

Orbital Spectrum Analysis of Non-Axisymmetric Perturbations of the Guiding-Center Particle Motion in Axisymmetric Equilibria

The presence of non-axisymmetric perturbations in an axisymmetric magnetic field equilibrium renders the Guiding Center (GC) particle motion non-integrable and may result in particle, energy and momentum redistribution, due to resonance mechanisms. We analyse these perturbations in terms of their spectrum, as observed by the particles in the frame of unperturbed GC motion. We calculate semi-analytically the exact locations and strength of resonant spectral components of multiple perturbations. The presented Orbital Spectrum Analysis (OSA) method is based on an exact Action-Angle transform that fully takes into account Finite Orbit Width (FOW) effects. The method provides insight into the particle dynamics and enables the prediction of the effect of any perturbation to all different types of particles and orbits in a given, analytically or numerically calculated, axisymmetric equilibrium.

4.1 Introduction

Guiding Center (GC) theory has been widely used for more than four decades as the basis for the study of single and collective particle dynamics in toroidal magnetic fields utilized in fusion devices (Cary and Brizard, 2009). The theory has been originally formulated in a non-canonical (Littlejohn, 1979) description which was later extended to a canonical one

(White and Chance, 1984). The former has the advantage of being applicable to any type of coordinates, whereas the latter, while being more abstract, has the advantage of an elegant structure of the described dynamics, accompanied by an arsenal of powerful mathematical methods (see Chapter 1 and Chapter 3).

The GC motion of charged particles in an axisymmetric magnetic field is known to be regular, due to the existence of three integrals of motion, namely the energy, the magnetic moment and the canonical toroidal momentum (Littlejohn, 1983, White and Chance, 1984). However, the presence of any non-axisymmetric perturbation results in symmetry breaking, non-integrability and complex particle dynamics. In realistic tokamaks, non-axisymmetric perturbations are introduced due to static magnetic field fluctuations, magnetohydrodynamic (MHD) modes or radio frequency (RF) waves. The effect of these perturbations is the re-distribution of particles, energy and momentum, through local (e.g energy absorption) and non-local processes (e.g. energy transport), that are based on resonant interactions with the 3 degrees of freedom of the GC motion (White, 2012, White et al., 2010).

Significant interaction with any perturbative mode takes place when the mode is resonant with the unperturbed particle motion. Fundamental understanding of the perturbed motion requires the knowledge of the position of the resonant orbits in phase space, where the resonant condition - involving the 3 frequencies of the unperturbed motion - is met. However, this is not sufficient for obtaining a clear picture of the perturbed –single, or collective – particle dynamics. Some measures of the strength and the extent of the resonance in the phase space are also required.

The collective particle dynamics under symmetry-breaking perturbations can be studied on the basis of single particle GC theory, described above. This is the Gyro-Kinetic (GK) theory, which has been formulated either in non-canonical or canonical coordinates (Brizard and Hahm, 2007), with the latter resulting in a kinetic equation of the Fokker-Planck type in the Action space (Kaufman, 1972a). This is the standard quasilinear transport theory formulated either by the trajectory integral approach (Brambilla, 1999, Eester and Koch, 1998, Lamalle, 1993) or by the Hamiltonian approach, both made possible due to the canonical structure of the GC phase space (Wang, 2006, White et al., 1982, White and Chance, 1984). Common to the two approaches is the requirement that the quasilinear diffusion operator be expressed in terms of constants of the unperturbed motion. The former approach relies on the application of integration operators on the perturbations, the constants of motion being used to label the unperturbed orbits, whereas in the latter, the constants of motion are the Action variables (Gambier and Samain, 1985, Hazeltine et al., 1981, Kaufman, 1972a, Kominis, 2008, Kominis et al., 2008, 2010)

Although the Action-Angle description is accompanied by powerful mathematical tools (Goldstein, 1956, Lichtenberg and Lieberman, 1992) and is widely appreciated for its elegance, applications have been restricted to either formal derivations (Gambier and Samain, 1985, Kaufman, 1972a, Kominis, 2008, Kominis et al., 2008, 2010) or calculations under strict assumptions (Abdullaev et al., 2006, Hazeltine et al., 1981). Explicit calculations of AA variables have been carried out only for the simple case of *Large Aspect Ratio (LAR)* equilibria for transit and banana orbits, under the approximation of zero drift from the magnetic surfaces or *Zero Orbit Width (ZOW)* approximation (Brizard, 2011, Hazeltine et al., 1981). However, it is known that energetic particle orbits deviate strongly from the magnetic surfaces. Even the simple case of concentric circular magnetic surface equilibria supports 10 orbit types other than the transit and banana orbits (Eriksson and Porcelli, 2001, Gott and Yurchenko, 2014) of *Standard Neoclassical Theory (SNT)*. The effect of such orbits has been long debated (Bergmann et al., 2001, Helander, 2000, Lin et al., 1997, Shaing et al., 1997, Shaing and Peng, 2004), and though it seems that the contribution from low energy non–standard orbits is not significant (Helander, 2000), this cannot be argued for energetic orbits as well, since the bounce and drift frequencies can become comparable (Eriksson and Porcelli, 2001), giving rise to new interactions and instabilities, which SNT cannot predict. White and al. (White, 2012, White et al., 2010) have recently provided a method of numerically locating resonances with a particular mode in phase space, by means of the vector rotation criterion. This involves particle tracing, the time consuming process of numerically integrating particle orbits with initial conditions that span the entire phase space for long enough integration times so that the resonance is manifested and for every perturbation separately.

Undoubtedly, the AA formalism provides the appropriate description and concepts for understanding the particle motion, due to its direct relation to the three adiabatic constant of GC dynamics. No wonder the scientific community have decided to include it in most textbooks on plasma physics or fusion (e.g. (Chen, 2013, Wesson, 2004)). The widespread notion that the AA formalism cannot provide specific results for realistic magnetic field configurations (e.g. (Eester, 1999, Lamalle, 1993)) stems from the fact that so far no general method for obtaining the transform from configuration variables to AA variables has been presented, rather than from some intrinsic obscurity of the Hamiltonian formalism itself. So do the aforementioned restrictions and approximations. In fact, we argue that it is the AA formalism that elucidates the dynamics and separates the timescales of different degrees of motion. After all, it is the AA formalism that takes the most advantage of the Hamiltonian structure and fully exploits the canonical structure of GC dynamics.

In this chapter, we demonstrate a method for calculating the transform from configuration space variables to AA variables for any given axisymmetric equilibrium. The existence of a local transform to AA variable is guaranteed by the symmetries of the unperturbed system (Goldstein, 1956), and, though, in general, no such global transform exists, we are able to cover all phase space by calculating multiple AA transforms. The orbital frequencies, being constants of motion, are functions of the Actions alone, so that the resonances can be located and studied on the Action subspace. Since the Actions are both the canonical momenta and the integrals of motion, perturbation analysis is significantly simplified (Goldstein, 1956, Lichtenberg and Lieberman, 1992).

Based on the AA transform we introduce the *Orbital Spectrum Analysis (OSA)* method for analytically estimating the effects of particle interaction with different kinds of perturbations. In OSA, all different kinds of orbits are treated on equal footing, without referring to phenomenological taxonomies, which makes it straightforward to expand the analysis to equilibria more complex than LAR. One of the most significant advantages this approach has to offer is that the frequencies of the different degrees of freedom are readily calculated and that the resonance condition can be written in a simple form. *Full Orbit Width (FOW)* effects are intrinsically taken into account and the phase space location as well as the effective strength of resonances is automatically revealed. Moreover, the Actions, being both canonical momenta and constants of motion, provide an excellent framework for building an equilibrium distribution function, a task that until recently has been known to be problematic (Troia, 2012).

In section 4.2 the canonical GC motion is reviewed and the AA transform algorithm is outlined. In section 4.3 we introduce the Orbital Spectrum Analysis (OSA) method and demonstrate it by applying it to the case of synergetic interaction with two non resonant magnetic perturbations, where chaotic particle motion occurs, while the magnetic field lines remain regular and no magnetic surface destruction occurs. By means of OSA, the conditions for transition to chaos are analytically determined.

4.2 The Action Angle Transform

Assuming that the gyromotion is much faster than every other process involved, the magnetic moment remains constant and the particle motion is accurately approximated by the motion of its guiding center. The *Lagrangian of the Guiding Center (GC)* motion of a charged particle is

$$\mathcal{L} = \left(\mathbf{A} + \rho_{\|} \cdot \mathbf{B}\right) \cdot \mathbf{v} + \mu\dot{\xi} - H,$$

where $\mathbf{A}$ and $\mathbf{B}$ are the vector potential and the magnetic field respectively, $\mathbf{v}$ is the guiding center velocity, μ the magnetic moment, ξ, the gyrophase, $\rho_{\|}$ the parallel velocity to the magnetic field, normalized with B and

$$H = \rho_{\|}^2 B^2/2 + \mu B + \Phi \tag{4.1}$$

the Hamiltonian, with Φ the electric potential (Littlejohn, 1983). All quantities are evaluated at the guiding center position and normalized with respect to the nominal magnetic axis gyrofrequency and the major radius R. It has been shown that, when the magnetic coordinates (ψ, τ, χ) – ψ being the toroidal flux, τ and χ the poloidal and toroidal angle – are Boozer coordinates, the dynamical system is Hamiltonian and one can define P_τ and P_χ to be the canonical poloidal and toroidal momenta given by

$$P_\tau \equiv \psi + \rho_{\|} I \tag{4.2}$$

and

$$P_\chi \equiv \rho_{\|} g + \psi_p \tag{4.3}$$

respectively (White and Chance, 1984). The Hamiltonian in eq. 4.1 takes the form

$$H = \frac{\left(P_\chi + \psi_p\left(P_\tau, P_\chi\right)\right)^2}{2g^2\left(P_\tau, P_\chi\right)} B^2 + \mu B + \Phi. \tag{4.4}$$

In *axisymmetric equilibria*, the canonical position χ is ignorable and P_χ is conserved, so that the dynamical system, being reduced to one Degree Of Freedom (DOF), is integrable. However, the motion in phase space is non–trivial and there is no straightforward way to predict the behaviour of the system when perturbations are introduced and integrability is lost.

The conserved canonical momenta P_χ and μ are already the actions of the toroidal motion and the gyromotion respectively. The AA pair (J, θ) of the poloidal motion is found by integrating along a closed orbit in the poloidal plane:

$$J \;=\; \frac{1}{2\pi} \oint P_\tau d\tau \tag{4.5}$$

and defining θ as the normalized time

$$\theta \;=\; \omega_\theta\left(J, P_\chi, \mu\right) t, \tag{4.6}$$

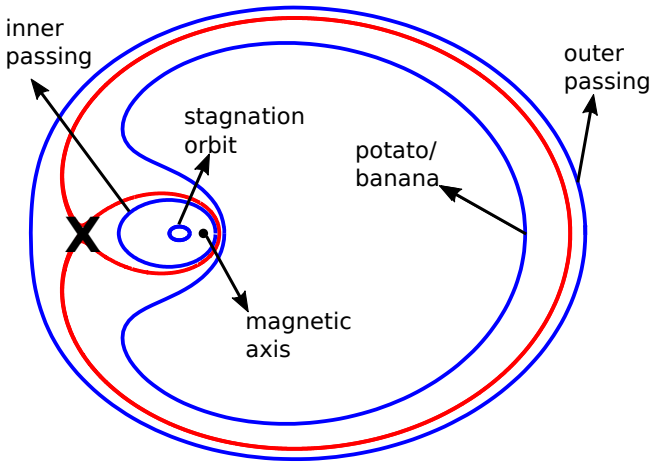

Figure 4.1 Schematic diagram of LAR characteristic orbits. Two separatrices, homoclinic to the x-point, are shown, each one acting as a boundary between two continents.

where ω_θ is the frequency of the poloidal motion and depends only on the three actions. By virtue of the Liouville–Arnlold theorem (Arnold, 1989), such a transform always exists locally. In particular we can cover all phase space with a measurable set of AA transforms, one for each phase space region that is bounded by a separatrix. From now on we shall call such a region a *continent*, while the set of transforms for all regions is called an *atlas*.

Fig. 4.1 depicts a poloidal projection of LAR orbits with fixed P_χ and μ. Each of the two separatrices (thick red lines) separates two continents. All orbits belonging to the same continent share the same topology and the behaviour of the dynamics varies continuously within each continent. The conventional orbit labelling (e.g. passing, trapped, stagnated) is phenomenological and refers to the magnetic axis, because it is the natural reference point of the magnetic field geometry and very close to the natural reference point of the slow particle dynamics, i.e. the elliptic point of the inner passing orbits (innermost continent in the figure). However, for the energetic particle dynamics, the magnetic axis is not special from the dynamics point of view, and conventional labelling is arbitrary and confusing. Fig. 4.1 depicts a poloidal projection of LAR orbits with the same P_χ and μ. Each of the two separatrices (thick red lines) separates two continents. All orbits belonging to the same continent share the same topology and the behaviour of the dynamics varies continuously within each continent. The conventional orbit labelling (e.g. passing, trapped, stagnated) is phenomenological and refers to the magnetic axis, because it is the natural reference point of the magnetic field geometry and very close to the natural reference point of the slow particle dynamics, i.e. the elliptic point of the inner passing orbits (first continent in the figure). However, for the energetic particle dynamics, the magnetic axis is not special from the dynamics point of view, and conventional labelling is arbitrary and confusing. For example, in Fig. 4.1, the

two orbits marked as stagnation and inner passing orbits share the shame topology, but their conventional labelling is not the same. It would be more reasonable to label the orbits with respect to the continent they belong to, this would not only underlines the dynamic characteristics of each orbit, but additionally it would serve the purpose of clarity and algorithmic simplicity.

Although the Hamiltonian H is integrable, finding an analytic solution to the AA transform problem is impracticable. Instead, we calculate the atlas numerically. The algorithm we follow relies on finding the boundaries of each continent in $(\tau, \psi, P_\chi, \mu)$ subspace, i.e. the separatrices, and then calculating numerically each AA transform defined by eqs. 4.5, 4.6 on a carefully chosen sample of closed orbits. The particulars of the algorithm will be discussed in Chapter 5.

In transforming from (τ, ψ) to (J, θ), the angles of the other two DOFs are redefined, so that eventually all DOFs are described by AA pairs. In each continent, the transform from $(\tau, \psi, P_\chi, \mu)$ to $\left(\theta, J, P_\chi, \mu\right)$ is implicitly generated by a function of the form $F_2 = F\left(\tau, J, P_\chi, \mu\right)$. Dependence of F_2 on P_χ and μ implies that the toroidal angle χ is also transformed to an new canonical angle variable

$$\hat{\chi} \;=\; \chi - f_\chi\left(J, \theta, P_\chi, \mu\right) \tag{4.7}$$

and so does the gyration angle ξ. Therefore, this procedure generates the transform to the AA pairs $\left(P_\chi, \hat{\chi}\right)$ and $\left(\mu, \hat{\xi}\right)$. The new angles differ from the original in that they evolve linearly with time, with frequencies $\omega_{\hat{\chi}}$ and Ω_c, which are the averaged drift frequency and the mean gyrofrequency respectively. By construction, the new poloidal angle θ evolves linearly as well, with the average poloidal frequency ω_θ, while the actions J, P_χ and μ are constants of motion.

4.3 Chaotic motion due to magnetic perturbations

There is little reason to calculate the AA transform, unless we intend to study the particle dynamics in the presence of perturbations. The dynamics of low energy particles is strongly correlated with the magnetic topology, because their guiding centre orbits are essentially parallel to the magnetic field lines. Thus, the particle motion is regular, provided that the magnetic surfaces are conserved. However, for higher energy particles, this is not necessarily true. Drift effects that are negligible for low energies, can no longer be neglected, and the topologies of these two spaces are disentangled. Consequently, appearance of chaotic

magnetic field lines may be a reliable criterion for predicting chaotic motion of low energy particles, but inevitably fails for energetic particles.

In the high energy domain, resonance location and resonance overlap are purely dynamic effects and particle motion can become chaotic without destruction of the magnetic surfaces. This is, of course, not the first time this phenomenon has been described (see, for example, (Matsuyama et al., 2014) and references therein), but here the analysis is restricted on the particulars of phase space alone, without resorting to configuration geometry concepts. The simplicity of this approach and the excellent quantitative results it can provide is a major advantage of the OSA method.

4.3.1 Orbital Spectrum Analysis

A perturbation of the form

$$\delta\mathbf{B} = \nabla \times \sigma\mathbf{B}$$

can be straightforwardly included in the guiding center Hamiltonian as (White, 2001)

$$H = (\rho_c - \sigma)^2 B^2/2 + \mu B + \Phi,$$

with

$$\rho_c = \rho_{\|} + \sigma,$$

and modified canonical momenta

$$P_\tau \equiv \psi + \rho_c I, \tag{4.8}$$

$$P_\chi \equiv \rho_c g + \psi_p \tag{4.9}$$

The first order perturbation Hamiltonian is

$$H_1 = -\rho_c \sigma B^2 + \Phi$$

and second order perturbation Hamiltonian

$$H_2 = \sigma^2 B^2/2.$$

For ideal MHD modes, the scalar potential Φ must be chosen so that it cancels out the parallel electric field induced by $d\delta\mathbf{B}/dt$, to account for the rapid response of the electrons.

Thus, a monochromatic mode with

$$\sigma = \sigma_{m,n}(\psi) \exp\left(i(m\chi + n\tau - \omega t)\right) \tag{4.10}$$

implies a scalar potential

$$\Phi = \Phi_{m,n}(\psi) \exp\left(i(m\chi + n\tau - \omega t)\right)$$

with $\Phi_{m,n}$ given by (White, 2013):

$$\Phi_{m,n} = \omega \frac{gq + I}{mq + n} \sigma_{m,n}.$$

Due to the nonlinear dependence of $\hat{\chi}$ on θ (eq. 4.7), the mode in eq. 4.10, which is monochromatic in the magnetic coordinates, gives rise to an infinite series of harmonics in the AA coordinates, for which the toroidal number is fixed and equal to the toroidal number m of the magnetic perturbation σ, but the poloidal number is not. The associated first order Hamiltonian H_1 has the general form

$$H_1 = \sum_s \mathcal{H}^1_{s,m}\left(J, P_\chi\right) \exp(i\left(m\hat{\chi} + s\theta - \omega t\right)), \tag{4.11}$$

The poloidal number n of the magnetic perturbation influences H_1 only by affecting the amplitudes of its harmonic components, which are given by

$$\mathcal{H}^1_{s,m}\left(J, P_\chi\right) = \frac{1}{2\pi} \oint H^1_{m,n}(\psi) \exp(i\left(n\tau + n f_\chi\left(J, P_\chi, \theta\right) - s\theta\right))d\theta \tag{4.12}$$

and there is no reason to assume any stronger connection between the two. For example, it may seem reasonable at first sight to assume that for a given $\sigma_{m,n}$, the spectrum of H_1 should peak at the same poloidal number n, but this assumption is utterly unjustified. For even if it happened to hold for some class of particle orbits, it would necessarily fail for orbits with different topology.

As equation eq. 4.11 indicates, the resonances of the perturbation are located in action space at the points where the resonance condition

$$m\,\omega_{\hat{\chi}}\left(J, P_\chi, \mu\right) + s\,\omega_\theta\left(J, P_\chi, \mu\right) - \omega\ = 0 \tag{4.13}$$

is met, s being any integer.

The toroidal to poloidal frequency ratio for passing particles tracing exactly the magnetic field lines is clearly

$$\frac{\omega_{\hat{\chi}}}{\omega_\theta} = q, \tag{4.14}$$

q being the safety factor, so that, eq. 4.13 becomes for $\omega = 0$

$$m\, q + s = 0, \tag{4.15}$$

This approximation is accurate for low energy particles. The dynamic properties of the particles (i.e. energy, magnetic moment) are not involved in the resonance condition and, since for $s = n$, eq. 4.15 takes the form of the condition for the destruction of the magnetic surfaces (White, 2001), the perturbed dynamics of the particles is closely linked to the perturbed magnetic topology.

As the energy increases, drift orbit effects come into play, a different kind of resonance appears and the connection between the destruction of the magnetic surfaces and the destruction of the integrals of motion breaks. The ZOW approximation does not take into consideration drifts across the magnetic surfaces, but allows for drift effects on the magnetic surface across magnetic field lines. The magnetic geometry is approximated by the circular Large Aspect Ratio (LAR) equilibrium, with $B \approx 1 - r\cos(\tau)$ and the poloidal and toroidal frequencies for trapped particles are given by the pendulum formulas (Brizard, 2011, White, 2001)

$$\omega_\theta \approx \frac{\pi\sqrt{\mu\, r(\psi)}}{2q(\psi)K(\kappa)}, \tag{4.16}$$

$$\omega_{\hat{\chi}} \approx \frac{\mu\left[(q' + 2q)\, E(\kappa) + (q'(\kappa - 1) - q)K(\kappa)\right]}{rK(\kappa)}, \tag{4.17}$$

with

$$\kappa \equiv \frac{H - \mu B}{2r\mu}, \tag{4.18}$$

where r is the normalized minor radius, $q' \equiv \partial q/\partial\psi$ the shear, K and E the complete elliptic integrals,

$$K(\kappa) = \int_0^{\frac{\pi}{2}} \frac{d\phi}{(1 - \kappa^2 \sin^2\phi)^{1/2}},$$

$$E(\kappa) = \int_0^{\frac{\pi}{2}} (1 - \kappa^2 \sin^2\phi)^{1/2} d\phi.$$

and all quantities are calculated at the low field point of the particle orbit. The equations above are more that just a correction to eq. 4.15, since they account for drifts from the magnetic line and thus allow for a different kind of resonance to take place, one which involves the dynamic characteristics of the particle. Had we ignored the drift motion, the toroidal drift frequency would be zero, and the only possible resonances would occur at $q =$ rational, i.e. only when the magnetic field lines are also in resonance with the perturbation. By allowing for drift motion, chaotic magnetic field lines do not imply chaotic particle orbits, nor do chaotic particle orbits necessarily suggest the existence of chaotic field lines.

For particles with even higher energies, drift across the magnetic surfaces becomes significant and a full orbit approach is necessary. When the AA transform is carried out and the unperturbed Hamiltonian H_0 is expressed as a function of the three actions, the frequencies are given by

$$\omega_\theta = \frac{\partial H_0(J, P_\chi, \mu)}{\partial J}, \tag{4.19}$$

$$\omega_{\hat{\chi}} = \frac{\partial H_0(J, P_\chi, \mu)}{\partial P_\chi}. \tag{4.20}$$

As we will demonstrate in the following subsection, using eqs 4.16, 4.17 outside their domain of validity can lead to significant misrepresentation of the particle dynamics.

The location of the resonances in action space depends only on the spectral parameters m and ω. The actual profile of the perturbation, i.e the depencence on n or ψ, is relevant in defining the amplitude of the resonant terms, but not in pinpointing their location in the orbital spectrum. Since s can take on any integer value, each bounded continent may contain a large number of such resonances, most of which are located in the narrow chaotic sea near the separatrix, where ω_θ approaches zero. In the bulk of each continent there are only a few, if any, sites where eq. 4.13 is satisfied.

Near a particular resonance $m\,\omega_{\hat{\chi}} + s\,\omega_\theta - \omega = 0$, the dynamics follow a pendulum– like Hamiltonian and a trapped area of width proportional to the square root of the perturbation amplitude is formed. This width depends on $\mathcal{H}_{s,m}\left(J, P_\chi\right)$ and can be easily calculated once the AA transform has been performed (more on this on Chapter 5).

4.3.2 Particle losses due to static magnetic perturbations

The advantages of the Orbital Spectrum Analysis method are highlighted, when it used to predict the conditions under which perturbations may lead to loss of ion confinement. In this

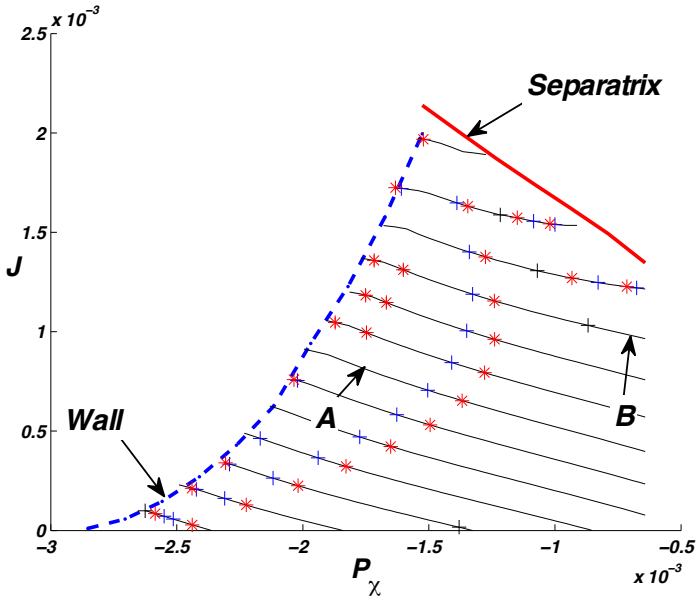

Figure 4.2 Resonance chart cross section in μ. The solid black lines depict the energy surfaces, crosses and stars correspond to resonances with $m = 10$ and $m = 8$ respectively.

section we apply it to the study of the dynamics in a LAR peaked equilibrium [1] in the presence of two static magnetic perturbations ($\omega = 0$). The case of time independent perturbations may b3 particularly simple, but is rather indicative of the power of the AA transform and the OSA method.

The perturbations are chosen to be of the form

$$\sigma_i = A_i(\psi) \exp\left[i\left(m\chi + n\tau\right)\right], \quad i = 1, 2,$$

with toroidal numbers $m = 8$ and $m = 10$ respectively, while the poloidal number equals $n = -1$ for both perturbations. The amplitudes of the perturbation are assumed to be such that

$$\delta B/B \approx 10^{-4} - 10^{-3},$$

[1] The safety factor, defined as $q = \mathbf{B} \cdot \nabla\chi / \mathbf{B} \cdot \nabla\tau$, is determined by the balance of the pressure and the magnetic force and, as its name suggests, its profile is an important characteristic of the equilibrium. It is a flux function in straight magnetic field line coordinates (see Chapter 2). It is known that, for LAR equilibria, q profiles of the form

$$q = q_0 \left(1 + (\psi/\psi_0)^{\nu}\right)^{\frac{1}{\nu}} \tag{4.21}$$

are acceptable solutions of the force balance condition. Equilibria with $\nu = 1, 2, 3$ are referred to as peaked, rounded and flat respectively (White, 2001).

well inside the domain of validity of perturbation theory. Moreover, the safety factor q is chosen to range from 1 to 1.8, so that it is nowhere equal to $-n/m$ and thus the magnetic field lines are non resonant with the perturbation and no flux surface is destroyed.

The Hamiltonian is conserved and near any given m/s resonance, the quantity

$$P'_{\chi} = P_{\chi} - m/sJ$$

is an adiabatic invariant. The cases where the ratio m/s or s/m becomes very large are of little interest, since the adiabatic invariant coincides with one of the actions, so that no significant redistribution takes place. Without assuming any particular knowledge about the actual profile of the perturbations, other than their toroidal numbers, it is possible to chart the location of the resonances in the action space of each continent, by requiring the resonance condition

$$\frac{m\omega_{\hat{\chi}}}{\omega_{\theta}} \;=\; \text{integer.} \tag{4.22}$$

to be satisfied. Since the frequencies, given by eqs 4.19, 4.20, are functions of the three actions alone, eq. 4.22 describes a set of two–dimensional surfaces in the action space. Moreover, since the Hamiltonian is conserved, the perturbed particle motion will necessarily take place near the surfaces of constant unperturbed energy $H_0\left(J, P_{\chi}, \mu\right)$.

The AA transform enables us to visualize the constant energy surfaces in Action space. Fig. 4.2 depicts the cross section of the 3D chart of the $m = 10$ and $m = 8$ resonances in a potato–banana continent with the $\mu = 8 \cdot 10^{-6}$ plane. A set of constant unperturbed energy subsurfaces, near which the perturbed motion will be confined, due to time independence of the perturbation, are plotted with solid black lines. The locations of the resonances on the energy surfaces are marked with crosses and stars for the $m = 10$ and $m = 8$ perturbations respectively. The location of the separatrix that bounds the banana continent is given by $J_s(P_{\chi}, \mu)$. It is depicted as a thick red line in Fig. 4.2. Finally the last closed magnetic surface with $\psi = \psi_{\text{wall}}$ is visualised by depicting the surface $\psi_{\text{max}}(J, P_{\chi}, \mu) = \psi_{\text{wall}}$, where ψ_{max} is the maximum ψ value along the orbit defined by the three actions.

Coexistence of more than one resonances on the same energy surface can lead to chaotic redistribution, due to destruction of the adiabatic invariant. On the energy surface denoted by A in Fig. 4.2 there are two neighbouring resonances located at

$$P_{\chi,1} \approx -1.5 \cdot 10^{-3}$$

and

$$P_{\chi,2} \approx -1.37 \cdot 10^{-3}.$$

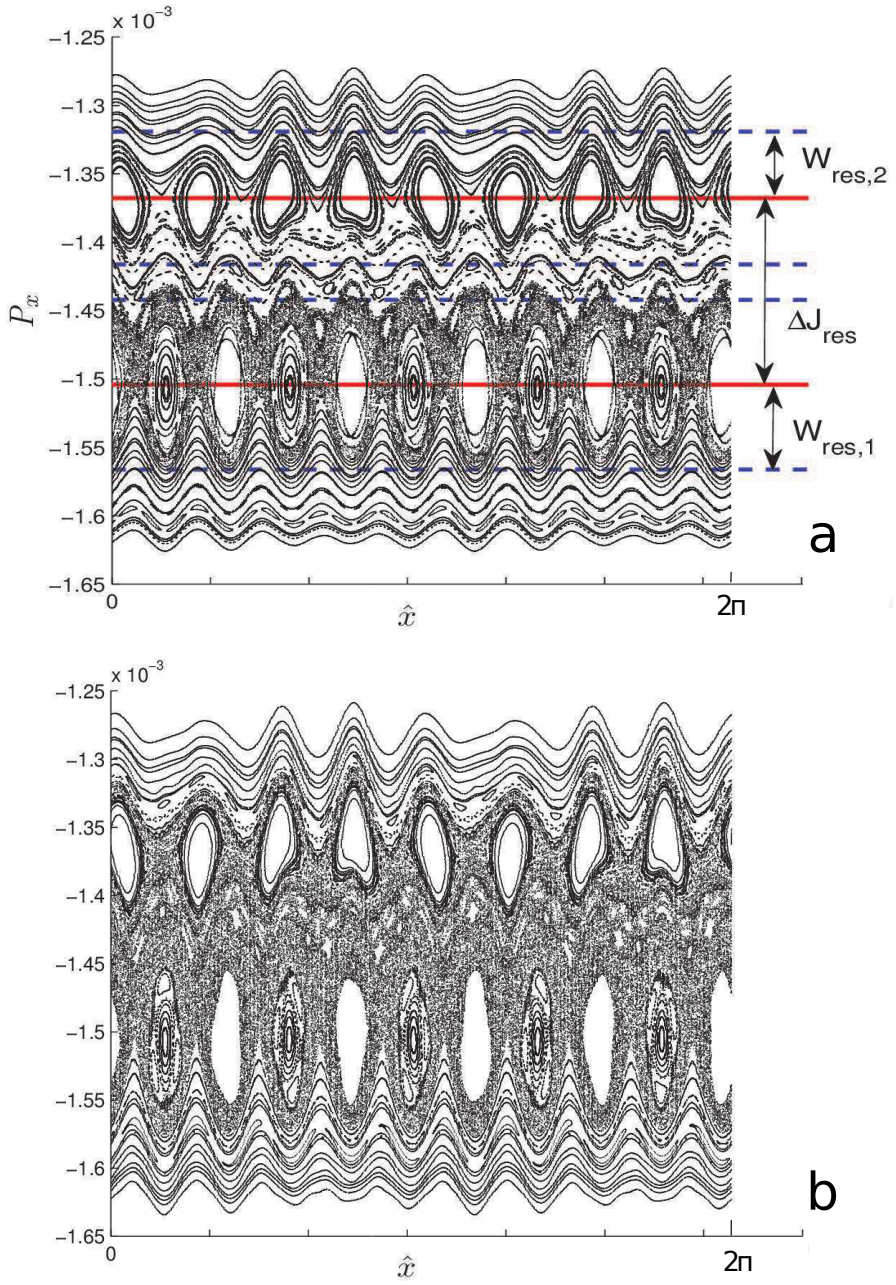

Figure 4.3 Inspection of the resonance chart can reveal the phase space regions when mode synergy can be significant. The analytically calculated resonance positions, width and overlap conditions are in excellent agreement with the simulations. a) Poincare plot on the surface A of Fig. 4.2 for two modes with subcritical amplitude. The semianalitically calculated positions of the resonances as well as their widths are denoted with solid and dashed lines respectively. b) The same Poincare plot for perturbations with critical amplitude. KAM lines between the two resonances have been destroyed and significant redistribution can take place.

Chiricov criterion (Lichtenberg and Lieberman, 1992) provides a simple estimation for the onset of chaotic motion, by requiring that the resonances overlap. The resonance widths $W_{\text{res},i}$ are estimated by approximating the motion around the resonances with the pendulum Hamiltonian (see Section 5.4). The criterion requires that for chaotic motion

$$\Delta J \leq W_{\text{res},1} + W_{\text{res},2}, \tag{4.23}$$

where ΔJ is the distance between two neighbouring resonances.

As demonstrated in Fig. 4.3, the OSA method predicts both the location of the resonance center as well as the resonance width in the phase space. Moreover, application of the Chirikov criterion is shown very successful in predicting the transition from weak to strong chaos. Fig. 4.3a displays a Poincare plot of the perturbed motion, when the amplitude of the perturbation $A = A_{\text{subcrit}}$ is lower than the analytically computed critical amplitude A_{crit}. Some chaos is present, due to the existence of higher order resonances, but the primary resonances are well separated by KAM surfaces and no significant particle redistribution takes place. Superimposed on the Poincare plot are the analytically calculated locations of the resonances (solid lines) and the resonance widths (dashed lines). It is evident that the resonances do not overlap. The situation changes for $A = A_{\text{crit}} = A_{\text{Chiricov}}$ (Fig. 4.3b), for which the KAM surfaces have been destroyed and there is a chaotic sea between the two primary resonances.

The case of the energy surface B in Fig. 4.2 is of particular importance, because there is a sequence of resonances linking a deeply trapped part of phase space to the plasma wall (dashed blue line). When all consecutive resonances overlap, significant particle loss will take plac3. Application of the Chirikov criterion overestimates the critical amplitude at $A_{\text{Chirikov}} = 1.2 \cdot 10^{-3}$, due to the strong presence of higher order resonances (see fig. 4.4).

The location of the resonances is determined by requiring that

$$\omega_{\hat{\chi}}/\omega_\theta = s/10$$

or

$$\omega_{\hat{\chi}}/\omega_\theta = s/8,$$

where s is any integer. In the above, it is important that we make use of the frequencies calculated through the full orbit width approach (eqs 4.19, 4.20). The closed form estimations of the poloidal and toroidal frequencies in eq. 4.16 and eq. 4.17 that are valid under the zero orbit width assumption are much easier to compute, but not nearly accurate enough for our purposes. Figure 4.5 compares the frequency ratio curve on the energy surface B (Fig. 4.2) ob-

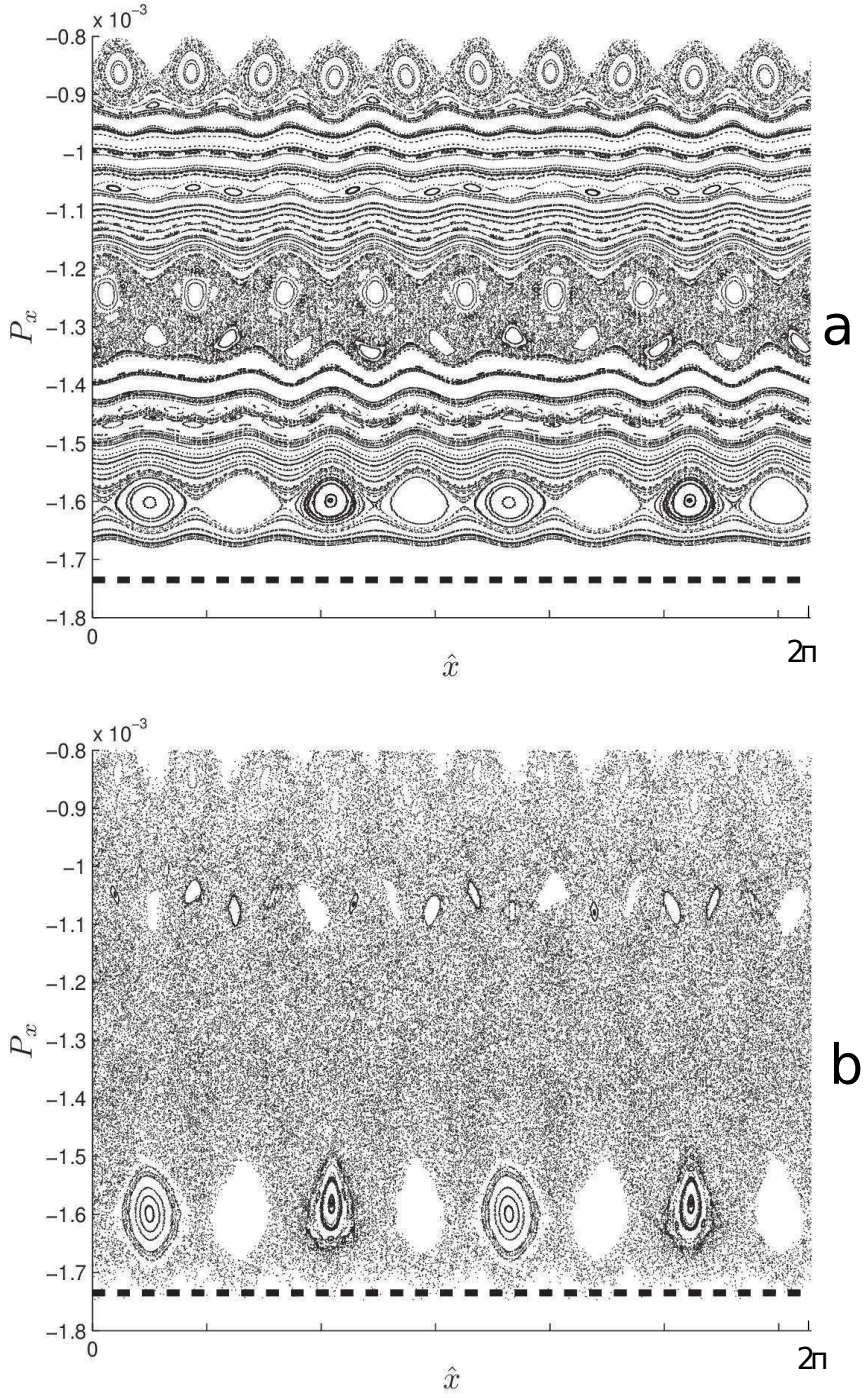

Figure 4.4 The OSA method as a tool for estimating conditions for confinement loss. The outer closed flux surface is marked with a thick dashed line. a) Poincare cut for the energy surface B of Fig. 4.2 and subcritical amplitude $0.08\ A_{\text{Chirikov}}$. Only two of the resonances have partially overlapped. b) The same, with amplitude $0.3\ A_{\text{Chirikov}}$. Although, this is still below the critical value determined by Chirikov criterion, the KAM surfaces have been destroyed. Chirikov criterion overestimates the critical amplitude, by ignoring higher order resonances.

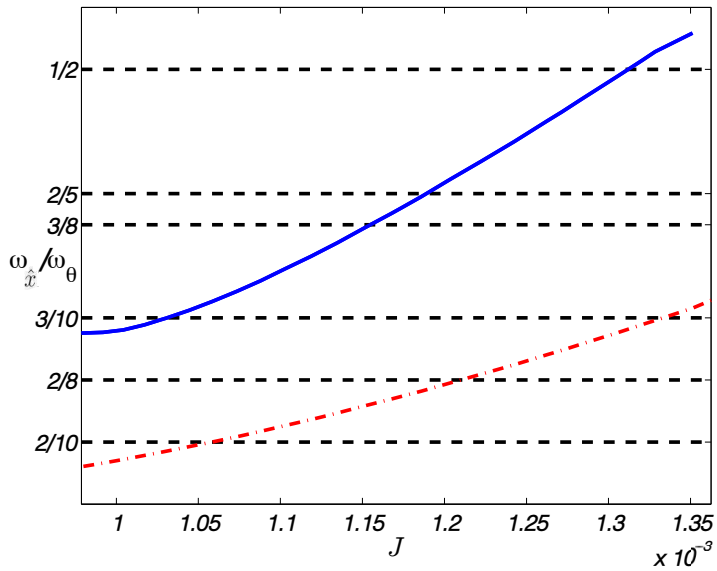

Figure 4.5 Toroidal over poloidal frequency ratio as a function of J on the energy surface B. The resonances with the $m = 8$ and $m = 10$ are located at the intersections with the horizontal dashed lines. Solid curve: The frequencies are calculated numerically through eq. 4.19 and eq. 4.20, taking into account full orbit width effects. Dashed-dotted curve: The frequencies are calculated using the closed form formulas in eq. 4.16 and eq. 4.17 under the zero orbit width assumption. The two approaches lead to qualitatively different predictions.

tained through the numerical FOW approach, eqs 4.19, 4.20, with the one obtained through the closed form approximate formulas. It is quite obvious that the two approaches predict entirely different resonance ratios and locations. Even for a LAR equilibrium, the ZOW approximation leads to incorrect predictions for the resonances experienced by energetic particles. It is expected to be more inaccurate for an equilibrium with significant triangularity and elongation (see (Zohm, 2014)), where the assumption of approximately circular magnetic surfaces is not satisfied.

Up to this point, our analysis was limited to single particle motion. However, the Action Angle formalism is ideally suited to the kinetic modelling of the *collective particle dynamics* as well. In the absence of any nonaxisymmetric perturbation, an equilibrium distribution function can be expressed as a function of any triplet of independent conserved quantities (Troia, 2012). Any such triplet would be valid, but, for the purposes of the study of the perturbed dynamics, the most useful of them is the triplet of Actions. The presence of nonaxisymmetric perturbations results in collisionless particle and momentum redistribution, either through phase mixing effects in the resonance islands, or through diffusion in phase space, when the KAM surfaces are destroyed (see Chapter 1). This implies some time evolution of the distribution function and possibly net exchange of energy and momentum between the particles and the perturbations.

In case of strong chaos, when most of the KAM surfaces have been destroyed, this process is governed by a Focker–Plank equation for the evolution of the Angle-averaged distribution function in Action space (Kaufman, 1972b, Lichtenberg and Lieberman, 1992). Since the Action variables are related to magnetic moment, parallel momentum and radial position (or energy), particle, momentum and energy transport is also described by the corresponding Action-dependent quasilinear diffusion tensor.

For perturbations for which the guiding centre approximation applies, the magnetic moment remains constant and the resonance condition is given by Eq. 4.13. At the points where the resonance condition is met, the diffusion tensor is given by

$$\bar{\mathbf{D}} = \pi \sum_{\mathbf{r}} \mathbf{r}\mathbf{r} \left|\mathcal{H}^1_{\mathbf{r}}\right|^2 \delta(\mathbf{r}\cdot\boldsymbol{\omega}), \tag{4.24}$$

where $\mathbf{r} = (s, m)$ is the vector of the harmonic numbers and $\boldsymbol{\omega} = (\omega_\theta, \omega_{\hat{\chi}})$ the vector of frequencies.

The actual diffusion tensor

$$\mathbf{D} = \begin{pmatrix} D_{J,J} & D_{J,P_\chi} \\ D_{J,P_\chi} & D_{P_\chi,P_\chi} \end{pmatrix}$$

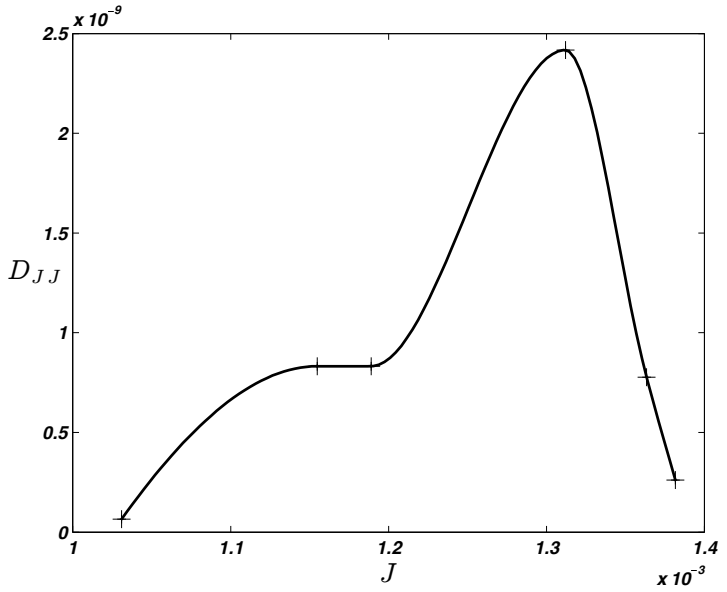

Figure 4.6 The J, J element of the quasilinear tensor for the case of Fig. 4.4b.

used in the Focker–Plank equation is a tensor whose elements smoothly interpolate the elements of the singular diffusion tensor $\bar{\mathbf{D}}$ at the resonance points, to account for the spreading of resonances, i.e. the appearance of resonance islands, due to nonlinear effects (Kaufman, 1972a). Finally, the Focker–Plank equation is given by

$$\frac{\partial}{\partial t} f\left(\mathbf{I}, \mu; t\right) \;=\; \frac{\partial}{\partial \mathbf{I}} \cdot \left(\mathbf{D} \cdot \frac{\partial}{\partial \mathbf{I}} f\left(\mathbf{I}, \mu; t\right) \right), \tag{4.25}$$

where $\mathbf{I} = (J, P_{\chi})$ is the vector of Actions and f is the distribution function (Abdullaev, 2006, Kaufman, 1972b). The fact that the diffusion tensor can be expressed explicitly in Action space is one of the many advantages of the AA formalism.

Chapter 5

Path integral theory for Orbital Spectrum Analysis

The Hamiltonian of the gyrocenter motion in unperturbed axisymmetric equilibria with no electric field is given by (see eq 4.4):

$$H_{\text{gc}} = \frac{\left(P_\zeta + \psi_p\left(p, P_\zeta\right)\right)^2}{2g^2\left(p, P_\zeta\right)} B(p, q, P_\zeta)^2 + \mu B(p, q, P_\zeta). \tag{5.1}$$

Here p and q are the canonical momentum-position pair for the poloidal motion, while P_ζ is the canonical momentum for the toroidal motion. Its conjugate position ζ is not present in the unperturbed Hamiltonian, so that P_ζ is constant. The unperturbed gyrocenter Hamiltonian is one example of the family of 2 DOM Hamiltonians with one ignorable angle, which have the form

$$H = H(p, q; F),$$

where F is the canonical momentum conjugate to the ignorable angle. For the gyrocenter Hamiltonian H_{gc}, the canonical toroidal momentum P_ζ plays the role of F. All such Hamiltonians are integrable, but in order for them to serve as the starting point for canonical perturbation analysis, they need to be expressed as functions of the Actions alone

$$K = K(J, F).$$

Calculating the Action Angle transform involves calculating a diffeomorphism (a smooth invertible function with a smooth inverse) parametrized by F

$$\phi|_F : (p, q) \to (J, \theta),$$

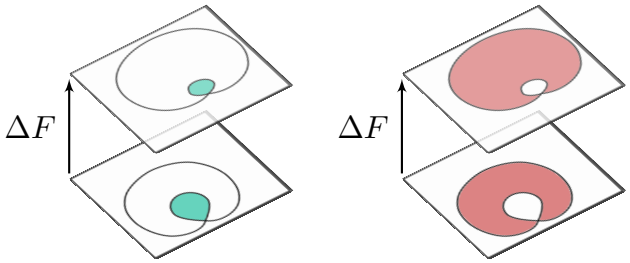

Figure 5.1 Correspondence of phase space continents for different values of F.

so that (J, θ) is a canonical pair and the new Hamiltonian K is independent of θ, i.e. $K = K(J, F)$. Doing so analytically is only practical for only a few exceptional Hamiltonians, so in general such transforms must be carried out numerically. This is, of course the numerical Action Angle transform discussed at some length in Chapter 4. As we have also pointed out, for each $F = \text{const.}$ slice of phase space, a multitude of such transforms is generally required, one for each continent bounded by a separatrix.

Calculating the Action Angle transform is half the battle. The other half is building models of $K(J, F)$ from the samples of (J, F, K) calculated through numerical integration. This requires that the samples are grouped by continent, which in turn requires the knowledge of the shape of separatrices and the location of the critical points on each $F = \text{const.}$ slice. This is by no means a trivial task, but one we had to automate, before we could carry out our calculations for Chapter 4.

For the purposes of canonical perturbation analysis, we even need to go a step further and find a way to model the derivatives of K with respect to F. For example, as we discuss in length in sec. 5.4, estimating the width of resonant islands requires the calculation of the *Hessian matrix* of K with respect to the actions. This would not present a major challenge, if there only was only one continent on each slice, but now that there are many, we need to find a way to connect associated continents on neighbouring slices with one another (see fig. 5.1). In other words, we need to model the *topological skeleton* of the unperturbed phase space. Moreover, this must be done efficiently and with no prior assumption about the number, shape and location of the phase space continents on each slice. All calculations in Chapter 4 where carried out without having automated the steps above. Matching equivalent continents on neighbouring slices relied by human inspection, which proved painstakingly slow, error– prone, hard to reproduce, counter productive and in general defied good software engineering practices that require separation of library and user code.

Building an automated tool for fast and reliable modelling of the topological skeleton of $1\ 1/2$ DOM phase spaces proved to be a very challenging task. Until this problem had been tackled successfully, Orbital Spectrum Analysis was doomed to be nothing more than

mathematical extravagance, far from the useful tool we aspired it to become. In this chapter we discuss how we came to bypass these difficulties by taking an alternative approach, one that does not presuppose any knowledge of topological characteristics, but relies only on *local* information about the unperturbed dynamics. We shall begin by calculating the derivatives of the Action Angle transform by means of path integrals along unperturbed orbits and we shall proceed to calculating the Hessian matrix of the transformed Hamiltonian K in a similar way. This improved *topology agnostic* Orbital Spectrum Analysis is benchmarked by applying it to the extended pendulum Hamiltonian, from which valuable conclusions can be drawn.

5.1 A bit of differential forms

For the calculations that follow, some elementary aspects of differential forms is necessary (Flanders, 1989). All required theorems and definitions are quoted here for reference, with no attempt for mathematical rigour.

Definition 5.1.1. A differential form of degree 1, or a 1-form on $\mathbf{R}^n$ is an expression of the form

$$\alpha = \sum_i f_i dx_i$$

Definition 5.1.2. If f is a 0-form, i.e. a smooth function on $\mathbf{R}^n$, df is the 1-form

$$df = \sum_i \frac{\partial f}{\partial x_i} dx_i.$$

The operator d is linear and satisfies a generalized Leibniz rule.

Suppose we have an open set $U \in \mathbf{R}^n$, an open set $V \in \mathbf{R}^m$. Let us denote the coordinates in V with

$$\mathbf{y} = \begin{pmatrix} y_1 \\ y_2 \\ \vdots \\ y_m \end{pmatrix}.$$

Consider now a 1-form on V

$$\alpha = \sum_i f_i dy_i,$$

where f_i are functions on V.

Now suppose a smooth function $\phi : U \to V$. Write

$$\mathbf{y} = \phi(\mathbf{x}) = \begin{pmatrix} \phi_1(x_1, x_2, \cdots, x_n) \\ \phi_2(x_1, x_2, \cdots, x_n) \\ \vdots \\ \phi_m(x_1, x_2, \cdots, x_n) \end{pmatrix}$$

Definition 5.1.3. Given a smooth map ϕ from U to V, there is an operator ϕ^* called *pullback* that maps k-forms on V to k-forms on U. Applied to 0-forms, ϕ^* gives

$$\phi^*(f_i) = f_i \circ \phi.$$

Applied to the 1-form $\alpha = \sum f_i dy_i$, ϕ^* gives

$$\phi^*(\alpha) = \sum \phi^*(f_i) d\phi_i. \tag{5.2}$$

The pullback operation is

1. linear, $\phi^*(a\alpha + b\beta) = a\phi^*(\alpha) + b\phi^*(\beta)$,
2. multiplicative, $\phi^*(\alpha\beta) = \phi^*(\alpha)\phi^*(\beta)$,
3. natural, $\phi^*\big(\psi^*(\alpha)\big) = (\psi \circ \phi)^*(\alpha)$.

Observe that the pullback operation "turns the arrow around." When ϕ maps stuff on U to stuff on V, ϕ^* maps other stuff on V to other stuff on U.

From eq. 5.2 we see that

$$\phi^*(dy_i) = d\phi_i = d(y_i \circ \phi) = d\phi^*(y_i).$$

Theorem 5.1.1. *Let $\phi : U \to V$ a smooth map and α a k-form on V, then $\phi^*(d\alpha) = d(\phi^*)$, or*

$$\boxed{\phi^* d = d\phi^*.}$$

Theorem 5.1.1 means that the exterior derivative of a differential form is independent of the coordinate system in which it is computed.

5.1.1 Path integrals of 1–forms

Let U be an open set on $\mathbf{R}^n$. A path on U is a smooth mapping $c : [a, b] \in \mathbf{R} \to U$. For our purposes we will always assume that paths are bounded. Consider a 1-form α on U. The pullback $c^*(\alpha)$ is a 1-form on $[a, b]$ so it can be written as $c^*(\alpha) = h(t)dt$.

Definition 5.1.4. The integral of a differential form α on U over the path c is defined by

$$\int_c \alpha = \int_{[a,b]} c^*(\alpha) = \int_a^b h(t)dt.$$

Note that, if $t : U \to V$ is a smooth map so that $\hat{c} = t \circ c$ is a well defined path on V and β is a 1-form on V, then

$$\int_{\hat{c}} \beta = \int_{[a,b]} \hat{c}^*(\beta) = \int_{[a,b]} (t \circ c)^*(\beta) = \int_{[a,b]} c^*(t^*(\beta)).$$

Therefore

$$\int_{\hat{c}} \beta = \int_c t^*(\beta) \tag{5.3}$$

Our calculations will be based largely on the application of eq. 5.3.

5.2 Calculation of the action derivatives

Suppose phase space U open in $\mathbf{R}^2$, with a Hamiltonian $H(p, q; F)$, where $(p, q) \in U$ and F is a real parameter. Let us define the orbit through (p_0, q_0) for $F = F_0$ as the closed path $c(p_0, q_0; F_0) \equiv c_0$ that satisfies $(p_0, q_0) \in c_0([0, 1])$ and $H(c_0(t)) = \text{const.} = H(p_0, q_0; F_0)$. Then the action at (p_0, q_0) is given by

$$J(p_0, q_0; F_0) = \frac{1}{2\pi} \oint_{c_0} pdq.$$

Suppose there is a canonical transform from the phase space $(p, q) \in U$ to the phase space $(J, \theta) \in V$ and the Hamiltonian of the new phase space has the functional form $K(J; F)$, i.e. it is independent of the angle variable θ. Then, since the transform is time independent, the two Hamiltonians are equal to one another,

$$H(p, q; F) = K(J; F)$$

and so are their differentials

$$dH = dK = \frac{\partial K}{\partial J}dJ + \frac{\partial K}{\partial F}dF = \omega\frac{\partial J}{\partial p}dp + \omega\frac{\partial J}{\partial q}dq + (\frac{\partial K}{\partial J}\frac{\partial J}{\partial F} + \frac{\partial K}{\partial F})dF \Rightarrow$$
$$\frac{\partial H}{\partial p}dp + \frac{\partial H}{\partial q}dq + \frac{\partial H}{\partial F}dF = \omega\frac{\partial J}{\partial p}dp + \omega\frac{\partial J}{\partial q}dq + (\frac{\partial K}{\partial J}\frac{\partial J}{\partial F} + \frac{\partial K}{\partial F})dF,$$

where of course ω is the frequency. Therefore,

$$\frac{\partial J}{\partial p} = \frac{1}{\omega}\frac{\partial H}{\partial p} = \frac{\dot{q}}{\omega}, \tag{5.4}$$

$$\frac{\partial J}{\partial q} = \frac{1}{\omega}\frac{\partial H}{\partial p} = -\frac{\dot{p}}{\omega}, \tag{5.5}$$

$$\frac{\partial K}{\partial F} = \frac{\partial H}{\partial F} - \omega\frac{\partial J}{\partial F}. \tag{5.6}$$

In the next sections we will show how it is possible to calculate these derivatives as path integrals over the orbit c_0.

5.2.1 The derivatives of Action in phase space.

In this subsection we will calculate how the action changes due to small translations on phase space U. The parameter F is not going to play any role, so we will temporarily omit it from our formalism. We will reintroduce it in the following subsection. Write

$$H(p+\Delta p, q+\Delta q) \approx H(p,q) + \nabla H \cdot (\Delta p, \Delta q) = H(\mathbf{x}) + \nabla H \cdot \Delta \mathbf{x},$$

where obviously $\mathbf{x} = (p,q)$. Let us introduce the steepest descend translation operator

$$\tilde{T}(\Delta H) : \mathbf{x} \to \mathbf{x} + \Delta H \frac{\nabla H}{|\nabla H|^2}$$

Then, if $\tilde{T}(\Delta p \frac{\partial H}{\partial p}\big|_{\mathbf{x_0}}) \circ c_0$ is a path,

$$\tilde{T}(\Delta p \frac{\partial H}{\partial p}\big|_{\mathbf{x_0}}) \circ c_0 = c_{\Delta p} + O(\Delta p^2),$$

where $c_{\Delta p}$ is the orbit through $(p+\Delta p, q)$. Let us use $\tilde{T}_0 = \tilde{T}(\Delta p \frac{\partial H}{\partial p}\big|_{\mathbf{x_0}})$, for brevity The Action at $(p+\Delta p, q)$ is given by

$$J(p+\Delta p, q) \approx \frac{1}{2\pi}\oint_{\tilde{T}_0 \circ c_0} pdq = \frac{1}{2\pi}\oint_{c_0} \tilde{T}_0^{\,*}(pdq).$$

We have managed to express the Action at the translated point as an integral over the original orbit. All that is left is to calculate the 1-form $\tilde{T}_0^{\,*}(pdq)$. We have

$$\tilde{T}_0^{\,*}(p) = p + \Delta p \frac{\partial H}{\partial p}\big|_{\mathbf{x_0}} \frac{\partial_p H}{|\nabla H|^2} = p + \Delta H \frac{\partial_p H}{|\nabla H|^2}$$

and

$$\tilde{T}_{0,q} = q + \Delta H \frac{\partial_q H}{|\nabla H|^2}$$

Therefore

$$d\tilde{T}_{0,q} = dq + \Delta H d\left(\frac{\partial_q H}{|\nabla H|^2}\right),$$

So that

$$\begin{aligned}\tilde{T_0}^*(pdq) &= \left(p + \Delta H \frac{\partial_p H}{|\nabla H|^2}\right)\left(dq + \Delta H d\left(\frac{\partial_q H}{|\nabla H|^2}\right)\right) \\ &= pdq + \Delta H\left[\frac{\partial_p H}{|\nabla H|^2}dq + pd\left(\frac{\partial_q H}{|\nabla H|^2}\right)\right] + O(\Delta H^2).\end{aligned}$$

Therefore the partial derivative of J with respect to p is given by the integral over the orbit

$$\boxed{\frac{\partial J}{\partial p} = \frac{1}{2\pi}\frac{\partial H}{\partial p}\Big|_{\mathbf{x_0}} \oint_{c_0} \frac{\partial_p H}{|\nabla H|^2}dq + pd\left(\frac{\partial_q H}{|\nabla H|^2}\right).} \tag{5.7}$$

Comparing eq. 5.4 and eq. 5.7 we see that the integral above is equal to the orbit period, or that

$$\boxed{\frac{1}{\omega} = \frac{1}{2\pi}\oint_{c_0} \frac{\partial_p H}{|\nabla H|^2}dq + pd\left(\frac{\partial_q H}{|\nabla H|^2}\right),} \tag{5.8}$$

a result which will later prove useful.

5.2.2 The derivative of Action with respect to the free parameter

In this subsection we reintroduce the dependence on the parameter F. We follow the path we took in the previous calculation, but now instead of varying the initial point in phase space, we vary the value of F. We have

$$H(\mathbf{x_0}; F_0 + \Delta F) = H(\mathbf{x_0}; F_0) + \frac{\partial H}{\partial F}\Big|_0 \Delta F + O(\Delta F^2)$$

and of course

$$H(\mathbf{x_0} + \Delta\mathbf{x}; F_0 + \Delta F) \approx H(\mathbf{x_0}; F_0) + \nabla H \cdot \Delta\mathbf{x} + \frac{\partial H}{\partial F}\Big|_0 \Delta F.$$

Let us denote with $c_0 = c(\mathbf{x_0}; F_0)$ the orbit through (p_0, q_0) for $F = F_0$ and $c_{\Delta F} = c(\mathbf{x_0}; F_0 + \Delta F)$ the orbit through the same point (p_0, q_0) for $F = F_0 + \Delta F$. As we did

earlier, we seek a smooth transformation that approximately maps c_0 on $c_{\Delta F}$ up to first order on ΔF.

Proposition 5.2.1. *Let $\tilde{T}(\Delta H)$ a translation operator so that*

$$\tilde{T}(\Delta H) : \mathbf{x} \to \mathbf{x} + \Delta H \frac{\nabla H}{|\nabla H|^2}$$

as before. Then, if $\tilde{T}\left(\Delta F\left[\frac{\partial H}{\partial F}|_0 - \frac{\partial H}{\partial F}\right]\right) \circ c_0$ is a path,

$$\tilde{T}\left(\Delta F\left[\frac{\partial H}{\partial F}|_0 - \frac{\partial H}{\partial F}\right]\right) \circ c_0 = c_{\Delta F} + O(\Delta p^2).$$

Proof. Let us write $\tilde{T}$ for $\tilde{T}\left(\Delta F\left[\frac{\partial H}{\partial F}|_0 - \frac{\partial H}{\partial F}\right]\right)$, for simplicity. It is sufficient to show that if $\mathbf{x} \in c_0$ is a point on the initial orbit , then the value of the Hamiltonian at the translated point $H(\tilde{T}\mathbf{x}; F_0 + \Delta F)$ is almost equal to the value of the Hamiltonian at the initial point $H(\mathbf{x_0}; F_0 + \Delta F)$, so that the translated point $\mathbf{x}' = \tilde{T}\mathbf{x}$ is very close to the orbit $c_{\Delta F}$ through $\mathbf{x_0}$ for $F = F_0$. Indeed we have

$$\begin{aligned} H(\tilde{T}\mathbf{x}; F_0 + \Delta F) &= H(\mathbf{x} + \Delta\mathbf{x}; F_0 + \Delta F) \approx H(\mathbf{x}; F_0) + \nabla H \cdot \Delta\mathbf{x} + \frac{\partial H}{\partial F}\Delta F \\ &= H(\mathbf{x}; F_0) + \nabla H \cdot \frac{\nabla H}{|\nabla H|^2}\left[\frac{\partial H}{\partial F}|_0 - \frac{\partial H}{\partial F}\right]\Delta F + \frac{\partial H}{\partial F}\Delta F \\ &= H(\mathbf{x}; F_0) + \left[\frac{\partial H}{\partial F}|_0 - \frac{\partial H}{\partial F}\right]\Delta F + \frac{\partial H}{\partial F}\Delta F \\ &= H(\mathbf{x}; F_0) + \frac{\partial H}{\partial F}|_0 \Delta F. \end{aligned}$$

But, since $\mathbf{x}$ is a point on the initial orbit,

$$H(\mathbf{x}; F_0) = H(\mathbf{x_0}; F_0)$$

so that

$$H(\tilde{T}\mathbf{x}; F_0 + \Delta F) = H(\mathbf{x_0}; F_0) + \frac{\partial H}{\partial F}|_0 \Delta F \approx H(\mathbf{x_0}; F_0 + \Delta F),$$

which proves our point. □

Proceeding as before, we can calculate the action

$$J(\mathbf{x_0}; F_0 + \Delta F) \approx \frac{1}{2\pi}\oint_{\tilde{T}\circ c} pdq = \frac{1}{2\pi}\oint_c \tilde{T}^*(pdq).$$

We have

$$\tilde{T}^*(p) = p + \left(\frac{\partial H}{\partial F}\Big|_0 - \frac{\partial H}{\partial F}\right)\frac{\partial_p H}{|\nabla H|^2}\Delta F$$

and

$$\begin{aligned}
\tilde{T}^*(dq) = d\tilde{T}_q &= dq + d\left(\Delta H \frac{\partial_q H}{|\nabla H|^2}\right) \\
&= dq + d\left(\Delta H\right)\frac{\partial_q H}{|\nabla H|^2} + \Delta H d\left(\frac{\partial_q H}{|\nabla H|^2}\right) \\
&= dq + \Delta F\left[-d\left(\frac{\partial H}{\partial F}\right)\frac{\partial_q H}{|\nabla H|^2} - \frac{\partial H}{\partial F}d\left(\frac{\partial_q H}{|\nabla H|^2}\right) + \frac{\partial H}{\partial F}\Big|_0 d\left(\frac{\partial_q H}{|\nabla H|^2}\right)\right] \\
&= dq + \Delta F\left[\frac{\partial H}{\partial F}\Big|_0 d\left(\frac{\partial_q H}{|\nabla H|^2}\right) - d\left(\frac{\partial H}{\partial F}\frac{\partial_q H}{|\nabla H|^2}\right)\right].
\end{aligned}$$

Therefore, the pulled back 1 -form is up to first order

$$\begin{aligned}
\tilde{T}^*(pdq) = pdq &+ \Delta F\left(\frac{\partial H}{\partial F}\Big|_0 - \frac{\partial H}{\partial F}\right)\frac{\partial_p H}{|\nabla H|^2}dq \\
&+ p\Delta F\left[\frac{\partial H}{\partial F}\Big|_0 d\left(\frac{\partial_q H}{|\nabla H|^2}\right) - d\left(\frac{\partial H}{\partial F}\frac{\partial_q H}{|\nabla H|^2}\right)\right] \\
&= pdq + \Delta F\frac{\partial H}{\partial F}\Big|_0\left[\frac{\partial_p H}{|\nabla H|^2}dq + pd\left(\frac{\partial_q H}{|\nabla H|^2}\right)\right] \\
&- \Delta F\left[\frac{\partial H}{\partial F}\frac{\partial_p H}{|\nabla H|^2}dq + pd\left(\frac{\partial H}{\partial F}\frac{\partial_q H}{|\nabla H|^2}\right)\right]
\end{aligned}$$

And

$$\begin{aligned}
\frac{\partial J}{\partial F} =& \frac{1}{2\pi}\frac{\partial H}{\partial F}\Big|_0 \oint_c \frac{\partial_p H}{|\nabla H|^2}dq + pd\left(\frac{\partial_q H}{|\nabla H|^2}\right) \\
&- \frac{1}{2\pi}\oint_c \frac{\partial H}{\partial F}\frac{\partial_p H}{|\nabla H|^2}dq + pd\left(\frac{\partial H}{\partial F}\frac{\partial_q H}{|\nabla H|^2}\right).
\end{aligned}$$

Of the two terms above only the first depends on the initial point of the differentiation, through the dependence of the local derivative with respect to the free parameter. On the other hand, the two path integrals that appear above depend only on the whole orbit and are independent of the initial point $\mathbf{x}_0$. By comparing with eq. 5.8, the above becomes

$$\frac{\partial J}{\partial F} = \frac{1}{\omega}\frac{\partial H}{\partial F}\Big|_0 - \frac{1}{2\pi}\oint_c \frac{\partial H}{\partial F}\frac{\partial_p H}{|\nabla H|^2}dq + pd\left(\frac{\partial H}{\partial F}\frac{\partial_q H}{|\nabla H|^2}\right). \tag{5.9}$$

From eq. 5.6, we get

$$\frac{\partial K}{\partial F} = \frac{\partial H}{\partial F}\Big|_0 - \omega \frac{\partial J}{\partial F},$$

or

$$\boxed{\frac{\partial K}{\partial F} = \frac{\omega}{2\pi}\oint_c \frac{\partial H}{\partial F}\frac{\partial_p H}{|\nabla H|^2}dq + pd\left(\frac{\partial H}{\partial F}\frac{\partial_q H}{|\nabla H|^2}\right),} \tag{5.10}$$

where, as expected, the dependence on the specific point of reference $\mathbf{x_0}$ has disappeared and only the dependence on the whole closed orbit remains.

5.2.3 Application: Parametrized harmonic oscillator

Let us verify our findings, by applying them to the parametrized harmonic oscillator Hamiltonian

$$H = p^2 + Fq^2,$$

with $F > 0$ the spring constant. The orbit at $H = \text{const.} = E$ can be parametrized by

$$c : t \to \begin{matrix} q = \sqrt{\frac{E}{F}}\sin(t) \\ p = \sqrt{E}\cos(t) \end{matrix}.$$

The calculation of the Action is straightforward.

$$J = \frac{1}{2\pi}\oint_c pdq = \frac{1}{2\pi}\oint_0^{2\pi} \sqrt{E}\cos(t)\sqrt{\frac{E}{F}}\cos(t)dt = \frac{E}{2\sqrt{F}}.$$

Therefore

$$K(J;F) = 2\sqrt{F}J,$$
$$\frac{\partial K}{\partial J} = 2\sqrt{F}$$
$$\frac{\partial K}{\partial F} = \frac{J}{\sqrt{F}}.$$

Let us now apply eqs. 5.8, 5.10 to verify that they replicate the results above.

We have

$$\partial_p H = 2p,$$
$$\partial_q H = 2Fq,$$
$$|\nabla H|^2 = 4p^2 + 4F^2q^2$$

,

$$\frac{\partial_p H}{|\nabla H|^2} = \frac{2p}{4p^2 + 4F^2q^2},$$
$$\frac{\partial_q H}{|\nabla H|^2} = \frac{2Fq}{4p^2 + 4F^2q^2}.$$

Skipping some tedious algebra, we have

$$\oint_c \frac{\partial_p H}{|\nabla H|^2} dq = \frac{\pi}{\sqrt{F} + F}$$

and

$$\oint_c pd\left(\frac{\partial_q H}{|\nabla H|^2}\right) = \frac{\pi}{\sqrt{F} + 1},$$

So that

$$\frac{1}{\omega} = \frac{1}{2\pi}\oint_{c_0} \frac{\partial_p H}{|\nabla H|^2} dq + pd\left(\frac{\partial_q H}{|\nabla H|^2}\right) = \frac{1}{2\pi}\frac{\pi}{\sqrt{F}} = \frac{1}{2\sqrt{F},}$$

as expected.

Similarly

$$\oint_c \frac{\partial H}{\partial F}\frac{\partial_p H}{|\nabla H|^2} dq = \oint_c q^2 \frac{2p}{4p^2 + 4F^2q^2} dq = \frac{E\pi}{2\left(1 + \sqrt{F}\right)^2 F^{3/2}}$$

and

$$\oint_c pd\left(\frac{\partial H}{\partial F}\frac{\partial_q H}{|\nabla H|^2}\right) = \frac{E\left(2 + \sqrt{F}\right)\pi}{2\left(1 + \sqrt{F}\right)^2 F}$$

so that

$$\begin{aligned}\frac{\partial K}{\partial F} &= \frac{\omega}{2\pi}\oint_c \frac{\partial H}{\partial F}\frac{\partial_p H}{|\nabla H|^2} dq + pd\left(\frac{\partial H}{\partial F}\frac{\partial_q H}{|\nabla H|^2}\right) \\ &= \frac{\omega}{2\pi}\left[\frac{E\pi}{2\left(1 + \sqrt{F}\right)^2 F^{3/2}} + \frac{E\left(2 + \sqrt{F}\right)\pi}{2\left(1 + \sqrt{F}\right)^2 F}\right] \\ &= \frac{2\sqrt{F}}{2\pi}\frac{E\pi}{2F^{3/2}} = \frac{E}{2F} = \frac{J}{\sqrt{F}},\end{aligned}$$

again as expected.

5.3 Generalization to arbitrary integrals of motion

In this section, we build on the experience gained from the previous introductory section to clean up our formalism and derive more general conclusions. This approach will enable us to derive expressions for the calculation of the Jacobian of the Hamiltonian $K(J, F)$ as path integrals.

5.3.1 The bracket operator

Here we define the *bracket operator*, which will be of significant importance for what is to follow.

Definition 5.3.1. For any vector field $\mathbf{v} = (v_p, v_q)$, we define the bracket operator, which maps any one-form $\alpha = \alpha_p dp + \alpha_q dq$ to the one-form

$$[\mathbf{v}, \alpha] = (\partial_p \alpha_q - \partial_q \alpha_p)(v_p dq - v_q dp) + d(\mathbf{v} \cdot \alpha), \tag{5.11}$$

where

$$\mathbf{v} \cdot \alpha \equiv v_p \alpha_p + v_q \alpha_q$$

Proposition 5.3.1 reveals the elegant connection between the bracket operator and the pullback of a near identity transformation on a one-form. As we shall see in the next subsection, the bracket operator is closely connected to the derivatives of path integrals.

Proposition 5.3.1. *Consider a near identity infinitesimal transform $\phi_\epsilon : \mathbf{R}^2 \to \mathbf{R}^2$, with $\phi_\epsilon(\mathbf{x}) = \mathbf{x} + \epsilon \mathbf{v}(\mathbf{x})$ and $\mathbf{v} = (v_p, v_q)$. Also consider a one form $\alpha = \alpha_p dp + \alpha_q dq$. Then up to first order in ϵ the pullback of ϕ_ϵ on α can be written in terms of the bracket operator (eq. 5.11) as*

$$\phi_\epsilon^*(\alpha) = \alpha + \epsilon[\mathbf{v}, \alpha].$$

Proof. By definition, the pullback of ϕ_ϵ on α is

$$\phi_\epsilon^*(\alpha) = \phi_\epsilon^*(\alpha_p) d\phi_{\epsilon,p} + \phi_\epsilon^*(\alpha_q) d\phi_{\epsilon,q}.$$

The differentials of the zero forms $\phi_{\epsilon,i}$ are given by

$$d\phi_{\epsilon,p} = dp + \epsilon \frac{\partial v_p}{\partial p} dp + \epsilon \frac{\partial v_p}{\partial q} dq$$

and

$$d\phi_{\epsilon,q} = dq + \epsilon \frac{\partial v_q}{\partial p} dp + \epsilon \frac{\partial v_q}{\partial q} dq$$

and the pullback of ϕ_ϵ on the zero forms α_i is up to first order

$$\phi_\epsilon^*(\alpha_i) = \alpha_i + \epsilon\frac{\partial \alpha_i}{\partial p}v_p + \epsilon\frac{\partial \alpha_i}{\partial q}v_q + O(\epsilon^2).$$

Therefore

$$\begin{aligned}
\phi_\epsilon^*(\alpha) &= [\alpha_p + \epsilon\frac{\partial \alpha_p}{\partial p}v_p + \epsilon\frac{\partial \alpha_p}{\partial q}v_q][dp + \epsilon\frac{\partial v_p}{\partial p}dp + \epsilon\frac{\partial v_p}{\partial q}dq] \\
&\quad + [\alpha_q + \epsilon\frac{\partial \alpha_q}{\partial p}v_p + \epsilon\frac{\partial \alpha_q}{\partial q}v_q][dq + \epsilon\frac{\partial v_q}{\partial p}dp + \epsilon\frac{\partial v_q}{\partial q}dq] + O(\epsilon^2) \\
&= \alpha + \epsilon[\frac{\partial a_p}{\partial q}v_q dp + \frac{\partial a_p}{\partial p}v_p dp + \alpha_p\frac{\partial v_p}{\partial p}dp + \alpha_p\frac{\partial v_p}{\partial q}dq \\
&\quad + \frac{\partial a_q}{\partial q}v_q dq + \frac{\partial a_q}{\partial p}v_p dq + \alpha_q\frac{\partial v_q}{\partial p}dp + \alpha_q\frac{\partial v_q}{\partial q}dq] + O(\epsilon^2) \\
&= \alpha + \epsilon[\frac{\partial a_p}{\partial q}v_q dp + \left(\frac{\partial}{\partial p}(\alpha_p v_p)dp + \alpha_p\frac{\partial v_p}{\partial q}dq + \frac{\partial a_p}{\partial q}v_p dq\right) - \frac{\partial a_p}{\partial q}v_p dq \\
&\quad + \frac{\partial a_q}{\partial p}v_p dq + \left(\frac{\partial}{\partial q}(\alpha_q v_q)dq + \alpha_q\frac{\partial v_q}{\partial p}dp + \frac{\partial a_q}{\partial p}v_q dp\right) - \frac{\partial a_q}{\partial p}v_q dp] + O(\epsilon^2) \\
&= \alpha + \epsilon[\frac{\partial a_p}{\partial q}v_q dp - \frac{\partial a_p}{\partial q}v_p dq + d(\alpha_p v_p) \\
&\quad + \frac{\partial a_q}{\partial p}v_p dq - \frac{\partial a_q}{\partial p}v_q dp + d(\alpha_p v_p)] + O(\epsilon^2),
\end{aligned}$$

or, more compactly

$$\begin{aligned}
\phi_\epsilon^*(\alpha) &= \alpha + \epsilon[(\partial_q\alpha_p - \partial_p\alpha_q)v_q dp + (\partial_p\alpha_q - \partial_q\alpha_p)v_p dq + d(\mathbf{v}\cdot\alpha)] + O(\epsilon^2) \\
&= \alpha + (\partial_p\alpha_q - \partial_q\alpha_p)(v_p dq - v_q dp) + d(\mathbf{v}\cdot\alpha) + O(\epsilon^2) \\
&= \alpha + \epsilon[\mathbf{v}, \alpha] + O(\epsilon^2),
\end{aligned}$$

where

$$[\mathbf{v}, \alpha] = (\partial_p\alpha_q - \partial_q\alpha_p)(v_p dq - v_q dp) + d(\mathbf{v}\cdot\alpha).$$

□

5.3.2 Derivatives of path integrals

Suppose that s is an *explicit integral of motion*, i.e.

$$s(\mathbf{x_0}; F_0) = \oint_{c_0}\alpha = \oint_{c_0}\alpha_p dp + \alpha_q dq,$$

where c_0 is the orbit path passing through $\mathbf{x_0} = (p_0, q_0)$ for $F = F_0$. In other words c_0 is the closed path $c_0 \equiv c(p_0, q_0; F_0)$ that satisfies $(p_0, q_0) \in c_0([0,1])$ and $H(c_0(t)) = \text{const.} = H(p_0, q_0; F_0)$. We are interested in calculating the derivatives of explicit integrals of motion. We should distinguish between the derivatives due to translation in phase space $\mathbf{x} \to \mathbf{x} + \Delta\mathbf{x}$ and the derivative due to the variation of the free parameter $F \to F + \Delta F$.

A translation in phase space changes the starting point of the orbit path and this may or may not lead to a change in the path integral, depending on whether or not the new starting point lies on a different path than the original. If the translation takes place on a direction perpendicular to ∇H, the integral of motion s should remain unchanged.

Theorem 5.3.1. *If $s(\mathbf{x_0}; F_0) = \oint_{c_0} \alpha = \oint_{c_0} \alpha_p dp + \alpha_q dq$ is an explicit integral of motion, then*

$$\boxed{\nabla s = \nabla H \oint [\mathbf{f}, \alpha]\,,} \tag{5.12}$$

where

$$\mathbf{f} = \frac{\nabla H}{|\nabla H|^2} = \left(\frac{\partial_p H}{|\nabla H|^2}, \frac{\partial_q H}{|\nabla H|^2} \right).$$

Proof. First consider a translation in p, i.e. $\mathbf{x_0} = (p_0, q_0) \to \mathbf{x_1} = (p_0 + \Delta p, q_0)$ and the associated transformation in c_0, i.e. $c_0 \to c_{\Delta p}$. We seek a near identity transformation that takes c_0 to $c_{\Delta p}$ up to first order in Δp. As shown in subsection 5.2.1, the transformation

$$T_p : \mathbf{x} \to x + \Delta p \frac{\partial H}{\partial p}\Big|_0 \mathbf{f}(\mathbf{x}),$$

with

$$\mathbf{f}(\mathbf{x}) = \frac{\nabla H}{|\nabla H|^2}$$

satisfies these requirements. Then up to first order in Δp

$$s(\mathbf{x_1}) = \oint_{T_p \circ c_0} \alpha + O(\Delta p^2) = \oint_{c_0} T_p^*(\alpha) + O(\Delta p^2)$$

By virtue of proposition 5.3.1, this can be written as

$$s(\mathbf{x_1}) = \oint_{c_0} \alpha + [\Delta p \frac{\partial H}{\partial p}\Big|_0 \mathbf{f}, \alpha] + O(\Delta p^2) = s(\mathbf{x_0}) + \oint_{c_0} [\Delta p \frac{\partial H}{\partial p}\Big|_0 \mathbf{f}, \alpha] + O(\Delta p^2),$$

which, due to the bilinearity of the bracket operator can be further simplified to

$$s(\mathbf{x_0}) = s(\mathbf{x_0}) + \Delta p \frac{\partial H}{\partial p}\Big|_0 \oint_{c_0} [\mathbf{f}, \alpha] + O(\Delta p^2),$$

which means that

$$\frac{\partial s}{\partial p} = \frac{\partial H}{\partial p}|_0 \oint_{c_0} [\mathbf{f}, \alpha].$$

Similarly

$$\frac{\partial s}{\partial q} = \frac{\partial H}{\partial q}|_0 \oint_{c_0} [\mathbf{f}, \alpha],$$

Or, combining the two formulas above in a single formula

$$\nabla s = \nabla H \oint [\mathbf{f}, \alpha]$$

□

When the parameter F varies, the integral of motion s should in general change as well, but now there are two distinct ways through which the variation in F can lead to a change in the quantity s. As before, change in F might induce a deformation in the path c_0, which might result in a change of the value of the path integral. The other reason s might vary is due to any explicit dependence of the one-form α on F, which should result in a contribution of the form

$$\oint_{c_0} \frac{\partial \alpha}{\partial F}$$

to the total variation of s.

Theorem 5.3.2. *If $s(\mathbf{x_0}; F_0)$ is an explicit integral of motion with*

$$s(\mathbf{x_0}; F_0) = \oint_{c_0} \alpha = \oint_{c_0} \alpha_p dp + \alpha_q dq,$$

then

$$\boxed{\frac{\partial s}{\partial F} = \partial_F H \oint_{c_0} [\mathbf{f}, \alpha] + \oint_{c_0} D_F [\alpha]} \tag{5.13}$$

where

$$\boxed{D_F [\alpha] \equiv \partial_F \alpha - [(\partial_F H)\mathbf{f}, \alpha]} \tag{5.14}$$

and, as usual,

$$\mathbf{f} = \frac{\nabla H}{|\nabla H|^2} = \left(\frac{\partial_p H}{|\nabla H|^2}, \frac{\partial_q H}{|\nabla H|^2} \right).$$

Proof. Consider a variation in the free parameter $F_0 \to F_0 + \Delta F$. Then

$$s(\mathbf{x_0}; F_0 + \Delta F) = \oint_{c_{\Delta F}} \alpha(\mathbf{x}; F_0 + \Delta F),$$

where $c_{\Delta F}$ is the deformed path through $\mathbf{x_0}$, due to ΔF.

As in the previous proof, we seek a near identity transformation that takes c_0 to $c_{\Delta F}$ up to first order in ΔF. As shown in subsection 5.2.2, the transformation

$$T_F : \mathbf{x} \to \mathbf{x} + \Delta F \left[\frac{\partial H}{\partial F}\Big|_0 - \frac{\partial H}{\partial F} \right] \mathbf{f},$$

with

$$\mathbf{f}(\mathbf{x}) = \frac{\nabla H}{|\nabla H|^2}$$

as above, satisfies these requirements.

Therefore

$$\begin{aligned}
&s(\mathbf{x_0}; F_0 + \Delta F) = \oint_{c_{\Delta F}} \alpha(\mathbf{x}; F_0 + \Delta F) = \oint_{T_F \circ c_0} \alpha(\mathbf{x}; F_0 + \Delta F) + O(\Delta F^2) \\
&= \oint_{c_0} T_F^*(\alpha(\mathbf{x}; F_0 + \Delta F)) + O(\Delta F^2) \\
&= \oint_{c_0} (\alpha(\mathbf{x}; F_0 + \Delta F)) + \Delta F \oint_{c_0} [(\partial_F H\big|_0 - \partial_F H)\mathbf{f}, \alpha(\mathbf{x}; F_0 + \Delta F)] + O(\Delta F^2) \\
&= \oint_{c_0} (\alpha(\mathbf{x}; F_0) + \Delta F \oint_{c_0} \frac{\partial \alpha}{\partial F}(\mathbf{x}; F_0) \\
&+ \Delta F \partial_F H\big|_0 \oint_{c_0} [\mathbf{f}, \alpha(\mathbf{x}; F_0)] - \Delta F \oint_{c_0} [(\partial_F H)\mathbf{f}, \alpha(\mathbf{x}; F_0)] + O(\Delta F^2) \\
&= s(\mathbf{x}; F_0) + \Delta F \left[\oint_{c_0} \partial_F \alpha + \partial_F H\big|_0 \oint_{c_0} [\mathbf{f}, \alpha] - \oint_{c_0} [(\partial_F H)\mathbf{f}, \alpha] \right] + O(\Delta F^2).
\end{aligned}$$

Therefore

$$\begin{aligned}
\frac{\partial s}{\partial F} &= \partial_F H \oint_{c_0} [\mathbf{f}, \alpha] - \oint_{c_0} [(\partial_F H)\mathbf{f}, \alpha] + \oint_{c_0} \partial_F \alpha \\
&= \partial_F H \oint_{c_0} [\mathbf{f}, \alpha] + \oint_{c_0} D_F [\alpha]
\end{aligned}$$

□

Applying eq. 5.12 and eq. 5.13 to the action integral

$$J = \frac{1}{2\pi} \oint p dq,$$

we get

$$\nabla J = \frac{1}{2\pi}\nabla H \oint [\mathbf{f}, pdq] \tag{5.15a}$$

$$\frac{\partial J}{\partial F} = \frac{1}{2\pi}\partial_F H \oint_{c_0} [\mathbf{f}, pdq] - \frac{1}{2\pi}\oint_{c_0} [(\partial_F H)\mathbf{f}, pdq]\,. \tag{5.15b}$$

It is easily verified that the above expressions are compatible with eq. 5.7 and eq. 5.9. We will come across the one-forms and the path integrals that appear above so often that it is reasonable to give them a name. Let us define

$$\beta = 2\pi\,[\mathbf{f}, pdq]\,, \tag{5.16a}$$

$$T = \oint [\mathbf{f}, pdq] = \frac{1}{2\pi}\oint \beta \tag{5.16b}$$

and

$$\gamma = [(\partial_F H)\mathbf{f}, pdq]\,, \tag{5.17a}$$

$$G = \frac{1}{2\pi}\oint_{c_0} [(\partial_F H)\mathbf{f}, pdq] = \frac{1}{2\pi}\oint \gamma \tag{5.17b}$$

As we shall show in the next section, T is the orbital period on the (p, q) plane, while G is the ratio

$$G = \frac{\omega_F}{\omega},$$

where ω is the orbital frequency on the (p, q) plane and ω_F is the orbital frequency on the (ζ, F) plane. With these definitions in mind, the equations for the derivatives of the action J become:

$$\nabla J = \frac{T}{2\pi}\nabla H \tag{5.18a}$$

$$\frac{\partial J}{\partial F} = \frac{T}{2\pi}\partial_F H - G. \tag{5.18b}$$

5.3.3 Calculating the derivatives of Action quantities

The Action Angle transform can be regarded as a mapping Φ from the configuration manifold U to the action manifold V,

$$\Phi : (p, q, F) \in U \to (J, \theta, F) \in V$$

We use the coordinates (p, q, F) for points in the configuration space U and (J, θ, F) for points in the action space V, fig. 5.2

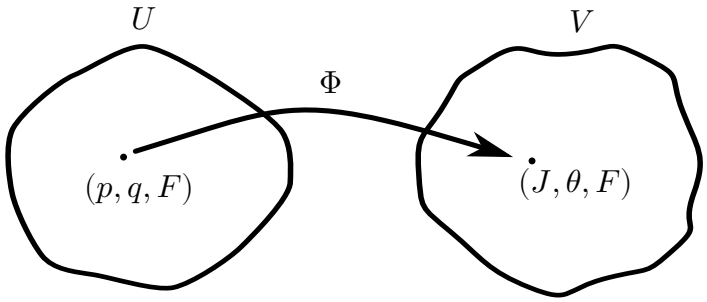

Figure 5.2 The Action Angle transform Φ as a mapping from the configuration manifold U to the action manifold V. We use the coordinates (p, q, F) for points in U and (J, θ, F) for points in V.

We say that a function $s : U \to \mathbf{R}$ is an *action quantity*, or an implicit integral of motion, if s is constant along any orbit in U. Then for any $s : U \to \mathbf{R}$, there is a function $S : V \to \mathbf{R}$ so that S is independent of θ, i.e. $S = S(J, F)$ and

$$s = \Phi^* S = S \circ \Phi.$$

By virtue of theorem 5.1.1, $ds = d(\Phi^* S) = \Phi^*(dS)$, so that, expanding the differentials on both sides of the equation, we get

$$\frac{\partial s}{\partial p}dp + \frac{\partial s}{\partial q}dq + \frac{\partial s}{\partial F}dF = \Phi^* \left(\frac{\partial S}{\partial J}dJ\right) + \Phi^* \left(\frac{\partial S}{\partial F}dF\right).$$

But,

$$\Phi^*(dJ) = d\Phi_J = \frac{\partial J}{\partial p}dp + \frac{\partial J}{\partial q}dq + \frac{\partial J}{\partial F}dF$$

and

$$\Phi^*(dF) = dF,$$

so that

$$\frac{\partial s}{\partial p}dp + \frac{\partial s}{\partial q}dq + \frac{\partial s}{\partial F}dF = \left(\Phi^* \frac{\partial S}{\partial J}\right)\left[\frac{\partial J}{\partial p}dp + \frac{\partial J}{\partial q}dq + \frac{\partial J}{\partial F}dF\right] + \left(\Phi^* \frac{\partial S}{\partial F}\right)dF.$$

Which means that,

$$\begin{aligned}
\frac{\partial s}{\partial p} &= \left(\Phi^* \frac{\partial S}{\partial J}\right) \frac{\partial J}{\partial p} \\
\frac{\partial s}{\partial q} &= \left(\Phi^* \frac{\partial S}{\partial J}\right) \frac{\partial J}{\partial q} \\
\frac{\partial s}{\partial F} &= \left(\Phi^* \frac{\partial S}{\partial J}\right) \frac{\partial J}{\partial F} + \left(\Phi^* \frac{\partial S}{\partial F}\right),
\end{aligned}$$

Or, equivalently

$$\begin{aligned}
\nabla s &= \left(\Phi^* \frac{\partial S}{\partial J}\right) \nabla J \\
\frac{\partial s}{\partial F} &= \left(\Phi^* \frac{\partial S}{\partial J}\right) \frac{\partial J}{\partial F} + \left(\Phi^* \frac{\partial S}{\partial F}\right).
\end{aligned}$$

By substituting eqs. 5.18 in the above, we get

$$\boxed{\begin{aligned}
\nabla s &= \frac{T}{2\pi} \left(\Phi^* \frac{\partial S}{\partial J}\right) \nabla H && \text{(5.19a)} \\
\frac{\partial s}{\partial F} &= \left(\Phi^* \frac{\partial S}{\partial J}\right) \left(\frac{T}{2\pi} \frac{\partial H}{\partial F} - G\right) + \left(\Phi^* \frac{\partial S}{\partial F}\right). && \text{(5.19b)}
\end{aligned}}$$

The meaning of the special path integrals T and G

If $H(p, q, F)$ is the Hamiltonian in U and $K(J, F)$ the Hamiltonian in V, the relation between them is

$$H = \Phi^* K = K \circ \Phi,$$

Then, from eq. 5.19a, we have

$$\nabla H = \left(\Phi^* \frac{\partial K}{\partial J}\right) \nabla J.$$

But, from eq. 5.18a, we have

$$\nabla J = \frac{T}{2\pi} \nabla H = \nabla H \oint [\mathbf{f}, p dq],$$

so that

$$\nabla H = \left(\Phi^* \frac{\partial K}{\partial J}\right) \frac{T}{2\pi} \nabla H,$$

from which we conclude that

$$\Phi^* \frac{\partial K}{\partial J} = \frac{2\pi}{T} = \frac{4\pi^2}{\oint \beta}. \tag{5.20}$$

But the derivative of the Hamiltonian K in Action Angle space with respect to the Action J is equal to the orbital frequency ω on the (p, q) plane and the expression

$$\omega = \Phi^* \frac{\partial K}{\partial J},$$

should be interpreted as the frequency ω expressed as a function on U. It then follows that the explicit integral of motion

$$T = \oint [\mathbf{f}, pdq] = \frac{1}{2\pi} \oint \beta = \frac{2\pi}{\omega}$$

is indeed equal to the orbital period on the (p, q) plane.

Moreover, applying eq. 5.19b to the pair H and K, we get

$$\begin{aligned} \frac{\partial H}{\partial F} &= \left(\Phi^* \frac{\partial K}{\partial J}\right) \left(\frac{T}{2\pi} \frac{\partial H}{\partial F} - G\right) + \left(\Phi^* \frac{\partial K}{\partial F}\right) \\ &= \omega \left(\frac{1}{\omega} \frac{\partial H}{\partial F} - G\right) + \left(\Phi^* \frac{\partial K}{\partial F}\right), \end{aligned}$$

or

$$\Phi^* \frac{\partial K}{\partial F} = \omega G.$$

Again the derivative of the Hamiltonian K in Action Angle space with respect to the Action F is equal to the orbital frequency ω_F on the (ζ, F) plane and the expression

$$\omega_F = \Phi^* \frac{\partial K}{\partial F},$$

should be interpreted as the frequency ω_F expressed as a function on U. We have thus proved our assertion that the explicit integral of motion

$$G = \frac{1}{2\pi} \oint \gamma$$

is equal to the ratio of the orbital frequencies ω_F and ω, i.e.

$$G = \frac{\omega_F}{\omega}.$$

Finally, we have succeeded in expressing the first derivatives of the Hamiltonian K in *Action Space* V by through path integrals in *configuration space* U,

$$\boxed{\begin{aligned}\Phi^* \frac{\partial K}{\partial J} &= \frac{2\pi}{T} = \frac{4\pi^2}{\oint \beta}. && \text{(5.21a)}\\ \Phi^* \frac{\partial K}{\partial F} &= \omega G = \frac{\omega}{2\pi} \oint \gamma. && \text{(5.21b)}\end{aligned}}$$

The quantity G is for dynamical systems the equivalent of the safety factor q for Tokamak equilibria. Obviously, G is an important quantity for the study of the behaviour of the dynamic system near resonances. There is only one more gap to fill before we are able to calculate the Hessian matrix of K, i.e. the matrix of second derivatives, in a similar manner. This is the subject of the next paragraph.

The derivatives of explicit integrals of motion in Action Space

Let us now apply eqns 5.19 to the special case when s is an *explicit integral of motion*, i.e.

$$s = \oint_{c_0} \alpha.$$

Equating the right hand sides of eq. 5.19a and eq. 5.12 we get

$$\nabla s = \frac{1}{\omega} \left(\Phi^* \frac{\partial S}{\partial J} \right) \nabla H = \nabla H \oint [\mathbf{f}, \alpha],$$

from which we infer that the derivative of any explicit integral of motion with respect to J can be calculated by means of two other integrals of motion, i.e.

$$\boxed{\Phi^* \frac{\partial S}{\partial J} = \omega \oint_{c_0} [\mathbf{f}, \alpha].} \qquad \text{(5.22)}$$

Similarly we can compute $\partial_F S$, by equating the right hand sides of eq. 5.19b and eq. 5.13, so that

$$\begin{aligned}\frac{\partial s}{\partial F} &= \left(\Phi^* \frac{\partial S}{\partial J} \right) \left(\frac{1}{\omega} \frac{\partial H}{\partial F} - G \right) + \left(\Phi^* \frac{\partial S}{\partial F} \right) \\ &= \partial_F H \oint_{c_0} [\mathbf{f}, \alpha] + \oint_{c_0} D_F [\alpha],\end{aligned}$$

which gives, by means of eq. 5.22

$$-G\left(\Phi^*\frac{\partial S}{\partial J}\right)+\left(\Phi^*\frac{\partial S}{\partial F}\right)=\oint_{c_0} D_F\left[\alpha\right],$$

or

$$\boxed{\left(\Phi^*\frac{\partial S}{\partial F}\right)=G\left(\Phi^*\frac{\partial S}{\partial J}\right)+\oint_{c_0} D_F\left[\alpha\right].} \tag{5.23}$$

The Hessian of K

We are now ready to calculate the second derivatives of the Hamiltonian in Action space V. By construction, the first derivatives $\partial_J K$ and $\partial_F K$ are both Action quantities, in that they are independent of the angle coordinate θ, so that they remain constant along the orbit. This means that the formulas in eqns 5.19 hold for the first derivatives $\partial_J K$ and $\partial_F K$ as well.

Take

$$S=\frac{\partial K}{\partial F},$$

so that

$$s=\Phi^*\frac{\partial K}{\partial F}.$$

On the one hand we know from eq. 5.21b that

$$s=\omega G=\frac{2\pi}{T}G,$$

so that

$$\nabla s=\frac{2\pi}{T}\nabla G-\frac{2\pi}{T^2}G\nabla T.$$

This, combined with the definitions

$$G=\frac{1}{2\pi}\oint_{c_0}\gamma$$

and

$$T=\frac{1}{2\pi}\oint_{c_0}\beta$$

as explicit integrals of motion and the application of the formula in 5.12eq.

$$\nabla G=\frac{1}{2\pi}\nabla H\oint\left[\mathbf{f},\gamma\right],$$
$$\nabla T=\frac{1}{2\pi}\nabla H\oint\left[\mathbf{f},\beta\right],$$

lead to

$$\begin{aligned}\nabla s &= \frac{2\pi}{T}\frac{1}{2\pi}\nabla H \oint [\mathbf{f},\gamma] - \frac{2\pi}{T^2}\frac{G}{2\pi}\nabla H \oint [\mathbf{f},\beta] \\ &= \frac{\omega}{2\pi}\left[\oint [\mathbf{f},\gamma] - \frac{G}{T}\oint [\mathbf{f},\beta]\right]\nabla H.\end{aligned}$$

On the other hand, we know from eq. 5.19a that

$$\nabla s = \frac{1}{\omega}\left(\Phi^* \frac{\partial S}{\partial J}\right)\nabla H.$$

Equating the above, we get

$$\frac{1}{\omega}\left(\Phi^* \frac{\partial S}{\partial J}\right)\nabla H = \frac{\omega}{2\pi}\left[\oint [\mathbf{f},\gamma] - \frac{G}{T}\oint [\mathbf{f},\beta]\right]\nabla H,$$

or

$$\boxed{\Phi^* \frac{\partial^2 K}{\partial F \partial J} = \frac{\omega^2}{2\pi}\left[\oint [\mathbf{f},\gamma] - \frac{G}{T}\oint [\mathbf{f},\beta]\right]}. \tag{5.24}$$

Similarly we have on one hand

$$\frac{\partial s}{\partial F} = \frac{2\pi}{T}\frac{\partial G}{\partial F} - \frac{2\pi}{T^2}G\frac{\partial T}{\partial F} = \omega\frac{\partial G}{\partial F} - \frac{\omega}{T}G\frac{\partial T}{\partial F}$$

along with

$$\begin{aligned}\frac{\partial T}{\partial F} &= \frac{1}{2\pi}\partial_F H \oint_{c_0} [\mathbf{f},\beta] + \frac{1}{2\pi}\oint_{c_0} D_F[\beta], \\ \frac{\partial G}{\partial F} &= \frac{1}{2\pi}\partial_F H \oint_{c_0} [\mathbf{f},\gamma] + \frac{1}{2\pi}\oint_{c_0} D_F[\gamma]\end{aligned}$$

so that

$$\begin{aligned}\frac{\partial s}{\partial F} &= \partial_F H \frac{\omega}{2\pi}\left[\oint_{c_0} [\mathbf{f},\gamma] - \frac{G}{T}\oint_{c_0} [\mathbf{f},\beta]\right] + \frac{\omega}{2\pi}\left[\oint_{c_0} D_F[\gamma] - \frac{G}{T}\oint_{c_0} D_F[\beta]\right] \\ &= \frac{\partial_F H}{\omega}\left(\Phi^* \frac{\partial S}{\partial J}\right) + \frac{\omega}{2\pi}\left[\oint_{c_0} D_F[\gamma] - \frac{G}{T}\oint_{c_0} D_F[\beta]\right].\end{aligned}$$

On the other hand, from eq. 5.19b we have

$$\frac{\partial s}{\partial F} = \left(\Phi^* \frac{\partial S}{\partial J}\right)\left(\frac{\partial_F H}{\omega} - G\right) + \Phi^* \frac{\partial S}{\partial F}$$

So that, equating the above, we get

$$\Phi^* \frac{\partial S}{\partial F} = G\left(\Phi^* \frac{\partial S}{\partial J}\right) + \frac{1}{T}\oint_{c_0} D_F\left[\gamma\right] - \frac{G}{T^2}\oint_{c_0} D_F\left[\beta\right],$$

or

$$\boxed{\Phi^* \frac{\partial^2 K}{\partial F^2} = G\left(\Phi^* \frac{\partial^2 K}{\partial F \partial J}\right) + \frac{1}{T}\oint_{c_0} D_F\left[\gamma\right] - \frac{G}{T^2}\oint_{c_0} D_F\left[\beta\right].} \tag{5.25}$$

Finally, the second derivative of K with respect to J can be calculated by taking

$$s = \omega = \frac{2\pi}{T}.$$

and, choosing $\tilde{T}$ so that $T = T^*$. Therefore

$$S = \frac{2\pi}{\tilde{T}},$$

and

$$\frac{\partial S}{\partial J} = -\frac{2\pi}{\tilde{T}^2}\frac{\partial \tilde{T}}{\partial J}.$$

or, equivalently

$$\Phi^* \frac{\partial S}{\partial J} = -\frac{2\pi}{T^2}\frac{\partial T}{\partial J}.$$

Using the definition of T as an explicit integral of motion eq. 5.16b, as well as the formula for the J-derivative of explicit integrals of motion in Action Space, eq. 5.22, the equation above becomes

$$\Phi^* \frac{\partial S}{\partial J} = -\frac{2\pi}{T^2}\frac{1}{2\pi}\omega \oint_{c_0} \left[\mathbf{f}, \beta\right] = -\frac{\omega^3}{(2\pi)^2}\oint_{c_0} \left[\mathbf{f}, \beta\right],$$

or

$$\boxed{\Phi^* \frac{\partial^2 K}{\partial J^2} = -\frac{\omega^3}{(2\pi)^2}\oint_{c_0} \left[\mathbf{f}, \beta\right]}. \tag{5.26}$$

5.4 Dynamics near resonances

Here we follow the exposition in Lichtenberg and Lieberman (Lichtenberg and Lieberman, 1992).

Assume a Hamiltonian in Action Space with a small perturbation term

$$H = H_0(J, F) + \epsilon H_1(J, \theta, F, \phi)$$

Suppose that for some (J, F) there is a resonance between

$$\omega = \frac{\partial H_0}{\partial J}$$

and

$$\omega_F = \frac{\partial H_0}{\partial F}$$

so that

$$\frac{\omega_F}{\omega} = \frac{r}{s}, \quad r, s \text{ co-prime integers}$$

Then the canonical perturbation methods we employ when we are away from resonances fail, due to small denominators. We can however remove the resonance by applying the following strategy. Let us choose a transform generator

$$\mathcal{F}_2 = (r\theta - s\phi)\hat{J} + \phi\hat{F}$$

so that

$$J = \frac{\partial \mathcal{F}_2}{\partial \theta} = r\hat{J}$$
$$F = \frac{\partial \mathcal{F}_2}{\partial \phi} = \hat{F} - s\hat{J}$$
$$\hat{\theta} = \frac{\partial \mathcal{F}_2}{\partial \hat{J}} = r\theta - s\phi$$

and

$$\hat{\phi} = \frac{\partial \mathcal{F}_2}{\partial \hat{F}} = \phi$$

The Jacobian of the transformation is

$$\mathcal{J} = \begin{bmatrix} \frac{\partial J}{\partial \hat{J}} & \frac{\partial J}{\partial \hat{F}} \\ \frac{\partial F}{\partial \hat{J}} & \frac{\partial F}{\partial \hat{F}} \end{bmatrix} = \begin{bmatrix} r & 0 \\ -s & 1 \end{bmatrix}, \tag{5.27}$$

while for the Hessian, we have in Einstein notation

$$\frac{\partial^2 H_0}{\partial \hat{z}_i \partial \hat{z}_j} = \frac{\partial z_k}{\partial \hat{z}_i}\frac{\partial z_m}{\partial \hat{z}_j}\frac{\partial^2 H_0}{\partial z_k \partial z_m}$$

or, in matrix form

$$\text{Hess}(H_0(\hat{J},\hat{F})) = \mathcal{J}^T \cdot \text{Hess}(H_0(J,F)) \cdot \mathcal{J},$$

which means

$$\text{Hess}(H_0(\hat{J},\hat{F})) = \begin{bmatrix} r^2 H_{JJ} + s(sH_{FF} - 2rH_{JF}) & rH_{JF} - sH_{FF} \\ rH_{JF} - sH_{FF} & H_{FF} \end{bmatrix} \tag{5.28}$$

In the new coordinates the Hamiltonian takes the form

$$\hat{H} = \hat{H}_0(\hat{J},\hat{F}) + \epsilon H_1(\hat{J},\hat{\theta},\hat{F},\hat{\phi}).$$

Near the resonance $\dot{\hat{\theta}} \approx 0$, which means that the new angle $\hat{\theta}$ changes much more slowly than the angle $\hat{\phi} = \phi$. We can use this time scale separation to average out the fast angle contribution to the perturbation component, so that the Hamiltonian becomes independent of $\hat{\phi}$ up to first order and the associated action $\hat{F}$ is an integral of motion, i.e.

$$\hat{F} = F - \frac{s}{r}J = \text{ const.} \tag{5.29}$$

Notice that for $s \gg r$ or $r \gg s$ eq. 5.29 becomes $J =$ const and $F =$ const respectively. Hence the only resonances of importance for modifying the invariants are those with low harmonic numbers s and r. The actual averaging can be carried out by Fourier expanding the perturbation as

$$\begin{aligned} H_1 &= \sum_{l,m} H_{l,m} \exp[i(l\theta + m\phi)] \\ &= \sum_{l,m} H_{l,m} \exp[\frac{i}{r}(l\hat{\theta} + (sl + mr)\hat{\phi})] \end{aligned}$$

and dropping any terms that depend on $\hat{\phi}$ to get

$$H_1 \approx \bar{H}_1 = \sum_p H_{-pr,ps} \exp[-ip\hat{\theta}].$$

We also choose to neglect all terms with $|p| > 1$, since the Fourier coefficients generally fall off rapidly. This significantly simplifies H_1, which becomes

$$\begin{aligned} H_1 \approx \bar{H}_1 &\approx H_{0,0} + H_{-r,s}\exp[-i\hat{\theta}] + H_{r,-s}\exp[i\hat{\theta}] \\ &= H_{0,0} + |H_{-r,s}|\exp[-i(\hat{\theta}-\theta_0)] + |H_{r,-s}|\exp[i(\hat{\theta}-\theta_0)] \\ &= H_{0,0} + 2|H_{-r,s}|\cos(\hat{\theta}-\theta_0), \end{aligned}$$

where

$$\theta_0 = \arg(H_{-r,s}).$$

Finally, we end up with a much simplified Hamiltonian

$$\boxed{\bar{H} = \hat{H}_0(\hat{J},\hat{F}) + \epsilon H_{0,0}(\hat{J},\hat{F}) + 2\epsilon|H_{-r,s}(\hat{J},\hat{F})|\cos(\hat{\theta}-\theta_0),} \tag{5.30}$$

with $\hat{F} = \text{const}$. Hence $\bar{H}$ is effectively a single degree Hamiltonian. The stationary points are determined by

$$\frac{\partial \bar{H}}{\partial \hat{\theta}} = 0 \quad and \quad \frac{\partial \bar{H}}{\partial \hat{J}} = 0 \tag{5.31}$$

The first condition gives the $\hat{\theta}_{\text{res}}$ coordinates of the resonances, which must satisfy

$$-2\epsilon|H_{-r,s}(\hat{J},\hat{F})|\sin(\hat{\theta}_{\text{res}}-\theta_0), \tag{5.32}$$

implying that

$$\hat{\theta}_{\text{res}} = \theta_0, \tag{5.33}$$

or

$$\hat{\theta}_{\text{res}} = \theta_0 \pm \pi \tag{5.34}$$

The second condition then becomes

$$\frac{\partial \hat{H}_0}{\partial \hat{J}} + \epsilon\frac{\partial H_{0,0}}{\partial \hat{J}} \pm 2\epsilon\frac{\partial |H_{-r,s}|}{\partial \hat{J}} = 0,$$

with the positive sing corresponding to $\hat{\theta}_{\text{res}} = \theta_0$ and the negative sign to $\hat{\theta}_{\text{res}} = \theta_0 \pm \pi$. To lowest order this reproduces the resonance condition, i.e.

$$\frac{\partial \hat{H}_0}{\partial \hat{J}} = 0,$$

or

$$r\frac{\partial H_0}{\partial J} - s\frac{\partial H_0}{\partial F} = r\omega - s\omega_F = 0.$$

From now on we will restrict ourselves to the case where the resonance condition is met only locally for particular values of J and F. This is called *accidental degeneracy* and has different qualitative features that *intrinsic degeneracy*, for which the resonance condition is satisfied for a local neighbourhood in J and F. In other words, we assume that a small excursion from the resonance point, takes us away from resonance, or equivalently that

$$\frac{\partial^2 \hat{H}_0}{\partial \hat{J}^2} \neq 0.$$

The perturbation terms cause a small displacement of the fixed points away from the resonance condition. We can estimate a first order correction $\hat{J}_c$ of the fixed point positions, by expanding the zero order term, i.e.

$$\frac{\partial^2 \hat{H}_0}{\partial \hat{J}^2}\hat{J}_c + \epsilon\frac{\partial H_{0,0}}{\partial \hat{J}} \pm 2\epsilon\frac{\partial |H_{-r,s}|}{\partial \hat{J}} = 0 \Rightarrow$$

$$\hat{J}_c = -\epsilon\left(\frac{\partial^2 \hat{H}_0}{\partial \hat{J}^2}\right)^{-1}\left[\frac{\partial H_{0,0}}{\partial \hat{J}} \pm 2\frac{\partial |H_{-r,s}|}{\partial \hat{J}}\right] \Rightarrow \tag{5.35}$$

$$\hat{J}_c = -\frac{\epsilon}{r^2 H_{JJ} + s(sH_{FF} - 2rH_{JF})}\left[\frac{\partial H_{0,0}}{\partial \hat{J}} \pm 2\frac{\partial |H_{-r,s}|}{\partial \hat{J}}\right] \tag{5.36}$$

with

$$J_c = r\hat{J}_c \tag{5.37}$$

and

$$F_c = -s\hat{J}_c \tag{5.38}$$

The displacement of the stationary points away from the resonance surface takes place tangentially to the surface $H_0 = \text{const}$, due to the relation of the integers r and s with the partial derivatives of the unperturbed Hamiltonian at the resonance location.

Inspection of eq. 5.30 shows that in the excursions in $\hat{J}$ are of order , $\dot{\hat{J}} = O(\epsilon H_{-r,s})$, while the excursions in $\hat{\theta}$ are of zeroeth order, so we can expand about the stationary point in $\hat{J}$ but not in $\hat{\theta}$.

We have

$$\hat{H}_0(\hat{J}, \hat{F}) = H_{0,res} + \frac{\partial \hat{H}_0}{\partial \hat{J}}\Delta\hat{J} + \frac{1}{2}\frac{\partial^2 \hat{H}_0}{\partial \hat{J}^2}\left(\Delta\hat{J}\right)^2.$$

The linear term

$$\frac{\partial \hat{H}_0}{\partial \hat{J}} \Delta \hat{J}$$

is zero, due to the resonance condition and we can drop the constant term $H_{0,res}$. The resulting Hamiltonian, governing the motion near the resonance is

$$\Delta \bar{H} = \frac{1}{2} M (\Delta \hat{J})^2 - K \cos(\hat{\theta} - \theta_0), \tag{5.39}$$

with

$$M = \frac{\partial^2 \hat{H}_0}{\partial \hat{J}^2} = r^2 H_{JJ} + s(sH_{FF} - 2rH_{JF}) \tag{5.40}$$

and

$$K = -2\epsilon |H_{-r,s}(\hat{J}, \hat{F})|. \tag{5.41}$$

It follows that *the motion near the resonance is governed by the pendulum Hamiltonian*. The stable fixed point is

$$\hat{\theta} = \begin{cases} \theta_0, & M < 0 \\ \theta_0 \pm \pi & M > 0 \end{cases}$$

The effective mass of the pendulum $M_{\text{eff}} \equiv |M|$ is determined by the second derivatives of the unperturbed Hamiltonian on the location of the resonance and on the resonance ratio r/s. The maximum excursion from the resonance curve is small, occurs at the separatrix and is given by half the separatrix width $\Delta \hat{J}_{\max}$. This occurs for $\Delta \bar{H} = K$ and $\hat{\theta} = \theta_0$, so that

$$\Delta \hat{J}_{\max} = 2 \left| \frac{K}{M} \right|^{1/2} = 2\epsilon^{1/2} \left| \frac{2|H_{-r,s}(\hat{J}, \hat{F})|}{r^2 H_{JJ} + s(sH_{FF} - 2rH_{JF})} \right|^{1/2} \tag{5.42}$$

Since $\Delta \hat{J}_{\max} = O(\epsilon^{1/2})$ the excursion in action due to libration around the fixed points usually dominates over the displacement of the fixed point from the resonance $\hat{J}_c$ due to finite perturbation strength, which is of order $O(\epsilon)$. Referring back to the original Action space, near the resonance, the perturbation gives rise to a change in the topology of the phase space orbits, with the creation of a separatrix centerd around the fixed points and extending on the tangential plane of the $H_0 = \text{const.}$ surface, with half widths

$$\begin{aligned} \Delta J_{\max} &= |r| \Delta \hat{J}_{\max} = 2 \left| \frac{r^2 K}{M} \right|^{1/2} \\ &= 2\epsilon^{1/2} \left| \frac{2r^2 |H_{-r,s}(\hat{J}, \hat{F})|}{r^2 H_{JJ} + s(sH_{FF} - 2rH_{JF})} \right|^{1/2} \end{aligned} \tag{5.43}$$

and

$$\Delta F_{\max} = |s|\Delta\hat{J}_{\max} = 2\left|\frac{s^2K}{M}\right|^{1/2}$$
$$= 2\epsilon^{1/2}\left|\frac{2s^2|H_{-r,s}(\hat{J},\hat{F})|}{r^2H_{JJ}+s(sH_{FF}-2rH_{JF})}\right|^{1/2}. \tag{5.44}$$

5.4.1 The Special Case of a Monochromatic Perturbation in the ignorable angle

A ϕ-monochromatic perturbation is the special perturbation with a single harmonic m in the ϕ direction, with Fourier representation

$$H_1 = \sum_l \sum_{k=\pm m} H_{l,k}\exp[i(l\theta+k\phi)]$$
$$= \sum_l \sum_{k=\pm m} H_{l,k}\exp[\frac{i}{r}(l\hat{\theta}+(sl+kr)\hat{\phi})].$$

The first order adiabatic terms are those with

$$sl = -kr = \mp mr$$

or

$$l = \mp\frac{mr}{s}. \tag{5.45}$$

Since we have prescribed r and s to be co-prime integers, eq. 5.45 can be satisfied only if s divides m, or

$$m = ps, \quad p \text{ integer}. \tag{5.46}$$

Then eq. 5.45 gives

$$l = \mp pr \tag{5.47}$$

If there is no such p, i.e. if s does not divide m, then the perturbation is non-resonant and no first order islands are formed on the resonance curve. When the resonance condition eq. 5.46 is satisfied, we can follow the footsteps of the previous paragraph, only we now cannot choose $p = 1$.

As before, we need to determine the adiabatic component of the perturbation, which is

$$\bar{H_1} = H_{-pr,m}\exp[-ip\hat{\theta}] + H_{pr,-m}\exp[+ip\hat{\theta}]$$
$$= 2|H_{-pr,m}|\cos(p(\hat{\theta}-\theta_0)),$$

with

$$\theta_0 = \frac{1}{p}\arg(H_{-pr,m}).$$

Near the resonance, the motion is governed by the Hamiltonian

$$\Delta\bar{H} = \frac{1}{2}M(\Delta\hat{J})^2 - K\cos(p(\hat{\theta}-\theta_0)), \tag{5.48}$$

with

$$M = \frac{\partial^2\hat{H}_0}{\partial\hat{J}^2} = r^2H_{JJ} + s(sH_{FF} - 2rH_{JF}) \tag{5.49}$$

as before and

$$K = -2\epsilon|H_{-pr,m}(\hat{J},\hat{F})|. \tag{5.50}$$

This differs from the standard Hamiltonian of the general case in two places. First the presence of p as a multiplying constant in the argument of the potential in eq. 5.48, which has no effect other than increasing the number of fixed points. Second in specifying the relevant Fourier amplitude that determines K. Other than this, all the previous conclusions hold. Namely, the maximum excursion in $\hat{J}$ is determined by the half width of the pendulum separatrix, which is given by

$$\Delta\hat{J}_{\max} = 2\left|\frac{K}{M}\right|^{1/2} = 2\epsilon^{1/2}\left|\frac{2|H_{-pr,m}(\hat{J},\hat{F})|}{r^2H_{JJ} + s(sH_{FF} - 2rH_{JF})}\right|^{1/2} \tag{5.51}$$

which in the original Actions translates to

$$\begin{aligned}\Delta J_{\max} &= |r|\Delta\hat{J}_{\max} = 2\left|\frac{r^2K}{M}\right|^{1/2} \\ &= 2\epsilon^{1/2}\left|\frac{2r^2|H_{-pr,m}(\hat{J},\hat{F})|}{r^2H_{JJ} + s(sH_{FF} - 2rH_{JF})}\right|^{1/2}\end{aligned} \tag{5.52}$$

and

$$\begin{aligned}\Delta F_{\max} &= |s|\Delta\hat{J}_{\max} = 2\left|\frac{s^2K}{M}\right|^{1/2} \\ &= 2\epsilon^{1/2}\left|\frac{2s^2|H_{-pr,m}(\hat{J},\hat{F})|}{r^2H_{JJ} + s(sH_{FF} - 2rH_{JF})}\right|^{1/2}.\end{aligned} \tag{5.53}$$

5.5 Computing the orbital spectrum

In this section we will consider perturbations of the general form

$$H_1 = P(p,q)e^{im\phi} + \text{cc.} \tag{5.54}$$

where cc. stands for complex conjugate. The choice of such general form has a clear physical meaning. It represents a perturbation with a monochromatic component in the ϕ "toroidal" direction modulated by prescribed profile $P(p,q)$ in the (p,q) "poloidal" plane. In the Action Angle coordinates, H_1 can be written as

$$H_1 = \sum_n A_n(J,F)e^{i(n\theta+m\bar{\phi})} + cc. \tag{5.55}$$

We will demonstrate how to compute the amplitudes $A_n(J,F)$ the of Fourier series in eq. 5.55 from the prescribed from in eq. 5.54.

The trick is to keep $\bar{\phi}$ fixed and treat H_1 as a function of only the poloidal angle θ. Then

$$\begin{aligned} H_1|_{\bar{\phi}} &= \sum_n A_n e^{in\theta+m\bar{\phi}} + \sum_n A_n^* e^{in\theta-m\bar{\phi}} \\ &= \sum_n \left(A_n e^{im\bar{\phi}} + A_{-n}^* e^{-im\bar{\phi}}\right) e^{in\theta} \\ &= \sum_n C_n(\phi) e^{in\theta}, \end{aligned}$$

where

$$C_n(\phi) = A_n e^{im\bar{\phi}} + A_{-n}^* e^{-im\bar{\phi}}.$$

The Fourier amplitudes C_n can be numerically estimated by means of a DFT on a sufficiently large number of samples of the projection of a closed orbit on the $\bar{\phi} = \text{const.}$ surface. Performing this operation twice, once for $\bar{\phi} = 0$ and once for $\bar{\phi} = \Delta\bar{\phi}$, we can determine the Fourier amplitudes A_n in eq. 5.55 by

$$A_n = \frac{C_{n,1}e^{im\Delta\bar{\phi}} - C_{n,0}}{e^{2im\Delta\bar{\phi}} - 1} \tag{5.56}$$

with

$$C_{n,1} = C_n(\Delta\bar{\phi})$$

and

$$C_{n,0} = C_n(0)$$

In eq. 5.56 the value of $\Delta\bar{\phi}$ must be chosen so that the denominator does not become so small as to be a threat for numerical accuracy. This means that $m\Delta\bar{\phi}$ must not come too close to an integer multiple of 2π. Since our domain of interest is for small non-zero integers m, this can be easily satisfied by taking $\Delta\bar{\phi}$ equal to a small integer. In our codes, we take $\Delta\bar{\phi} = 1$, which is a sufficiently good choice for our purposes, although it should be noted that it may not be adequate when Fourier amplitudes of very high harmonic number need to be specified. Therefore we have

$$A_n = \frac{C_{n,1}e^{im} - C_{n,0}}{e^{2im} - 1} \tag{5.57}$$

with

$$C_{n,1} = C_n(1)$$

and

$$C_{n,0} = C_n(0).$$

5.6 Application: The extended pendulum

In this section we make use of the knowledge acquired in this chapter, to study the dynamic behaviour of the *extended pendulum*. The Hamiltonian of this system is similar to the simple pendulum, but with an extra degree of freedom, whose canonical momentum F acts like the amplitude of the restoring force.

$$H(p, q, F) = \frac{1}{2}Mp^2 - F\cos q \tag{5.58}$$

Associated with F is the ignorable canonical position ϕ, a periodic variable with period equal to 2π. Of course, the extended pendulum phase space on a plane of positive $F =$ const. (fig. 5.3) looks exactly like the phase space of the simple pendulum. At $E_{sx} = F$, two marginal orbit curves emerge from the X-points located at $q = \pm\pi$. These form the *separatrix*, which separates the phase space into three regions, each of which is determined by the topology of the orbits contained within. For small energies, $E_{\text{lib}} < E_{\text{sx}}$, the orbits are bound around the O-point at the axes origin. For large enough energies $E_{\text{rot}} > E_{\text{sx}}$, there are two kinds of free orbits moving in opposite direction. When $F < 0$, the O-point and the X-point exchange position, but the topology of the phase space remains unchanged.

The extended pendulum is perhaps one of the most complex dynamic systems for which there is a known analytic solution for the Action Angle transform. Assuming $F > 0$, the

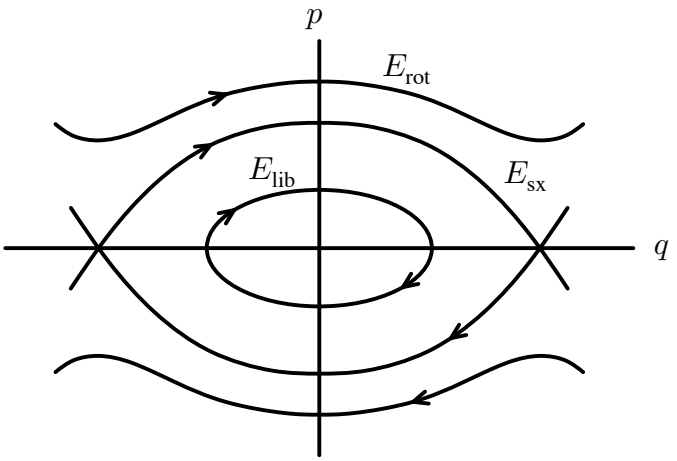

Figure 5.3 The Extended Pendulum phase space on a surface of constant $F > 0$.

action is given by

$$J = R\frac{8}{\pi}\begin{cases}\mathcal{E}(\kappa) - (1-\kappa^2)\mathcal{K}(\kappa), & \kappa < 1, \text{ libration} \\ \dfrac{\kappa}{2}\mathcal{E}(\kappa^{-1}), & \kappa > 1, \text{ rotation}\end{cases}, \tag{5.59}$$

where

$$\kappa = \left[\frac{1}{2}\left(1 + \frac{E}{F}\right)\right]^{1/2},$$
$$R = \left(\frac{F}{M}\right)^{1/2}$$

with $\mathcal{K}$ and $\mathcal{E}$ the complete elliptic integrals

$$\mathcal{K}(\kappa) = \int_0^{\frac{\pi}{2}} \frac{d\phi}{(1-\kappa^2 \sin^2\phi)^{1/2}},$$
$$\mathcal{E}(\kappa) = \int_0^{\frac{\pi}{2}} (1-\kappa^2 \sin^2\phi)^{1/2} d\phi.$$

Due to difference in orbit topology on the two sides of the separatrix, the action is a discontinuous function of the energy. This is demonstrated in fig. 5.4, in which there is a conspicuous drop of 50% when the energy crosses the marginal value $E_{\text{sx}} = F$. This reflects the fact that, as we have repeatedly stated, there can be no single continuous Action Angle transform

$$\Phi : (p, q) \in U \to (J, \theta) \in V,$$

when the domain U contains a separatrix. In order to treat the dynamic system in action angle coordinates, we need to treat separately each continent bound by a separatrix. In what

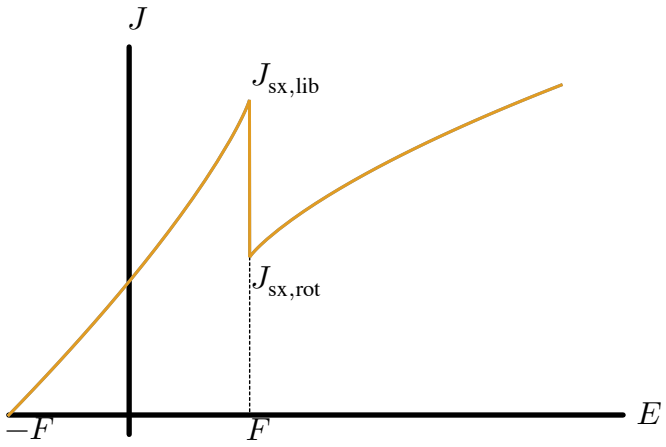

Figure 5.4 The extended pendulum Action as a function of the energy for constant $F > 0$. The discontinuity at the separatrix energy $E_{\text{sx}} = F$ is due to the different topology of orbits on either sides of the separatrix.

follows, unless otherwise stated, we shall limit our analysis to the libration continent defined by $E < E_{\text{sx}} = F$.

Moreover, although there is indeed a closed analytic expression for J as a function of the energy, i.e. J as a function of the Hamiltonian H, the equation relating the two, eq. 5.58, is transcendental, and it would be impractical, if not impossible to invert. In other words, this is a case, where $J(H, F)$ is known, but $K(J, F)$ is not. It is therefore a perfect test case for the theory we developed in the previous sections.

5.6.1 Polynomial Fitting of $H(J, F)$

Although the $K(J, F)$ is not known in a closed analytic form, it can be modelled by sampling $J(H, F)$ for a sufficiently large number of samples and then fitting a 2D polynomial of sufficient degree, so as to obtain an expression of the form

$$K(J, F) \approx P_n(J, F),$$

where P_n is a 2D polynomial of $n \times n$ degree. Then, we can approximate the derivatives of the Hamiltonian by the derivatives of P_n.

$$\frac{\partial^2 K}{\partial z_i \partial z_j} \approx \frac{\partial^2 P_n}{\partial z_i \partial z_j}.$$

What is the point of path integral theory, if we can make do with polynomial fitting? This will be answered at the end of this subsection.

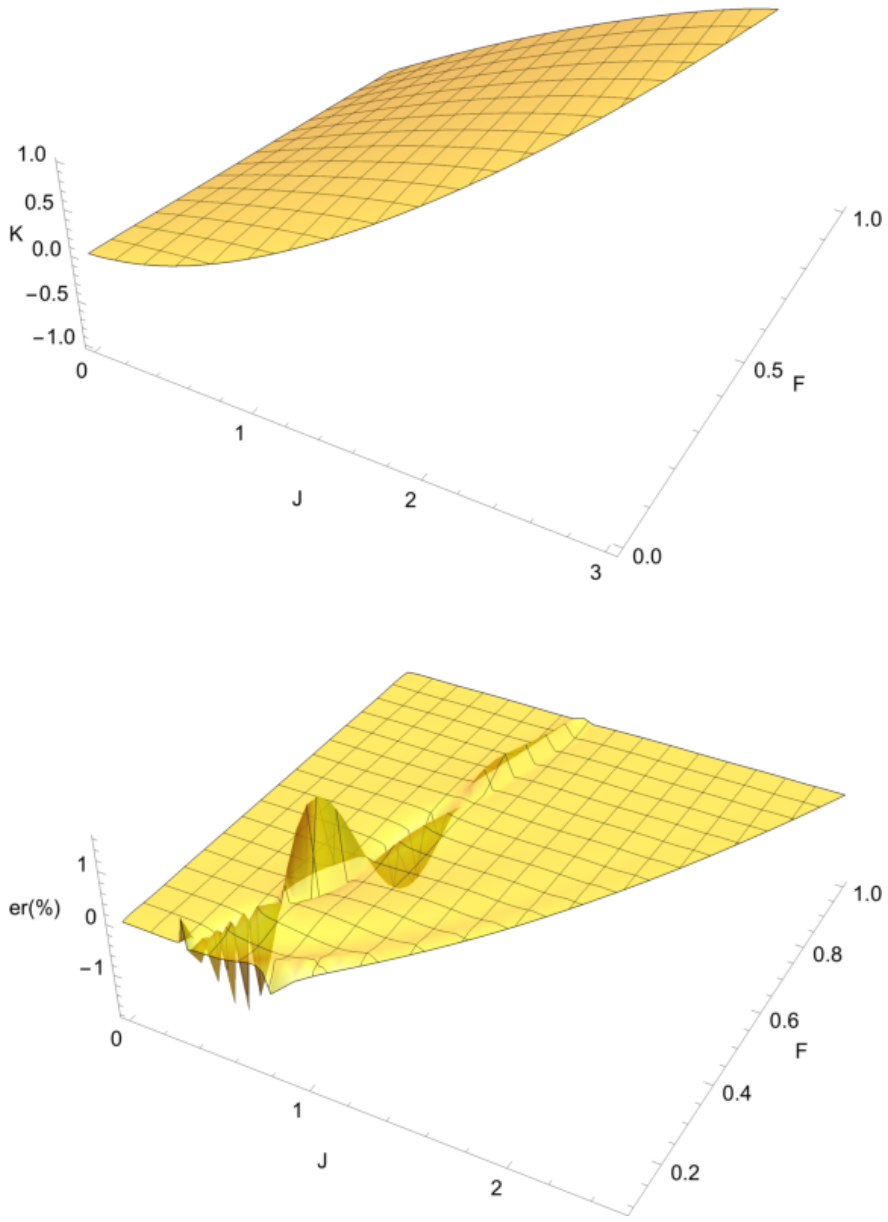

Figure 5.5 . The Hamiltonian $K(J, F)$ on a subset of the libration continent in action space. **Top**: Exact calculation of $K(J, F)$ by sampling eq. 5.59 for an extended pendulum with unit mass $M = 1$. **Bottom**: The relative error due to the approximation of K with a 10×10 degree polynomial. Apart from an apparent localized glitch at $K = 0$, the approximation is almost perfect.

In what follows, we test the method above, by applying it on a set of 1600 samples on the libration continent of a unit mass pendulum, $M = 1$, for $F \in [0.1, 1]$. The discussion below is not intended as an exhaustive study, but as a test case to illustrate the arguments made so far.

On the $F > 0$ action semi-plane, the libration continent is the subset

$$U_{\text{lib}} : \big((J, F), F > 0, 0 \leq J \leq J_{\text{sx,lib}}(F)\big),$$

where $J_{\text{sx,lib}}(F)$ is given by the libration branch of eq. 5.59, for $\kappa \to 1$. The Hamiltonian K is a very smooth function of the actions, as can be seen in fig. 5.5. This should make it easy to fit with a low degree polynomial, if it where not for the sharp edges of the domain U_{lib} and our need to approximate the second derivatives of K with sufficient accuracy.

As expected, a 10^{th}-degree polynomial P_{10} fits the samples of K almost perfectly, apart from an artificial glitch of about 1% error, at $K = 0$, where the relative error is ill-defined (see fig. 5.5). On the other hand, the second derivative is much harder to approximate, even when K has such smooth dependence on the action variables. Comparing $\dfrac{\partial^2 P_{10}}{\partial F^2}$, to the exact value of $\dfrac{\partial^2 K}{\partial F^2}$, calculated by means of eq. 5.25, we get a relative error of the order of 10% inside the sampling domain, which becomes much larger at the edges, as can be seen clearly in fig. 5.6.

For polynomials of "small" degree n, the quality of the approximation of the second order derivative, seems to improved with increasing n, see fig. 5.7, but of course this trend does not go on ad infinitum, see fig. 5.8. It follows that there is some optimal polynomial, but it seems very hard to determine what that is a priori.

Somewhat counter intuitively, polynomial fitting is not a trivial task, even in this example of particularly smooth functions. Comparison with path integral calculation is the only direct way of estimating the quality of the approximation of the second order derivatives. However, this is *not* the strongest argument in favour of path integral theory. The only reason we were able to use polynomial fitting in the first place, is that we already had a trivial model for the topological skeleton of the dynamics, namely $E < F$ for libration and $E > F$ for rotation. When the topological skeleton is not known a priori, which is usually the case, path integral theory is our only choice.

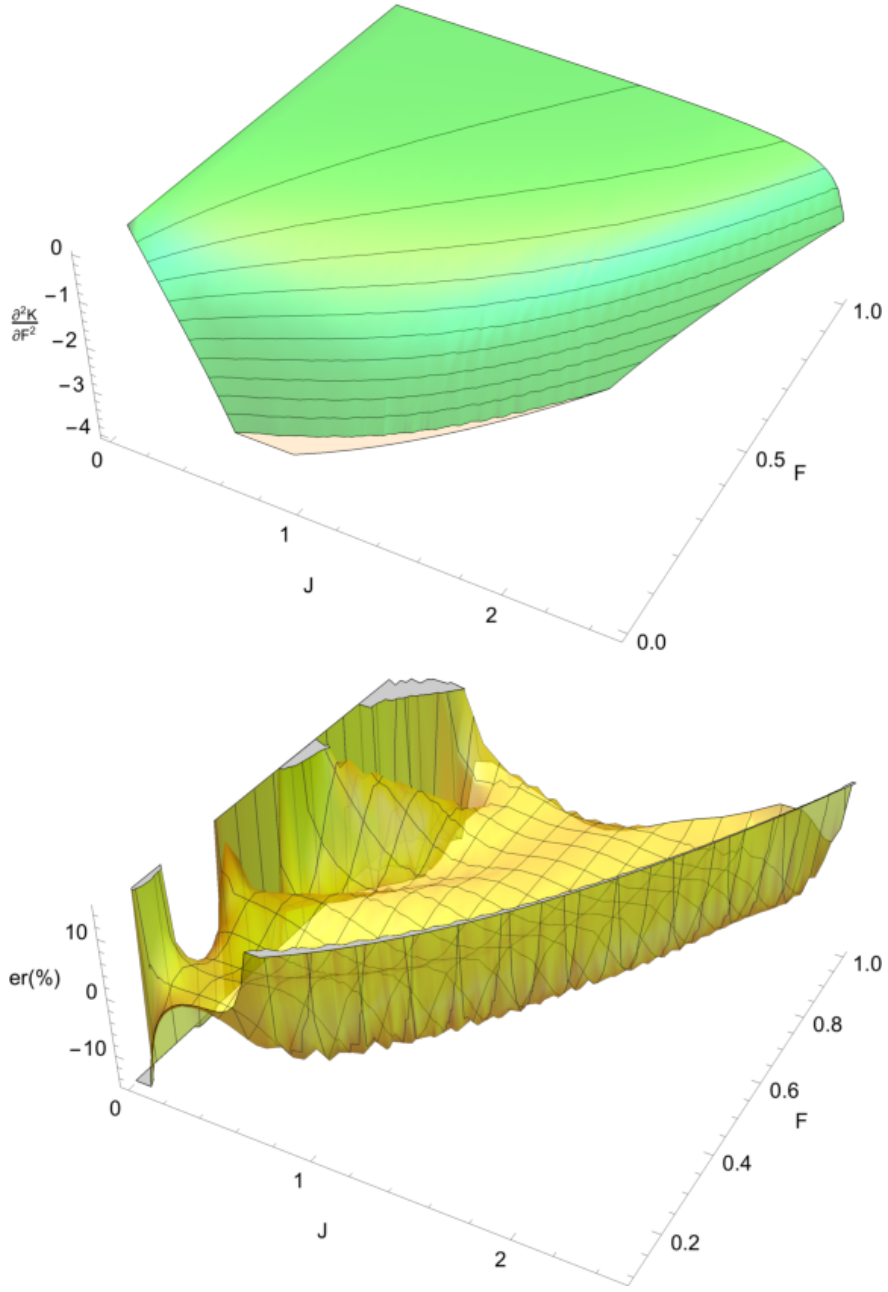

Figure 5.6 . Exact and approximate calculation of the second order derivatives of $K(J, F)$. **Top**: Exact calculation of the second derivative of K with respect to F in the libration continent for an extended pendulum with unit mass $M = 1$. The value grows towards negative infinity near the separatrix. **Bottom**: The relative error due to polynomial approximation of the same derivative. The approximation was done with a 10×10 degree polynomial. Even though $K(J, F)$ is very smooth, the relative error becomes significant, especially at the edges.

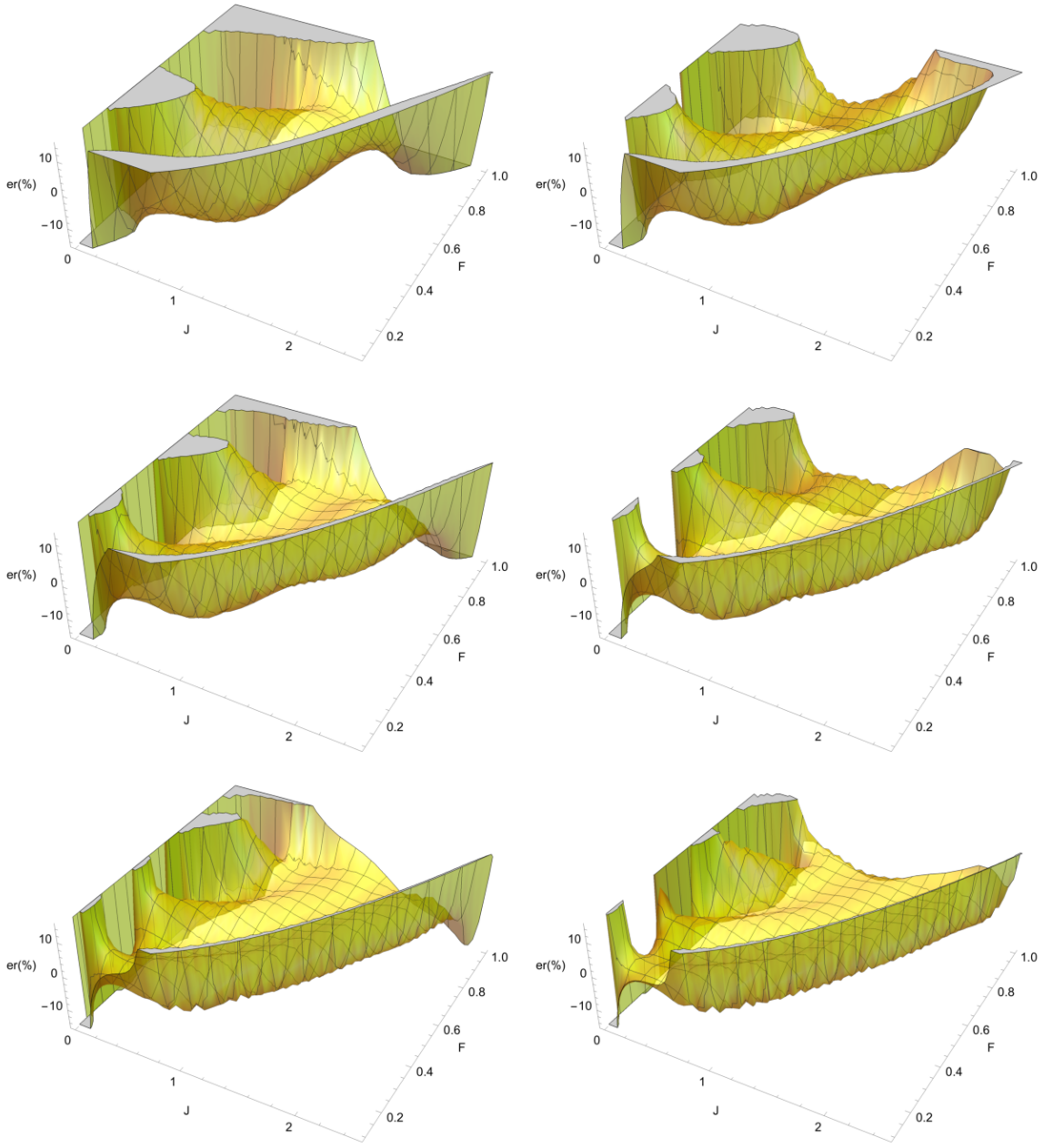

Figure 5.7 Effect of the degree of the polynomial model $P_{n,n}$, for "small" n. From top to bottom, left to right. The relative error in the estimation of the second derivative for n ranging from 5 to 10. The approximation improves as n increases. The dynamic parameters are kept the same as in fig. 5.6

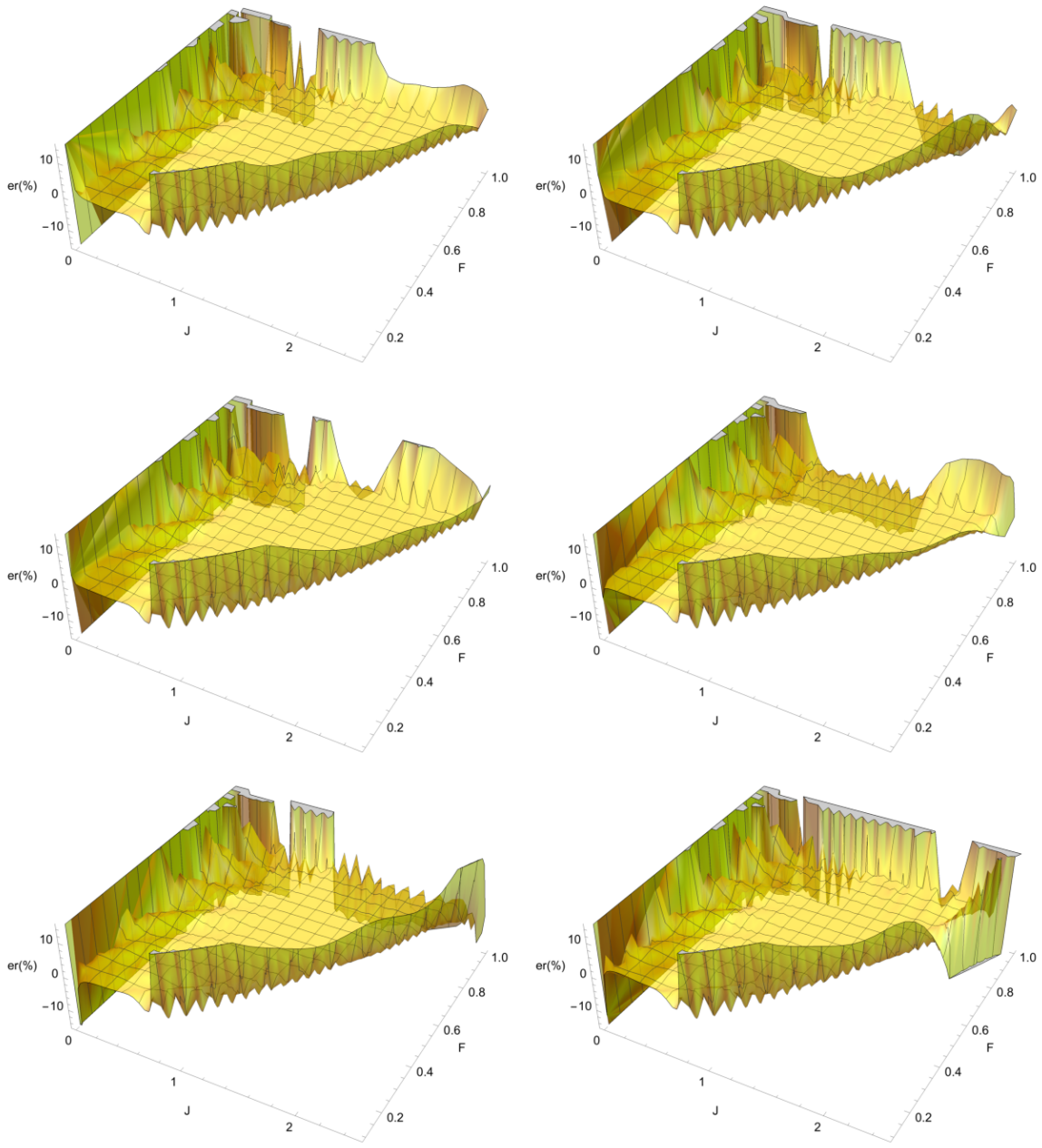

Figure 5.8 Effect of the degree of the polynomial model $P_{n,n}$, for "large" n. From top to bottom, left to right. The relative error in the estimation of the second derivative for n ranging from 25 to 30. There is no clear trend in the quality of the approximation as n increases, although some values lead to better performance than others. The dynamic parameters are kept the same as in fig. 5.6

5.6.2 Predicting the transition to deterministic chaos.

We now turn to the analysis of the perturbed extended pendulum. Assuming a time independent perturbation of the form

$$H_1 = A\cos(nq + m\phi),$$

the Hamiltonian of the perturbed system is

$$H = H_0 + H_1 = \frac{1}{2}Mp^2 - F\cos q + A\cos(nq + m\phi).$$

By writing the Hamiltonian above in Action Angle variables,

$$K(J,\theta,F,\phi) = K_0(J,F) + \sum_{\rho} A_{\rho,m}e^{i(\rho\theta+m\bar{\phi})} + \sum_{\rho} A_{\rho,-m}(J,F)e^{i(\rho\theta-m\bar{\phi})}$$

we can see clearly that the perturbation we have chosen is monochromatic in the angle variable $\bar{\phi}$ but not in the angle variable θ.

The appearance of the perturbation destroys the invariance of the Angles J and F, but, since the perturbation is time independent, the Hamiltonian is conserved and the perturbed orbits lie on the submanifold $H = \text{const}$. For small enough amplitudes, there exist Action variables $\bar{J}$ and $\bar{F}$ of the perturbed Hamiltonian, so that

$$K(J,\theta,F,\phi) = K(\bar{J},\bar{F}).$$

Their relation to the Action Angle variables of the unperturbed system can in principle be approximated to arbitrarily high order by perturbation methods discussed in previous chapters. When the perturbation amplitude becomes larger than some critical value, the integrals of motion $\bar{J}$ and $\bar{F}$ cease to exist. Then the orbits cover densely a finite subset of the $H = \text{const}$. submanifold and the motion becomes chaotic.

To predict the perturbation amplitude in which we have transition to chaos, we make use of the Chirikov criterion, which dictates that chaos occurs when the widths of two neighbouring first order resonances overlap. The first order resonances occur when

$$G \equiv \frac{\omega_{\bar{\phi}}}{\omega_\theta} = \frac{r}{s}, \quad r, s \text{ coprimes},$$

but, as we saw in subsec. 5.4.1, only those ratios for which s divides m are relevant.

We shall now apply the techniques we developed in the previous sections to analyse two qualitatively distinct cases. The deeply trapped and the weakly trapped orbits. For

demonstration purposes, we choose to limit ourselves to specific perturbation parameters. From now on, we choose $n = -5$ and $m = 4$ so that the perturbation becomes

$$H_1 = A\cos(4\phi - 5q).$$

The first order resonances will occur at $s = [1, ..., 4]$. We shall see that second order resonances also appear at $s = 8$.

Deeply Trapped Orbits

The perturbed orbit under the time independent perturbation H_1 conserves the Hamiltonian H. This means that to zeroeth order H_0 is also approximately conserved. In particular, orbits with negative unperturbed energy H_0 will continue to have $H_0 < 0$. But, for $F > 0$, these orbits are always trapped and they will continue to be trapped ad infinitum, unless H_0 was comparable to H_1 to begin with. This is evident from the fact that

$$\begin{aligned} &H \geq -F\cos q + A\cos(nq + m\phi) \Rightarrow \\ &F\cos q \geq -H - A\cos(nq + m\phi) \Rightarrow \\ &F \geq -H - A, \end{aligned}$$

which means that for negative H or H_0 sufficiently far from 0, F will always be positive and the orbit will never cross the separatrix, which occurs at $H_0 = F$. On the other hand F may become arbitrarily large, trapping the particle closer and closer to the fixed point $q = 0$.

For demonstration purposes, but with no loss of generality, we will examine the dynamics for a range of increasing perturbation amplitudes on the invariant surface $H = -0.5$.

The small amplitude perturbation case, where the motion is regular almost everywhere in phase space, arises for $A = 4 \cdot 10^{-3}$. On the left hand side of fig. 5.9 we have plotted the unperturbed frequency ratio G for different values of F on the invariant surface $H = -0.5$. We have also marked the location of the resonances with low harmonic numbers, with r and s taking small positive and negative values up to ± 5.

On the right hand side of fig. 5.9 we have plotted the corresponding Poincare surface for $A = 4 \cdot 10^{-3}$. The islands formed due to low harmonic first order resonances are easily distinguished. From top to bottom, they correspond to the ratios $-5/4, -1/1, -3/4$ and $-1/2$.

The calculated widths of the first order resonances are marked by the horizontal solid color bars. We have ignored the first order displacement of the fixed points from the resonance eq. 5.36, which depends on the derivatives of the perturbation with respect to the

Actions. Since the resonance widths are too small for the resonances to overlap, the motion is almost everywhere regular this patch of phase space, except for maybe the small areas near the secondary separatrices formed at the edges of the chains of resonant islands. This is in particular evident in the $-3/4$ resonant chain. Finally, if the reader pays close attention, he or she may be able to notice the two chains of 8 small second order islands at $-9/8$ and $-7/8$.

A somewhat different picture is painted when we double the perturbation amplitude to $A = 8 \cdot 10^{-3}$. As seen in fig. 5.10, the calculated resonant widths for the $-1/1$ and the $-3/4$ islands are still not big enough to satisfy the Chirikov criterion, yet a considerable portion of phase space between the two resonances is undoubtedly chaotically connected. This is clearly a case where Chirikov criterion overestimates the required conditions for the onset of chaos. The most probable explanation is twofold. First, there is the $-7/8$ second order resonance chain interposed between the first order chains. Second, there may be a finite first order displacement of the island centers from the resonance lines, see eq 5.36, which we have chosen to ignore. The combination of the two is probably what lowers the threshold for the onset of chaos.

Among other noteworthy features, is the notable first order displacement of the $-1/2$ chain, the appearance $-9/8$ second order chain, as well as the appearance of a $-2/3$ chain. Since 3 and 4 are obviously co-primes, the appearance of this chain is due to a first order correction of the orbit frequencies.

The reasonable conclusion that 'Chiricov criterion always overestimates the required amplitude for the onset of chaos', is far too hasty. As seen in fig. 5.11, which depicts the dynamics for $A = 2.2 \cdot 10^{-2}$, the calculated widths of the $-5/4$ and the $-1/1$ chains obviously overlap, but the two chains are not chaotically connected. However, this is probably due to a considerable first order displacement of the $-1/1$ centers from the $-1/1$ resonance level. One can see for themselves that the remaining $-1/1$ islands are not located in the center of the corresponding coloured stripe that marks the calculated island position and width. Including first order corrections for the resonant islands locations is a top priority for future work.

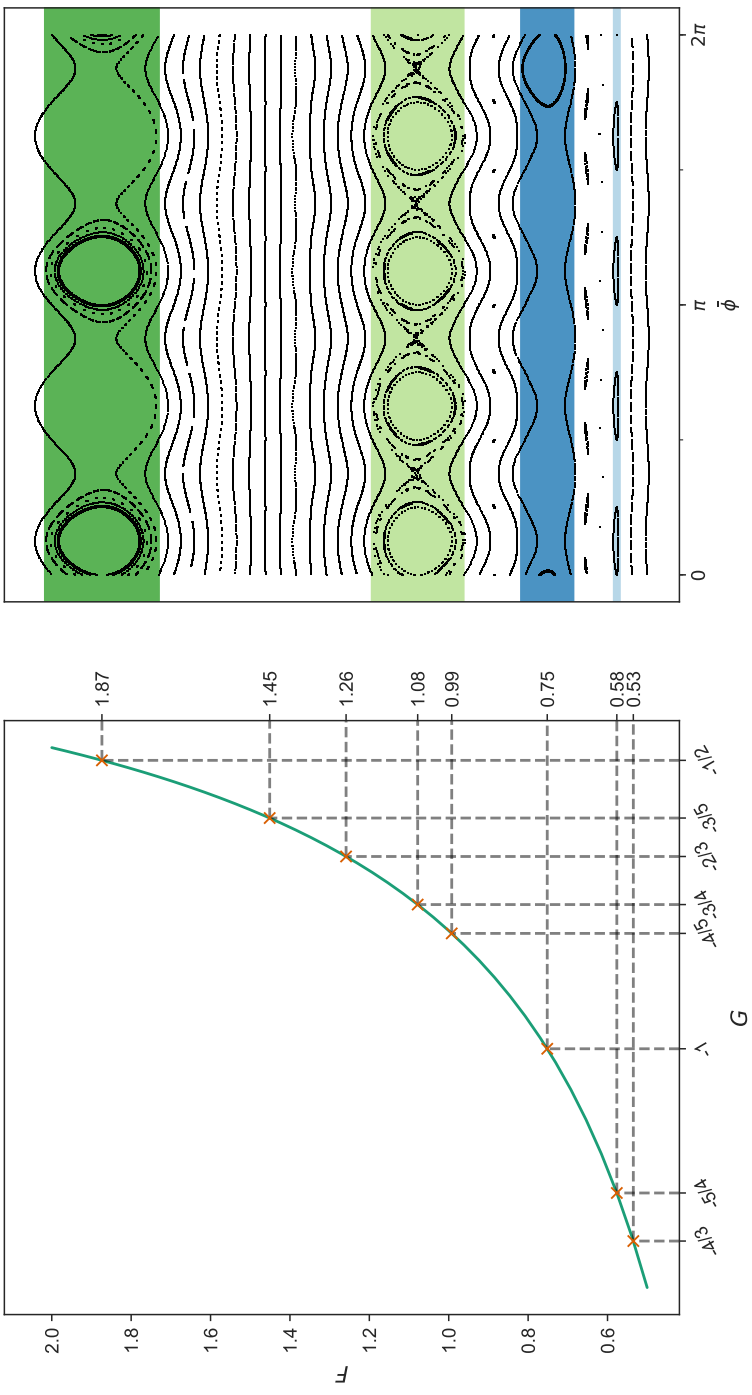

Figure 5.9 Left: The unperturbed frequency ratio G for different values of F on the invariant surface $H = -0.5$. The locations of the low harmonic resonances are marked with x's. The dotted lines facilitate the association of the harmonic resonances with the corresponding island chains on the Poincare diagram. Right: Poincare surface for $A = 4 \cdot 10^{-3}$. The calculated widths of the first order resonances are marked by the horizontal solid color bars.

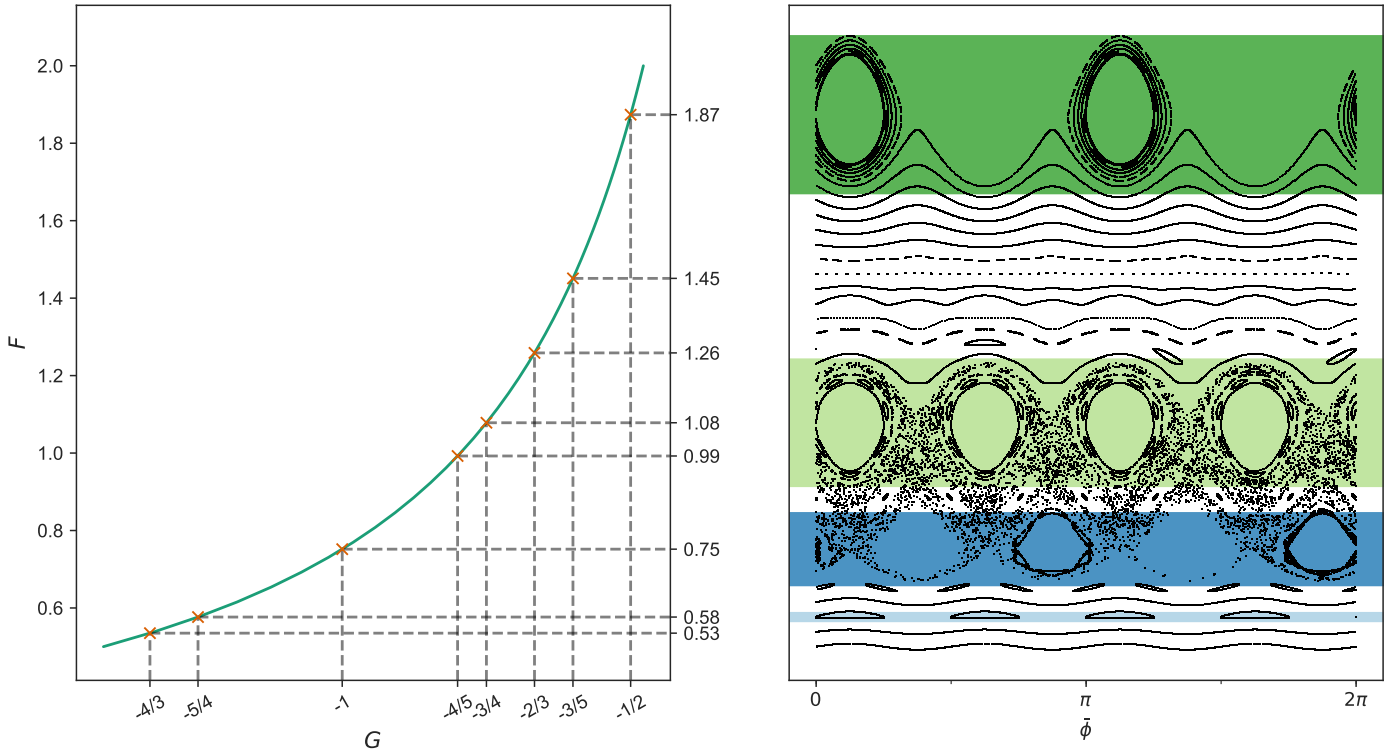

Figure 5.10 Same as in fig. 5.9, but for $A = 8 \cdot 10^{-3}$. Chirikov criterion fails to accurately predict the resonance overlap between the $-1/1$ and the $-3/4$ islands which are undoubtedly chaotically connected. A possible explanation is given in the text.

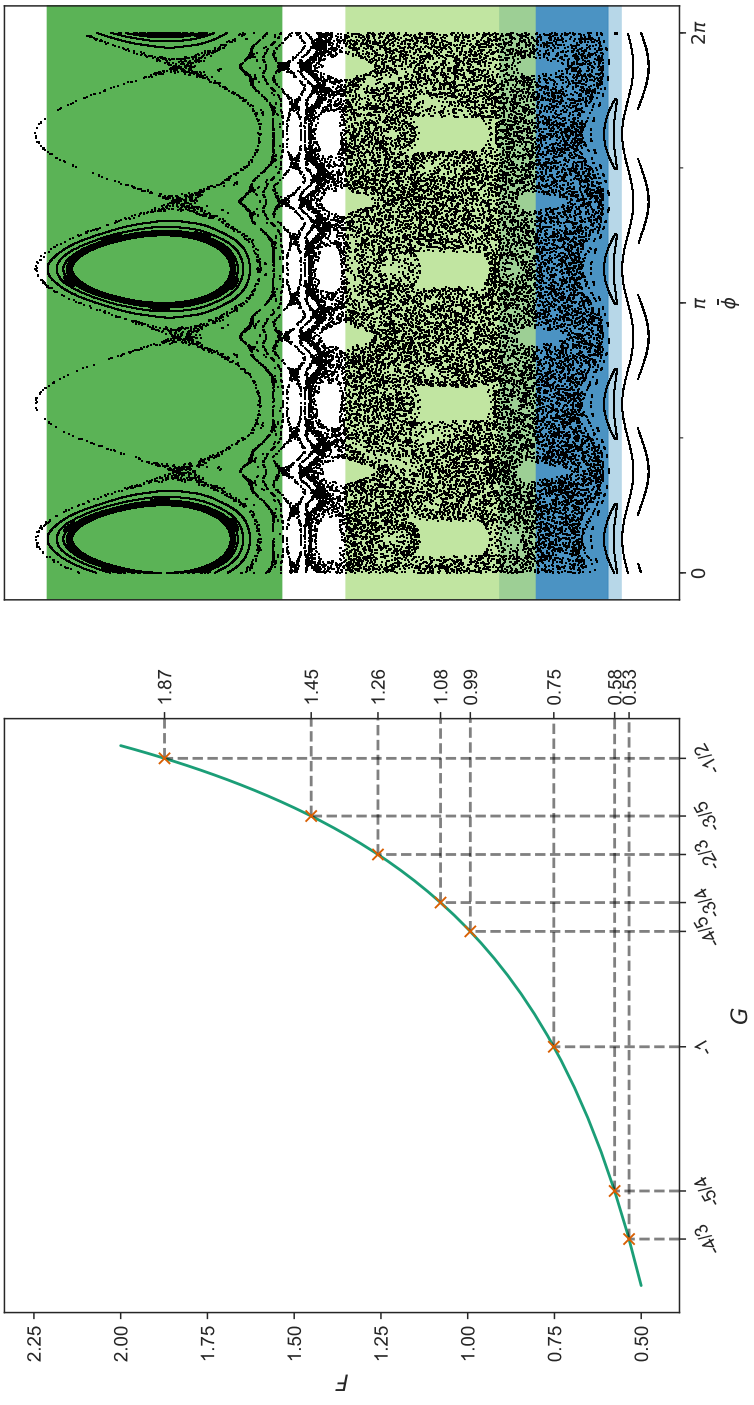

Figure 5.11 Same as in fig. 5.9 and fig. 5.10, but for $A = 2.2 \cdot 10^{-2}$. The calculated widths of the $-5/4$ and the $-1/1$ chains overlap, but the two chains are not chaotically connected. This is probably due to a considerable first order displacement of the $-1/1$ centers from the $-1/1$ resonance level.

Weakly Trapped Orbits

When the energy is positive, the invariant submanifold $H = \text{const.}$ contains a separatrix and the topology of the perturbed orbits can change from trapped to passing. This makes it a more interesting model for applications where one is concerned with determining the conditions of confinement loss in a dynamic equilibrium.

The existence of the separatrix means that there is an area where ω_θ goes to zero and the ratio of the frequencies $G = \omega_{\bar{\phi}}/\omega_\theta$ explodes to infinity. Near the separatrix there is an area densely populated with resonances. Consequently, near the separatrix, there is almost always some finite, although possibly very narrow, patch of phase space that exhibits chaotic behaviour for arbitrarily small perturbation amplitudes.

For symmetry reasons, we will now examine the dynamics on the invariant surface $H = 0.5$. The separatrix occurs at

$$F_{\text{sep}} = H = 0.5$$

For $F < F_{\text{sep}}$, the orbits are passing, while for $F > F_{\text{sep}}$ the orbits are weakly trapped. Trapped orbits can become passing and vice-versa when the part of phase space from which they originate becomes chaotically connected to the separatrix.

First we take $A = 8 \cdot 10^{-4}$, which is considerably smaller than the amplitudes we used for the deeply trapped case, although such comparisons are hardly meaningful here. The dynamics is depicted in fig. 5.12. The location of the separatrix is marked by a thick black horizontal line in both the resonance chart on the left hand side, as well as the Poincare plot on the right. The lowest harmonic resonances near the separatrix have been clearly marked, but since they are located tightly on the F axis, their labelling has been omitted. As predicted, some of the resonances have already started to overlap, so that a chaotic ribbon around the separatrix has already formed.

The low harmonic resonant islands of ratios $-1/4, 0/1, 1/4$ and $1/2$ are easily distinguishable on the Poincare chart and their calculated widths are marked with the superimposed horizontal coloured ribbons. Notice on the resonance chart on the left how the passing orbit branch, with $F < F_{\text{sep}}$, approaches the assymptote of the separatrix horizontal line much faster that the trapped orbit branch, with $F > F_{\text{sep}}$. This is the reason why the passing $1/2$ chain is already connected to the separatrix, while the trapped $1/2$ chain is not. A noteworthy characteristic is the passage of $\omega_{\bar{\phi}}$ through zero *without the existence of an associated separatrix*. This is a general characteristic of the class of Hamiltonians that we study in this chapter, but it is also a feature that surprised us the first time we encountered it. Finally, notice that since the harmonic content of the perturbation in the $\bar{\phi}$ coordinate is monochromatic with $m = 4$, no $n/5$ resonances appear on the Poincare plot.

The effects of increasing the perturbation amplitude to $A = 3 \cdot 10^{-3}$ are depicted in fig. 5.13. We can easily see that more trapped orbits are now allowed to escape, as the $1/2$ and $1/4$ resonances are now connected to the separatrix. The $0/1$ resonance is marginally separated from the chaotic sea. At the top edge of the chaotic sea, just bellow the $0/1$ chain, one can see the traces of the second order $1/8$ resonance.

To complete the picture, we have included fig. 5.14, which depicts the dynamics for $A = 4.5 \cdot 10^{-3}$. Now the $0/1$ chain is also connected to the chaotic sea, but note how the Chirikov criterion predicts that it should not, it's width not yet being large enough for resonance overlap. Again, we postulate that this is due to a combination of the effect of the second order resonances in $1/8$ with the fact that we have not accounted for the first order displacement of the centers of the islands from the resonant levels. The latter effect seems to be especially strong for the large but remote $-1/4$ islands.

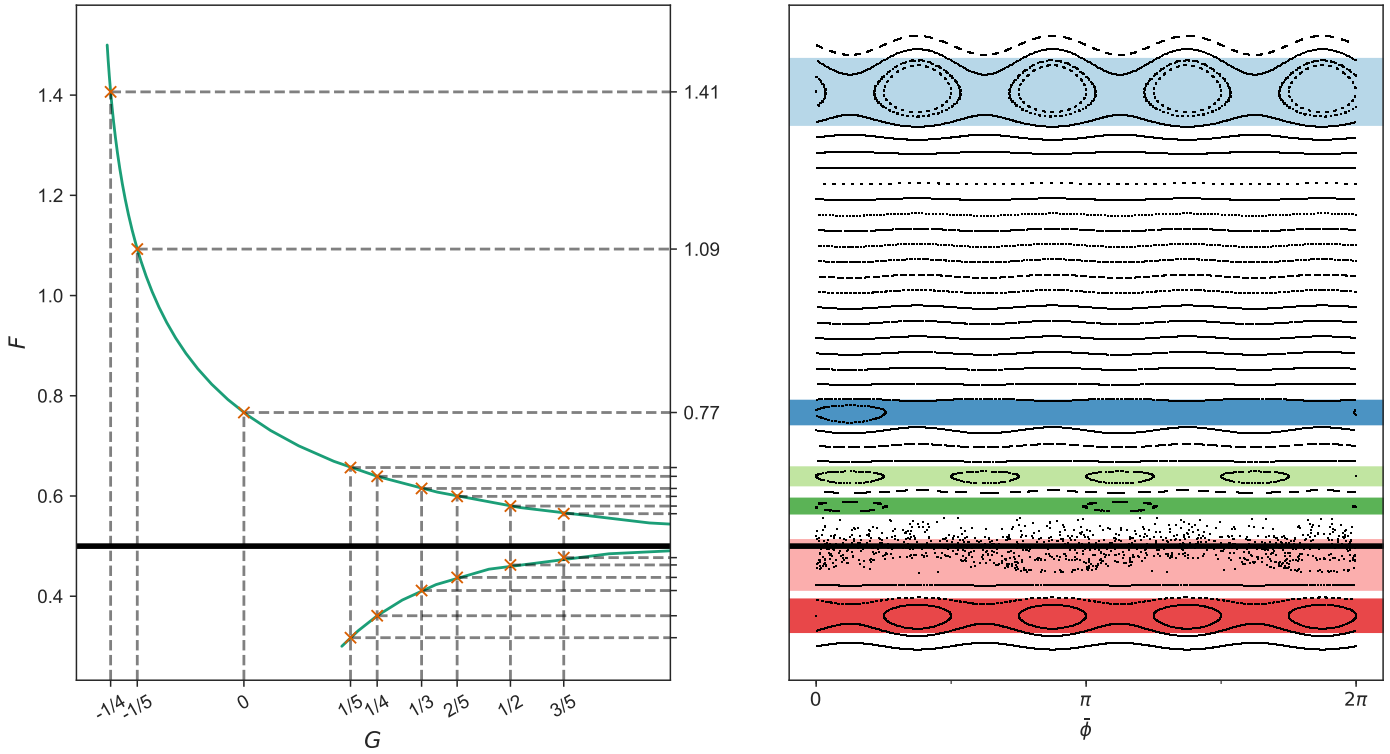

Figure 5.12 Left: The unperturbed frequency ratio G for different values of F on the invariant surface $H = 0.5$. The locations of the low harmonic resonances are marked with x's. The dotted lines facilitate the association of the harmonic resonances with the corresponding island chains on the Poincare diagram. Right: Poincare surface for $A = 8 \cdot 10^{-4}$. The calculated widths of the first order resonances are marked by the horizontal solid color bars. The location of the separatrix is marked by a thick black horizontal line in both diagrams.

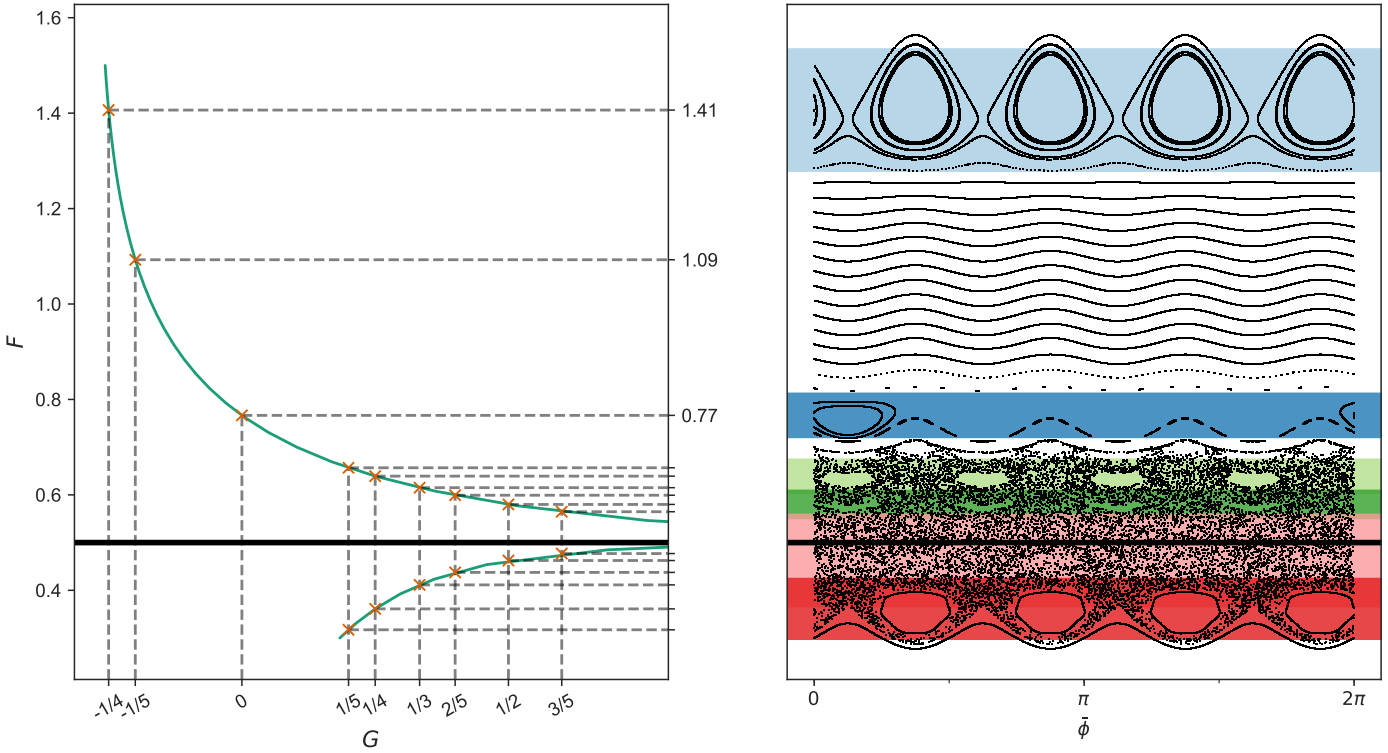

Figure 5.13 Same as in fig. 5.12, but for $A = 3 \cdot 10^{-3}$. More trapped orbits are now allowed to escape, as the $1/2$ and $1/4$ resonances are now connected to the separatrix. The $0/1$ resonance is marginally separated from the chaotic sea. At the top edge of the chaotic sea, just bellow the $0/1$ chain, one can see the remnants of the second order $1/8$ resonance.

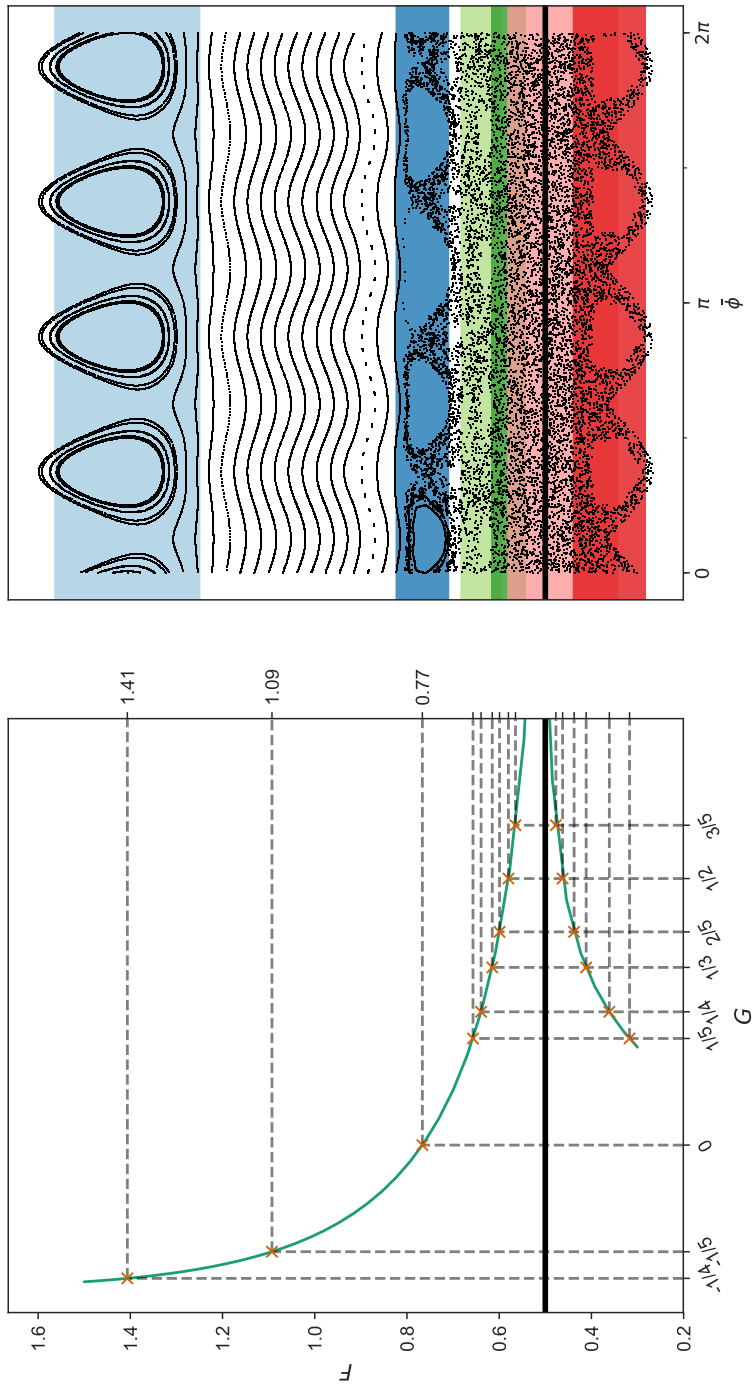

Figure 5.14 Same as in fig. 5.12 and fig. 5.13, but for $A = 4.5 \cdot 10^{-3}$. Contrary to the Chirikov criterion, the $0/1$ chain is now connected to the chaotic sea. This is probably due to a combination of the effect of the second order resonances in $1/8$ with the first order displacement of the centers of the islands from the resonant levels. The latter effect seems to be especially strong for the large remote $-1/4$ islands.

5.7 Conclusions

Path integral theory for orbital spectrum analysis bypasses the need to model the topological skeleton of integrable dynamical systems. Although the functional form of the Hamiltonian as a function of the Actions is in general not known, its Hessian and other quantities that are required for canonical perturbation analysis can be calculated by appropriate path integrals.

We have demonstrated the validity of the techniques developed in the first part of this chapter, by analysing the effect of perturbations on the *extended pendulum* Hamiltonian. In the course of this analysis we have gained experience on the unexpected difficulties that arise when performing perturbation analysis in this context, where quantities that one usually takes for granted are sometimes surprisingly difficult to calculate.

Bibliography

Abdullaev, S. S. (2006). *Construction of mappings for Hamiltonian systems and their applications*, volume 691 of *Lecture Notes in Physics*. Springer.

Abdullaev, S. S., Wingen, A., and Spatschek, K. H. (2006). Mapping of drift surfaces in toroidal systems with chaotic magnetic fields. *Phys. Plasmas*, 13(4).

Abramowitz, M. and Stegun, I. (1970). *Handbook of Mathematical Functions*. Dover, New York.

Arnold, V. I. (1989). *Mathematical methods of classical mechanics*. Springer-Verlag, New York.

Benisti, D., Ram, A. K., and Bers, A. (1997). Lower bound in energy for chaotic dynamics of ions. *Physics Letters A*, 233(3):209 – 215.

Bénisti, D., Ram, A. K., and Bers, A. (1998a). Ion dynamics in multiple electrostatic waves in a magnetized plasma. i. coherent acceleration. *Physics of Plasmas*, 5:3224.

Bénisti, D., Ram, A. K., and Bers, A. (1998b). Ion dynamics in multiple electrostatic waves in a magnetized plasma. ii. enhancement of the acceleration. *Physics of Plasmas*, 5:3233.

Bergmann, A., Peeters, A. G., and Pinches, S. D. (2001). Guiding center particle simulation of wide-orbit neoclassical transport. *Phys. Plasmas*, 8(12):5192.

Boozer, A. H. (1980). Guiding center drift equations. *Phys. Fluids*, 23(5):904.

Boozer, A. H. (1981). Plasma equilibrium with rational magnetic surfaces. *Physics of Fluids*, 24(11):1999.

Brambilla, M. (1998). *Kinetic Theory of Plasma Waves*. Clarendon Press.

Brambilla, M. (1999). Numerical simulation of ion cyclotron waves in tokamak plasmas. *Plasma Phys. Controlled Fusion*, 41(1):1.

Brizard, A. J. (2011). Compact formulas for guiding-center orbits in axisymmetric tokamak geometry. *Phys. Plasmas*, 18(2).

Brizard, A. J. and Hahm, T. S. (2007). Foundations of nonlinear gyrokinetic theory. *Rev. Mod. Phys.*, 79:421–468.

Carthy, P. J. M. (1999). Analytical solutions to the grad–shafranov equation for tokamak equilibrium with dissimilar source functions. *Physics of Plasmas*, 6(9):3554–3560.

Cary, J. R. (1981). Lie transform perturbation theory for hamiltonian systems. *Physics Reports*, 79(2):129 – 159.

Cary, J. R. and Brizard, A. J. (2009). Hamiltonian theory of guiding-center motion. *Rev. Mod. Phys.*, 81:693.

Cary, J. R. and Kaufman, A. N. (1981). Ponderomotive effects in collisionless plasma: A lie transform approach. *Physics of Fluids*, 24(7):1238–1250.

Cary, J. R. and Littlejohn, R. G. (1983). Noncanonical hamiltonian mechanics and its application to magnetic field line flow. *Annals of Physics*, 151(1):1 – 34.

Chen, F. (2013). *Introduction to Plasma Physics and Controlled Fusion: Volume 1: Plasma Physics*. Springer Science & Business Media.

Chu, K. R. (2004). The electron cyclotron maser. *Rev. Mod. Phys.*, 76:489–540.

Deprit, A. (1969). Canonical transformations depending on a small parameter. *Celestial Mechanics*, 1(1):12–30.

D'haeseleer, W. D., Hitchon, W. N. G., Callen, J. D., and Shohet, J. L. (1991). *Flux Coordinates and Magnetic Field Structure: A Guide to a Fundamental Tool of Plasma Theory (scientific Computation)*. Springer.

Eester, D. V. (1999). Trajectory integral and hamiltonian descriptions of radio frequency heating in tokamaks. *Plasma Phys. Controlled Fusion*, 41(7):L23.

Eester, D. V. and Koch, R. (1998). A variational principle for studying fast-wave mode conversion. *Plasma Phys. Controlled Fusion*, 40(11):1949.

Eriksson, L. G. and Porcelli, F. (2001). Dynamics of energetic ion orbits in magnetically confined plasmas. *Plasma Phys. Controlled Fusion*, 43(4).

Fisch, N. J. (1987). Theory of current drive in plasmas. *Rev. Mod. Phys.*, 59:175–234.

Flanders, H. (1989). *Differential Forms with Applications to the Physical Sciences*. Dover Publications Inc.

Fukuyama, A., Momota, H., Itatani, R., and Takizuka, T. (1977). Stochastic acceleration by an electrostatic wave near ion cyclotron harmonics. *Phys. Rev. Lett.*, 38:701–704.

Gambier, D. J. and Samain, A. (1985). Variational theory of ion cyclotron resonance heating in tokamak plasmas. *Nucl. Fusion*, 25(3):283.

Goldstein, H. (1956). *Classical mechanics*. Cambridge: Addison-Wesley.

Gott, Y. V. and Yurchenko, E. I. (2014). Topology of drift trajectories of charged particles in a tokamak. *Plasma Phys. Rep.*, 40(4).

Guazzotto, L. and Betti, R. (2005). Magnetohydrodynamics equilibria with toroidal and poloidal flow. *Physics of Plasmas*, 12(5):056107.

Hazeltine, R. D., Mahajan, S. M., and Hitchcock, D. A. (1981). Quasilinear diffusion and radial transport in tokamaks. *Phys. Fluids*, 24(6).

Helander, P. (2000). On neoclassical transport near the magnetic axis. *Phys. Plasmas*, 7(7):2878.

Hutchinson, I. H. (2005). *Principles of Plasma Diagnostics*. Cambridge University Press.

J. P. Goedbloed, S. P. (2008). *Principles of Magnetohydrodynamics*. Cambridge University Press.

Jorns, B. and Choueiri, E. Y. (2011). Ion heating with beating electrostatic waves. *Phys. Rev. Lett.*, 106:085002.

Jorns, B. and Choueiri, E. Y. (2013). Stochastic ion acceleration by beating electrostatic waves. *Phys. Rev. E*, 87:013107.

Jose, J. V. and Saletan, E. J. (1998). *Classical Dynamics: A Contemporary Approach*. Cambridge University Press.

Karney, C. F. F. (1978). Stochastic ion heating by a lower hybrid wave. *Physics of Fluids*, 21(9):1584–1599.

Karney, C. F. F. and Bers, A. (1977). Stochastic ion heating by a perpendicularly propagating electrostatic wave. *Phys. Rev. Lett.*, 39:550–554.

Kaufman, A. N. (1972a). Quasilinear diffusion of an axisymmetric toroidal plasma. *Phys. Fluids*, 15(6):1063.

Kaufman, A. N. (1972b). Reformulation of quasi-linear theory. *J. Plasma Phys.*, 8:1.

Kikuchi, M. and Azumi, M. (2012). Steady-state tokamak research: Core physics. *Rev. Mod. Phys.*, 84:1807–1854.

Kikuchi, M., Lackner, K., and Tran, M. Q., editors (2012). *Fusion Physics*. Intl atomic energy agency.

Kominis, Y. (2008). Nonlinear theory of cyclotron resonant wave-particle interactions: Analytical results beyond the quasilinear approximation. *Phys. Rev. E*, 77:016404.

Kominis, Y., Ram, A. K., and Hizanidis, K. (2008). Quasilinear theory of electron transport by radio frequency waves and nonaxisymmetric perturbations in toroidal plasmas. *Phys. Plasmas*, 15(12).

Kominis, Y., Ram, A. K., and Hizanidis, K. (2010). Kinetic theory for distribution functions of wave-particle interactions in plasmas. *Phys. Rev. Lett.*, 104:235001.

Kominis, Y., Ram, A. K., and Hizanidis, K. (2012). Interaction of charged particles with localized electrostatic waves in a magnetized plasma. *Phys. Rev. E*, 85:016404.

Lamalle, P. (1993). The nonlocal radio-frequency response of a toroidal plasma. *Phys. Lett. A*, 175(1):45–52.

Lao, L., John, H. S., Stambaugh, R., Kellman, A., and Pfeiffer, W. (1985). Reconstruction of current profile parameters and plasma shapes in tokamaks. *Nuclear Fusion*, 25(11):1611–1622.

Lichtenberg, A. and Liebermann, M. (1983). *Regular and Stochastic Motion*. Springer.

Lichtenberg, A. J. and Lieberman, M. A. (1992). *Regular and Chaotic Dynamics*, volume 38 of *Applied Mathematical Sciences*. Springer–Verlag.

Lin, Z., Tang, W. M., and Lee, W. W. (1997). Large orbit neoclassical transport. *Phys. Plasmas*, 4(5):1707.

Littlejohn, R. G. (1979). A guiding center hamiltonian: A new approach. *J. Math. Phys.*, 20(12):2445.

Littlejohn, R. G. (1983). Variational principles of guiding centre motion. *J. Plasma Phys.*, 29.

Markus, L. L. and Meyer, K. R. K. R. (1974). *Generic Hamiltonian dynamical systems are neither integrable nor ergodic*. American Mathematical Society, Providence. [by] L. Markus and K. R. Meyer., Bibliography: p. 51-52.

Matsuyama, A., Yagi, M., Kagei, Y., and Nakajima, N. (2014). Drift resonance effect on stochastic runaway electron orbit in the presence of low-order magnetic perturbations. *Nucl. Fusion*, 54(12):123007.

McClements, K. G. and Hole, M. J. (2010). On steady poloidal and toroidal flows in tokamak plasmas. *Physics of Plasmas*, 17(8):082509.

Meiss, J. D. and Hazeltine, R. D. (1990). Canonical coordinates for guiding center particles. *Physics of Fluids B: Plasma Physics*, 2(11):2563–2567.

Mouhot, C. and Villani, C. (2011). On landau damping. *Acta Mathematica*, 207(1):29–201.

Mukhovatov, V. S. and Shafranov, V. D. (1971). Plasma equilibrium in a tokamak. *Nuclear Fusion*, 11(6):605–633.

Peierls, R. (1979). *Surprises in Theoretical Physics*, chapter 1, pages 14–17. PRINCETON UNIV PR.

Peierls, R. E. and Urbano, J. N. (1968). The villars formalism for nuclear rotation. *Journal of Physics A: General Physics*, 1(1):1–10.

Porkolab, M., Bonoli, P. T., Pinsker, R. I., Prater, R., Temkin, R. J., and Wilson, J. R. (2012). *Fusion Physics*, chapter 6. Intl atomic energy agency.

Ram, A. K., Bers, A., and Benisti, D. (1998). Ionospheric ion acceleration by multiple electrostatic waves. *Journal of geophysical research*, 103:9431–9440.

Shaing, K. C., Hazeltine, R. D., and Zarnstorff, M. C. (1997). Ion transport process around magnetic axis in tokamaks. *Phys. Plasmas*, 4(3):771.

Shaing, K. C. and Peng, M. (2004). Transport theory for potato orbits in an axisymmetric torus with finite toroidal flow speed. *Phys. Plasmas*, 11(8):3726–3732.

Smith, G. R. and Kaufman, A. N. (1975). Stochastic acceleration by a single wave in a magnetic field. *Phys. Rev. Lett.*, 34:1613–1616.

Spektor, R. and Choueiri, E. (2004). Ion acceleration by beating electrostatic waves: Domain of allowed acceleration. *Physical Review E*, 69(4):046402.

Stix, T. H. (1992). *Waves in Plasmas*. American Inst. of Physics.

Strozzi, D. J., Ram, A. K., and Bers, A. (2003). Coherent acceleration of magnetized ions by electrostatic waves with arbitrary wavenumbers. *Physics of Plasmas*, 10(7):2722–2731.

Taylor, J. B. and Laing, E. W. (1975). Invariant for a particle interacting with an electrostatic wave in a magnetic field. *Phys. Rev. Lett.*, 35:1306–1307.

Troia, C. D. (2012). From the orbit theory to a guiding center parametric equilibrium distribution function. *Plasma Phys. Controlled Fusion*, 54(10):105017.

Wang, S. (2006). Canonical hamiltonian theory of the guiding-center motion in an axisymmetric torus, with the different time scales well separated. *Phys. Plasmas*, 13(5).

Wesson, J. (2004). *Tokamaks*. Oxford University.

White, R. (2012). Modification of particle distributions by MHD instabilities i. *Communications in Nonlinear Science and Numerical Simulation*, 17(5):2200.

White, R. and Zakharov, L. E. (2003). Hamiltonian guiding center equations in toroidal magnetic configurations. *Physics of Plasmas*, 10(3):573–576.

White, R. B. (2001). *The theory of toroidally confined plasmas*. Imperial College Press.

White, R. B. (2013). *The Theory Of Toroidally Confined Plasmas (third eddition)*. Imperial College Press.

White, R. B., Boozer, A. H., and Hay, R. (1982). Drift hamiltonian in magnetic coordinates. *Phys. Fluids*, 25(3).

White, R. B. and Chance, M. S. (1984). Hamiltonian guiding center drift orbit calculation for plasmas of arbitrary cross section. *Phys. Fluids*, 27(10).

White, R. B., Gorelenkov, N., Heidbrink, W. W., and Zeeland, M. A. V. (2010). Particle distribution modification by low amplitude modes. *Plasma Physics and Controlled Fusion*, 52(4):045012.

Zohm, H. (2014). *Magnetohydrodynamic Stability of Tokamaks*. Wiley VCH Verlag GmbH.

Index